Journal of Medicinal Chemistry

Article

Discovery of a Selective Aurora A Kinase Inhibitor by Virtual Screening

Falco Kilchmann, Maria Jose Marcaida, Sachin Kotak, Thomas Schick, Silvan D Boss, Mahendra Awale, Pierre Gönczy, and Jean-Louis Reymond

J. Med. Chem., **Just Accepted Manuscript** • DOI: 10.1021/acs.jmedchem.6b00709 • Publication Date (Web): 08 Jul 2016

Discovery of a Selective Aurora A Kinase Inhibitor by Virtual Screening

Falco Kilchmann,[a)§] Maria J. Marcaida,[a)c)§] Sachin Kotak,[b)d)] Thomas Schick,[a)] Silvan D. Boss,[a)] Mahendra Awale,[a)] Pierre Gönczy[b)]* and Jean-Louis Reymond[a)]*

[a)] *Department of Chemistry and Biochemistry, National Center of Competence in Research NCCR Chemical Biology and NCCR TransCure, University of Berne, Freiestrasse 3, 3012 Berne Switzerland;* e-mail: jean-louis.reymond@dcb.unibe.ch; [b)] *Swiss Institute for Experimental Cancer Research (ISREC), School of Life Sciences, National Center of Competence in Research NCCR Chemical Biology, Swiss Federal Institute of Technology (EPFL), CH-1015 Lausanne, Switzerland; e-mail:* pierre.gonczy@epfl.ch

[c)] *Present address: Institute of Bioengineering, School of Life Sciences, Swiss Federal Institute of Technology (EPFL), CH-1015 Lausanne, Switzerland*

[d)] *Present address: Department of Microbiology and Cell Biology (MCB), Indian Institute of Science (IISc), Bangalore, India*

[§] *These authors contributed equally to the work*

Abstract

Here we report the discovery of a selective inhibitor of Aurora A, a key regulator of cell division and potential anti-cancer target. We used atom category extended ligand overlap score (xLOS), a 3D ligand based virtual screening method recently developed in our group, to select 437 shape and pharmacophore analogs of reference kinase inhibitors. Biochemical screening uncovered two inhibitor series with scaffolds unprecedented among kinase inhibitors. One of them was successfully optimized by structure-based design to a potent Aurora A inhibitor (IC_{50} = 2 nM) with very high kinome selectivity for Aurora kinases. This inhibitor locks Aurora A in an inactive conformation and disrupts binding to its activator protein TPX2, which impairs Aurora A localization at the mitotic spindle and induces cell division defects. This phenotype can be rescued by inhibitor-resistant Aurora A mutants. The inhibitor furthermore does not induce Aurora B specific effects in cells.

Introduction

Computer-aided drug design exploits accumulated experimental and theoretical knowledge of drug-target interactions to preselect small sets of compounds for experimental evaluation enabling faster and more efficient drug discovery.[1-3] While structure-based methods exploit structural information on the protein targets,[4, 5] ligand-based virtual screening (LBVS) methods employ similarity to previously known compounds to propose new analogs for testing.[6] In LBVS substructure similarity searches, for example using Tanimoto similarity with Daylight-type substructure fingerprints,[7] can be used to find available analogs with varying substituents around conserved scaffolds. On the other hand shape and pharmacophore similarity methods, in particular those comparing the 3D structure of molecules either by overlays[8] (*e.g.* FlexS,[9] Topomer shape similarity searching,[10] Surflex-Sim,[11] pharmACOphore,[12] ROCS[13]) or via 3D-fingerprints[14] (e.g. USRCAT,[15] 3DXfp[16]) can suggest analogs with entirely different scaffolds and thus open the way to new compound series. This transition to new scaffolds while preserving shapes and pharmacophores is referred to as scaffold-hopping.[17]

Here we applied scaffold hopping LBVS to identify a new and selective inhibitor of Aurora A, an evolutionary conserved Ser/Thr kinase essential for proper progression through mitosis and one of the most intensively researched kinase targets due to its significance in cancer.[18, 19] Although many potent inhibitors of this kinase are known, most of these also inhibit Aurora B, a chromosomal passenger protein required notably for cytokinesis and which shares over 85% sequence homology with Aurora A in the kinase domain.[20, 21] Alisertib (MLN8237, **1**), one of the most selective Aurora A inhibitors reported to date,[22] is currently under advanced clinical investigation for the treatment of various solid and hematological malignancies (Figure 1).[23] Interestingly **1** and its close relative MLN8054 (**2**)[24] belong to a scaffold that is unique among the 4,874 scaffolds (as defined by Bemis and Murcko)[25] occurring in 11,286 kinase inhibitors with potencies better than 50 nM listed in ChEMBL.[26-32] Furthermore the diversity of scaffolds is quite

high among Aurora A kinase inhibitors, with 174 different scaffolds occurring among 329 inhibitors with potencies better than 50 nM listed in ChEMBL. This suggests that each inhibitor represents an already optimized compound for each scaffold, and that discovering further selective inhibitors for this particular kinase might require identifying different scaffolds, for example using scaffold hopping LBVS.[23, 24]

To perform scaffold hopping LBVS we used the atom category extended Ligand Overlap Score (xLOS),[33] a 3D shape and pharmacophore similarity algorithm recently developed in our group. The xLOS algorithm compares molecules by maximizing the ligand overlap score[34, 35] computed separately for three atom categories (hydrophobic, H-bond acceptor and H-bond donor atoms) previously found to be useful for pharmacophore fingerprint design.[36, 37] The method shows excellent scaffold hopping properties, which may be attributed to the fact that the algorithm compares molecules by atom positions only without considering atom connectivity patterns. Furthermore xLOS penalizes non-overlapping parts of seed and query molecule, and therefore gives higher scores to molecules with a relatively small size, which are most suitable for initial activity screening since these may later be optimized by the addition of substituents.[29, 30] In our initial implementation we used xLOS to optimize weak and unselective inhibitors of the calcium channel TRPV6 by early scaffold redesign, which enabled the identification of a new scaffold leading to the first potent and selective inhibitor for this target.[33] The method was also recently used for the identification of a new non-competitive inhibitor with an original scaffold for the iron transporter DMT1, for which only very few inhibitors have been described to date.[38]

As detailed below, we used xLOS to search commercial catalogs for shape and pharmacophore analogs of 16 known kinase inhibitors and assembled a kinase screening set of 437 compounds featuring mostly different scaffolds compared to known kinase inhibitors and kinase screening compounds. Biochemical screening against Aurora A gave 18 hits featuring 12 different scaffolds, two of which were pursued further. While attempts to optimize benzimidazole **5** only led to modest improvements with its hydroxyl analog **6**, we succeeded in modifying the phenylimino-

thiazolidinone hit **7** and its close analog **8** identified in a second round of LBVS using structure-based drug design and obtained the potent inhibitor **9**. Compound **9** is a type II kinase inhibitor displaying strong and selective binding to Aurora kinases against the entire kinome. Inhibitor **9** induces a selective Aurora A phenotype in cells without any Aurora B specific effects.

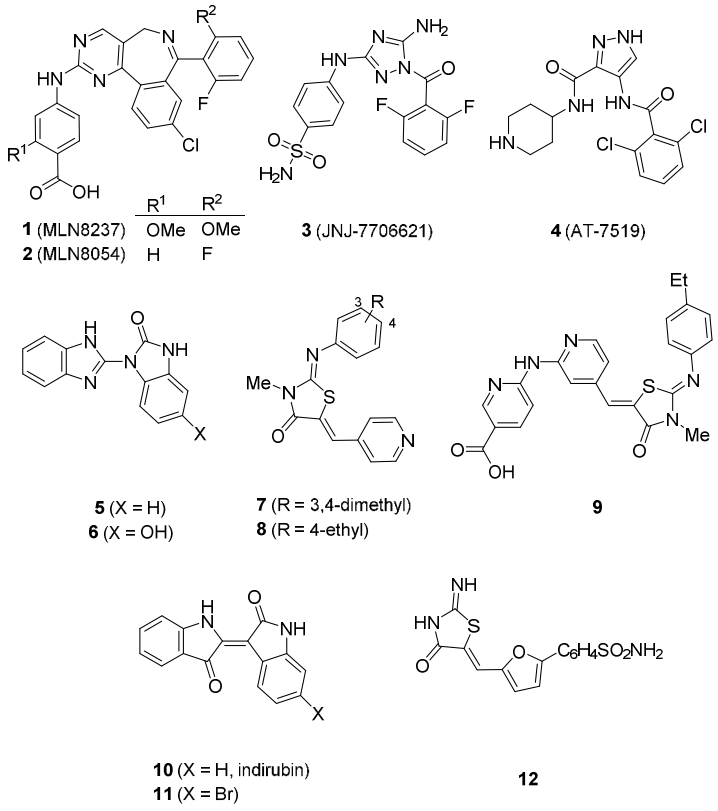

Figure 1. Structures of reference kinase inhibitors and new inhibitors discussed in this paper.

Results and Discussion

Virtual Screening

We assembled a kinase discovery set by searching the ZINC database comprising ~12 million compounds[39] for shape and pharmacophore analogs of 16 known inhibitors of Aurora A and other kinases (Supplementary Figure 1) using the xLOS algorithm described above. We focused our selection on two vendor catalogs totaling ~1.2 million compounds and purchased 437 compounds selected by clustering the 1000 top scoring compounds against each of the 16 references, taking into account scaffold diversity, potential for derivatization, and absence of reactive functional groups (aldehydes, quinones, chloroketones, imines, etc.). Pan assay interference compounds (PAINS) were however not specifically excluded.[40] Indeed the recently available automated tool at the docking.org website[41] flags 27 of the 437 compounds (6.2 %) as PAINS, which is significantly higher than for DrugBank (67 PAINS from 1775 drugs, 3.8 %) or a random selection of ChEMBL (86 PAINS from 2000 ChEMBL compounds, 4.3 %). The selected compounds had relatively high xLOS scores indicating significant shape and pharmacophore similarity to the reference inhibitors. These compounds also showed relatively low substructure similarity to these reference inhibitors as measured by the Tanimoto similarity coefficient relative to a 1024-bit Daylight type substructure fingerprint (TSfp < 0.7), although this similarity was still higher than the average Tanimoto value of 0.23 for all compounds used in LBVS (Figure 2a). Our screening set was comparable to commercially available kinase discovery sets in terms of molecular properties (molecular size, number of H-bond donor and acceptor atoms, number of rotatable bonds). Both of these discovery sets contained compounds that were on average smaller and with fewer H-bond donor atoms and rotatable bonds compared to kinase inhibitors reported in ChEMBL, in particular the more potent ones, reflecting the difference between screening compounds and optimized inhibitors (Figure 2c). Most importantly, our screening set showed very low overlap with known kinase inhibitors and discovery sets in terms of molecules and scaffolds, highlighting its potential for identifying scaffolds not previously used for kinase inhibition (Table 1).

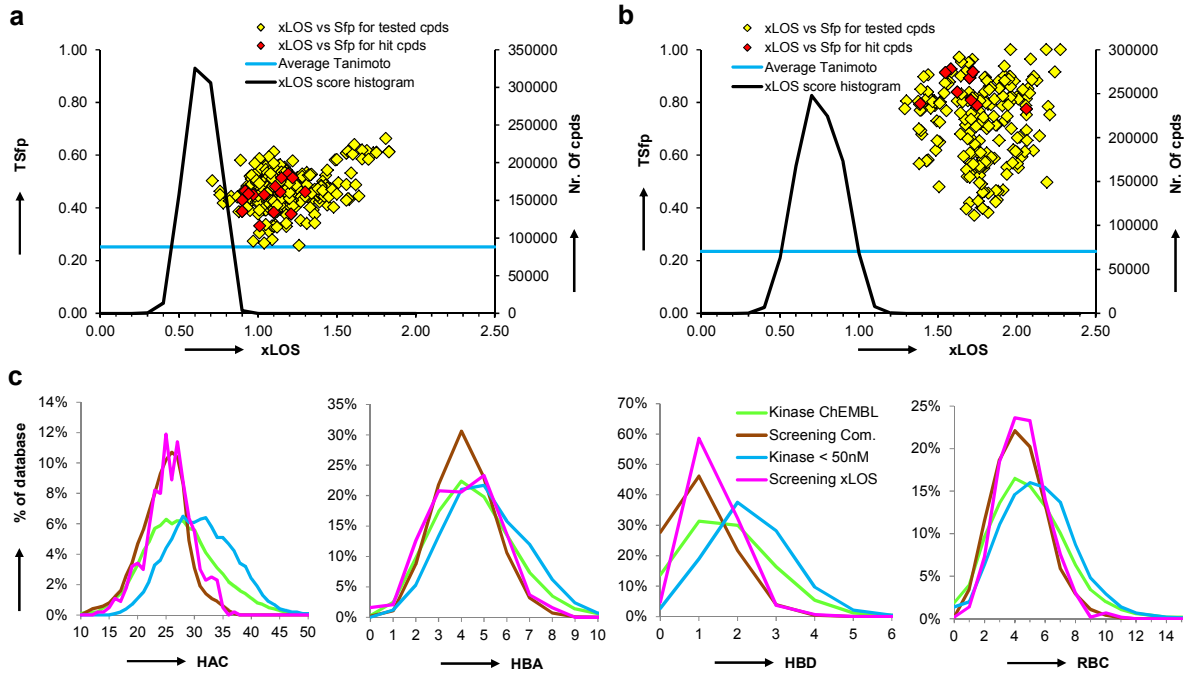

Figure 2. Kinase library design and screening. **a**. Combined frequency histogram as a function of xLOS score (black line, ~1.2 M commercial cpds from two catalogs, right vertical axis), and scatter plot of substructure similarity (TSfp: Tanimoto coefficient of a 1024-bit Daylight type substructure fingerprint) versus xLOS score for the selected 437 screening compounds (black dots) and active Aurora A hits (red dots) against their most similar reference inhibitor. **b**. Combined frequency histogram and similarity scatter plot as **a** for 212 compounds selected in the 2nd round of virtual screening compared to their reference 1st round hit. **c**. Property profile of kinase screening sets and inhibitors in terms of heavy atom count (HAC), hydrogen bond acceptor atoms (HBA), hydrogen bond donor atoms (HBD), and rotatable bond count (RBC). See Table 1 for details of the composition of the sets.

Table 1. Compound and scaffold overlap between different kinase inhibitor and screening sets.[a)]

Shared compounds	Kinase ChEMBL	Screening Commercial	Kinase 50nM	Aurora 50nM	Screening xLOS	Hits xLOS	**Unique**
Kinase ChEMBL	51643	139	11286	329	3	0	40222
Screening Commercial	139	23979	7	0	9	0	23831
Kinase 50nM	11286	7	11286	329	0	0	0
Aurora 50nM	329	0	329	329	0	0	0
Screening xLOS	3	9	0	0	437	15	410
Hits xLOS	0	0	0	0	15	24	9
Shared Scaffolds							
Kinase ChEMBL	23400	836	4874	174	66	4	17719
Screening Commercial	836	13447	61	1	58	5	12584
Kinase 50nM	4874	61	4874	174	9	1	0
Aurora 50nM	174	1	174	174	1	0	0
Screening xLOS	66	58	9	1	247	15	145
Hits xLOS	4	5	1	0	15	18	3 (12)[b)]

[a)] Kinase ChEMBL: all kinase inhibitors found in ChEMBL; Screening commercial: aggregated series of commercially available screening compounds for kinases; Kinase 50 nM: ChEMBL kinase inhibitors reported with IC_{50} < 50 nM; Aurora 50 nM: ChEMBL Aurora inhibitors with IC_{50} < 50 nM; Screening xLOS: screening set in the present study. Scaffolds are defined according to Bemis and Murcko.[b)] Scaffolds unique to the hits not considering overlap with the xLOS screening set.

Hit identification

We conducted a time-resolved FRET assay[42] to test the impact of our kinase screening set on Aurora A activity and found that 15 compounds inhibited Aurora A by more than 50 % at 10 μM (Supplementary Figure 2), corresponding to a 3.4 % hit rate comparable to other LBVS guided screens.[43] None of these hits were flagged as PAINS. An additional 205 analogs of these 15 hits were selected by further similarity searching using xLOS, which featured mostly very close analogs of the hits displaying both high xLOS and substructure similarity scores to these hits (Figure 2b). In this case a subsequent check at docking.org flagged six compounds as PAINS (see supporting information), none of which appeared as hits. Biochemical testing of these 2nd round LBVS compounds provided an additional 9 hits with comparable inhibition (Supplementary Figure 3). The compendium of 24 hits featured 18 scaffolds, 12 of which did not appear among commercial kinase screening compounds or known kinase inhibitors. Two of these hits were investigated closer, which were the benzimidazole **5** (IC_{50} = 6.5 μM), with a xLOS score of 1.1 relative to the known CDK and Aurora A/B inhibitor **3** (JNJ-7706621),[44] and the N-substituted thiazolidinone **7** (IC_{50} = 2.0 μM), with a xLOS score of 1.01 relative to the known CDK inhibitor **4** (AT-7519) (Figure 1).[45] Hit

7 was confirmed in the second round of virtual screening by the identification of a more potent analog **8** (IC_{50} = 0.39 μM). Both series represented scaffolds previously unknown among kinase inhibitors. Indeed only a single derivative of **5** and no bioactivity have been reported for this scaffold,[46] whereas the closest relative of **5** is the natural product indirubin (**10**), which is known to inhibit cyclin dependent kinases (CDKs), but with which **5** only shares the cyclic skeleton (scaffold not considering heteroatoms and double bonds).[47, 48] Furthermore, although a variety of bioactive compounds with N-substituted thiazolidinones are known,[49-52] only the N-unsubstituted thiazolidinone scaffold has been used in relationship with kinases in the case of compound **12** and analogs developed as PIM kinase and CDK2 inhibitors.[53, 54] Note that hit **7**, **8**, our optimized inhibitor **9**, the known inhibitor **12** as well as the various reported bioactive thiazolidinones[49-52] are not flagged by the PAINS tool at docking.org, and that their thiazolidinone core is allowed in the ZINC clean set.[41] In the present context the steep structure-activity relationship profile observed during the optimization of hit **7** and the relatively low glutathione reactivity observed for **9** (see below Figure 8) confirm that this structural type, although listed as "rhodanine-like" PAINS in the original publication,[40] does not behave as a typical PAINS.

Synthesis

Benzimidazole hit **5** was resynthesized from 1,2-diaminobenzene by condensation with carbonyl diimidazole to form the corresponding cyclic urea **13**, reaction with phosphorus oxychloride to form chlorobenzimidazole **19**, coupling with mono-boc protected 1,2-diaminobenzene to intermediate **25** and finally cyclization of the Boc group under basic conditions to form the cyclic urea group. This synthetic route was used to prepare **5** and its analogs **6** and **33-42** (Scheme 1). Coupling of the mono-boc protected 4-methyl-1,2-diaminobenzene **43** with chlorobenzimidazole **52** and cyclization gave benzimidazole **44** as an isomeric mixture. Oxidation of the methyl groups afforded the carboxylic acids **45** and **46** as a separable pair of isomers, which were subsequently converted to the corresponding N-methyl amide **47** and **48**. Finally syntheses involving N-methyl

chlorobenzimidazole **49** on the one hand and boc protected N-methyl-1,2-diaminobenzene **52** on the other hand afforded the selectively N-methylated analogs **51** and **53** (Scheme 2).

Analogs of phenylimino-thiazolidinone hit **7** were prepared by addition of various anilines to alkyl isothiocyanates, followed by regioselective cyclization with ethyl chloroacetate to form the thiazolidinone nucleus, and finally Knoevenagel condensation with aromatic aldehydes (Scheme 3).[55] The 2-aminopyridine analog **79**, prepared by condensation of intermediate **54** with Boc-protected 2-amino-4-formyl-pyridine followed by acidic deprotection (see supporting information), was further elaborated by coupling to carboxylic acids by amide bond formation to analogs **80-83**, or to aromatic bromides by palladium coupling to analogs **84-88** and **9** (Scheme 4). Alternatively, the exocyclic double bond of **79** was either cyclopropanated to yield diastereoisomeric cyclopropanes *rac*-**89**/*rac*-**90** or reduced by hydrogenation to yield *rac*-**91**, which was subsequently extended by coupling to 6-bromo-nicotinic acid to yield *rac*-**92**.

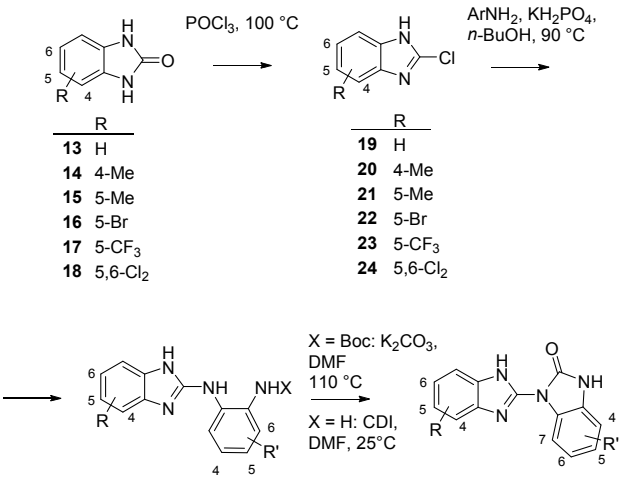

	R
13	H
14	4-Me
15	5-Me
16	5-Br
17	5-CF_3
18	5,6-Cl_2

	R
19	H
20	4-Me
21	5-Me
22	5-Br
23	5-CF_3
24	5,6-Cl_2

	X	R	R'
25	Boc	H	H
26	Boc	4-Me	H
27	Boc	5-Me	H
28	Boc	5-Br	H
29	Boc	5-CF_3	H
30	Boc	5,6-Cl_2	H
31	H	H	4-Cl
32	Boc	H	5-Cl

R (R' = H)		R' (R = H)	
H	**5**	7-OH	**38**
4-Me	**33**	6-Cl	**39**
5-Me	**34**	6-OH	**40**
5-Br	**35**	5-Cl	**41**
5-CF_3	**36**	5-OH	**6**
5,6-Cl_2	**37**	4-OH	**42**

Scheme 1. Synthesis of benzimidazole hit **5** and derivatives.

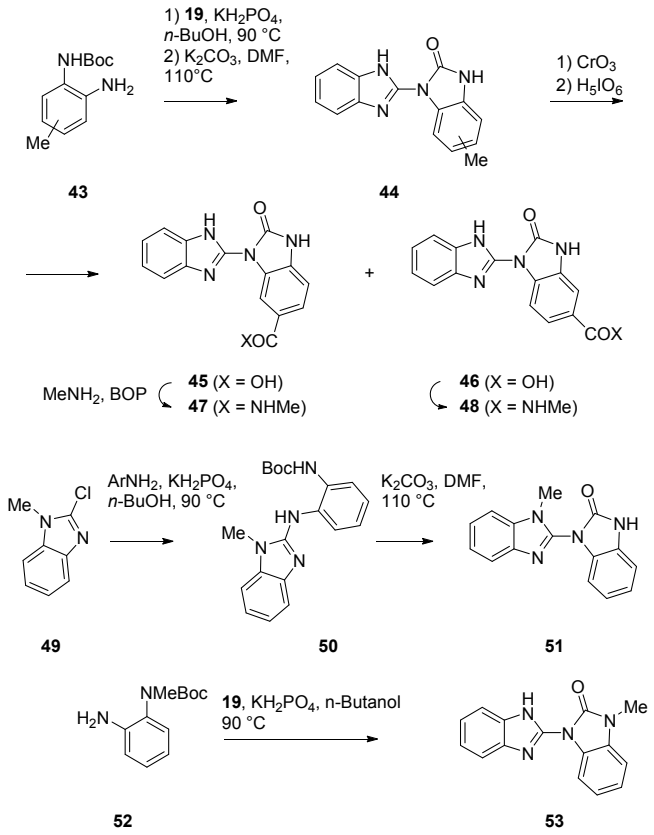

Scheme 2. Synthesis of further analogs of benzimidazole **5**.

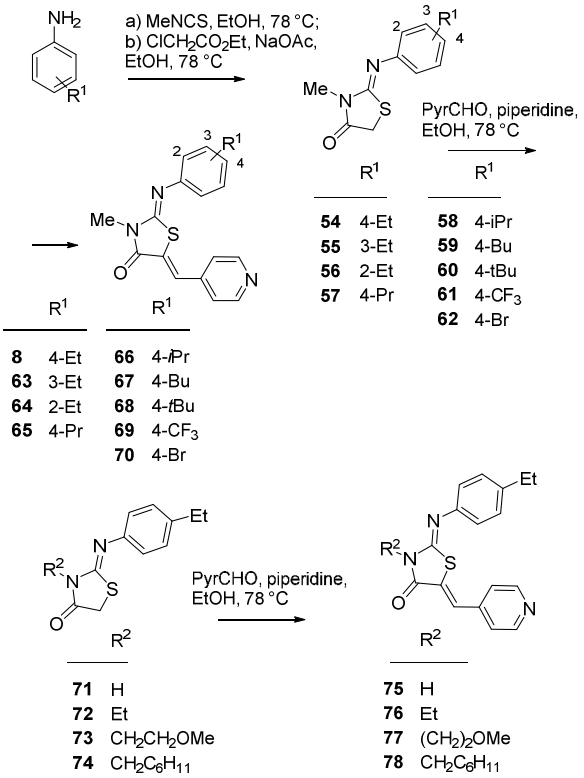

Scheme 3. Synthesis of phenylimino-thiazolidinones.

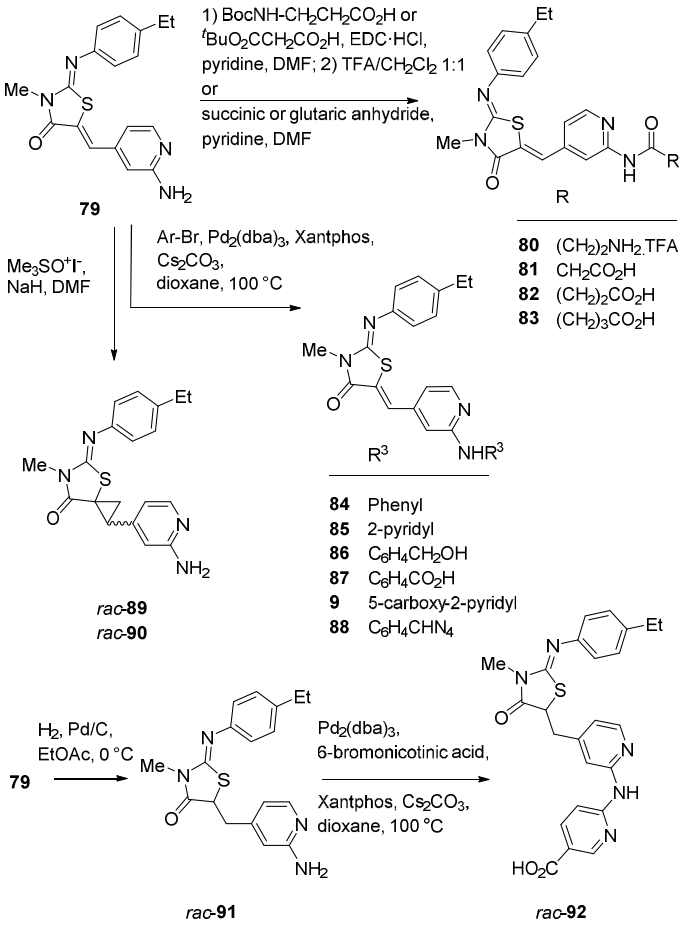

Scheme 4. Synthesis of further thiazolidinone analogs.

The indirubin-like benzimidazole 5 is a type I inhibitor

The benzimidazole derivative **5** was investigated first. Analogs **6**, **33-42, 45-48, 51** and **52** provided an initial structure-activity relationship profile. Many of these derivatives lost potency or only provided modest improvements compared to the initial hit compound. In particular N-methylation of the benzimidazole nitrogen atoms resulted in the inactive analogs **51** and **52**, suggesting that these hydrogen bond donor atoms were essential for activity and might therefore interact with the hinge region of the kinase. Furthermore a 3-fold gain in activity was observed upon introduction of a hydroxyl group at position 5 with **6** (IC_{50} = 2.3 μM, Figure 3a). The 5-carboxy analog **46** was almost as active, but activity returned to lower levels with the corresponding N-methyl carboxamide **48.**

To understand the inhibition mechanism of the best inhibitor **6** at the atomic level, we solved the crystal structure of **6** bound to Aurora A, revealing a typical Type I mode of inhibition including the activation loop in the active, DFG-in conformation (PDB code 4ZS0, 3.0-3.1 Å resolution, Supplementary Table 1 and Figure 3b).[56, 57] Compound **6** engaged in two hydrogen bonds between its benzimidazole and Ala213 in the hinge region of Aurora A, as suggested by the loss of activity observed upon N-methylation of the benzimidazole with analogs **51** and **52**. These interactions were analogous to those between the related 6-bromoindirubin (**11**) and its target CDK2 (PDB code 2BHE).[58] Moreover, **6** made additional hydrophobic contacts with Val147, Leu139, Leu194 and Leu263, and a hydrogen bond between its 6-hydroxyl group and Asp274 presumably explaining its stronger binding compared to **5** (Figure 3c). Although no breakthrough derivative (IC_{50} < 100 nM) could be identified in this series, the small size and high ligand efficiency of **6** (LE = 0.39) suggest that its rather original scaffold might be amenable to further optimization for Aurora A or other kinases.

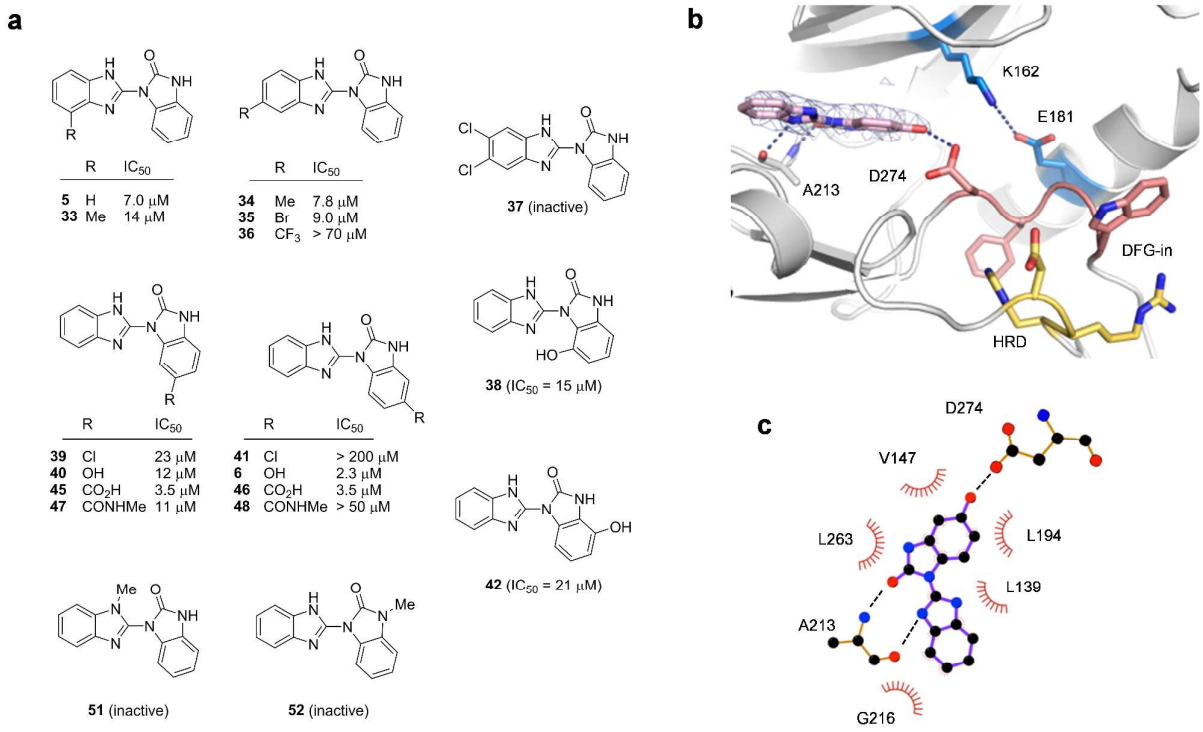

Figure 3. The indirubin-like scaffold **1**. **(a)** Structure-activity relationship profile. Aurora A inhibition was measured using an HTRF assay (see methods). **(b)** Crystal structure of the Aurora A ATP-binding site with bound **6** (PDB 4ZS0, Supplementary Table S1), with highlighted salt bridge between residues Lys162 and Glu181 (blue), DFG motif (pink) and HRD motif (yellow) characteristic of an active kinase conformation. **(c)** Schematic of contact residues between **6** and Aurora A. Dashed lines indicate hydrogen bonds and red arcs represent hydrophobic interactions.

The phenylimino-thiazolidinone 7 can be optimized to the potent and selective inhibitor 9

The phenylimino-thiazolidinones **7** was investigated next. Initial SAR profiling indicated potential for optimization upon variation of the N-phenyl substituents with **8** and pinpointed to the essential role of the 4-pyridine ring since several analogs of **7** with alkyl, halogen, hydroxy or methoxy substituted phenyl rings or a 3-pyridyl ring at that position were inactive (data not shown). Additional analogs were investigated to test if the initial gain in activity with **8** could be improved further (Figure 4a). Activity profiling confirmed the optimal 4-ethylphenylimino substituent of **8** (**63-70** and **93**) and the need for a small alkyl substituent on the endocyclic nitrogen atom of the thiazolidinone (**75-78**). Furthermore, crystal structures of **76** and **78** established the *Z*-stereochemistry of both exocyclic double bonds of the thiazolidinone core (Supplementary Figure 4).

A further crystal structure of **77** in complex with Aurora A (see below) suggested that placing an amino group at the 2-pyridyl position substituted with acyl or aromatic groups[59] might enhance hinge-binding interactions. Significant potency gains were indeed obtained by this approach, reaching low nanomolar values with **81-83** and **87**, **9** and **88** displaying substituents with a carboxylate or tetrazole group presumably interacting with Arg137 (Figure 4b).

These inhibitors were remarkably selective for Aurora A against Aurora B used in complex with its physiological activator INCENP (Figure 4c).[60] The most potent inhibitor **9** (IC_{50} = 2 nM) was selected for further in depth analysis because this compound was also the most potent when tested on cells (see below). A kinome scan of 456 kinases using an active site directed binding competition assay[61] followed by determination of binding affinities showed that **9** was remarkably selective and bound tightly only to Aurora A (K_D = 5 nM), Aurora B (without INCENP, K_D = 10 nM), and Aurora C (K_D = 11 nM) (Figure 4d).[62] Note that the biochemical inhibition and binding affinity measurements were both carried out with free Aurora A, which is autophosphorylated at T288, and gave comparable values. By contrast and due to the inactivity of the kinase alone the

biochemical inhibition of Aurora B was measured for its complex with its activator protein INCENP, to which it is always bound in cells, giving a 15-fold weaker value for inhibition of catalysis compared to the K_D value for binding measured with free Aurora B.

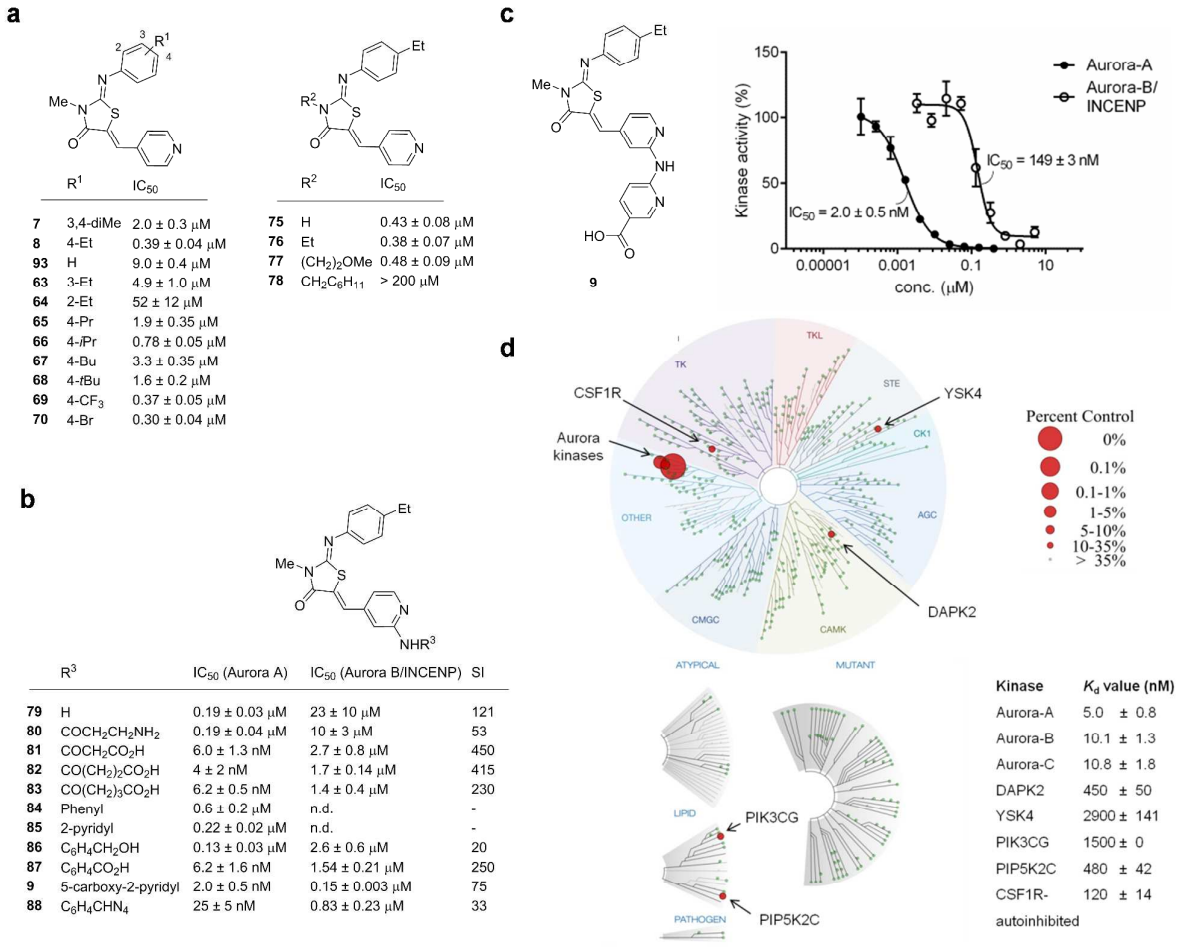

Figure 4. Optimization of the phenylimino-thiazolidinone hit **7** to the selective Aurora A inhibitor **9**. **(a)** Structure and activities of analogs with variations of R^1 and R^2. **(b)** Optimization of the 2-pyridyl substituent. SI = selectivity index: IC_{50}(Aurora B/INCENP)/IC_{50}(Aurora A). **(c)** Structure and IC_{50} curves for Aurora A and Aurora B/INCENP of the most potent inhibitor **9**. **(d)** Kinome profiling and K_D values for **9** towards its 9 best target kinases.

Binding of 9 to Aurora A excludes the activator protein TPX2

To understand the inhibition mechanism at the atomic level, we solved the crystal structures of Aurora A in complex with **77** from the initial SAR study, with the highest affinity inhibitor **9**, and with its phenyl tetrazole analog **88** (PDB codes 4ZTQ, 4ZTR and 4ZTS, resolution 2.8-2.9Å, Supplementary Table 1, Figure 5). All three inhibitors bind to the ATP pocket in the adenine binding region (Leu139, Val147, Ala160, Leu263) and occupy the hydrophobic back pocket (Leu194, Arg195, Leu196, Leu210, Phe275). The inhibitors induce an inactive DFG motif conformation also found in other Aurora A inhibitor complexes (PDB codes 4JBQ, 4JAI, 2J5O, 2BMC, 3P9J, 3R22, 3FDN, 3K5U, and 4BOG) with four characteristic features:[56, 57] (1) disruption of the R-spine (residues Leu196, Gln185, Phe275, His254, and Asp311), (2) an outward displacement of the αC helix compared to the active state (approximately 2.5 Å), (3) absence of the salt bridge between Lys162 and Glu181, and (4) disruption of the Asp256–Thr292–Lys258 hydrogen bond network. In this conformation Asp274 is pointing away from the ATP pocket and Phe275 is rotated upwards thereby contacting the phenylimino moiety of the inhibitors. Furthermore, Trp277 (or Arg255 of the HRD motif in the case of **9**) forms H-bonds with Gln185 and Asp274, an arrangement clearly different from classical DFG-in or DFG-out conformations,[63, 64] and which is specific of Aurora kinases, thus probably contributing to inhibitor selectivity.[65, 66] The pyridine/aminopyridine group of the inhibitors engages in one or two hydrogen bonds with Ala213 in the hinge region. Finally, the terminal carboxylate of **9** forms a salt bridge with Arg137 and Arg220, analogous to **1** in the structure bound to Aurora A (PDB code 2X81)[67], thus explaining its stronger affinity compared to **77**.

Tryptophan fluorescence experiments showed that binding of **9** and of its analogs **77** and **88** perturbed the environment of Trp277, reflecting the rearrangement of the DFG loop and Trp277 interactions with Gln185 occurring upon binding of these inhibitors, as suggested by inspection of the crystal structures. By contrast the type I inhibitor **6**, which does not induce rearrangement of the DFG loop, had no effect on tryptophan fluorescence (Supplementary Figure 5). Further analysis of

these crystal structures indicated that this rearrangement should be incompatible with the rotation of the αC-helix and the subsequent salt bridge formation between Lys162 and Glu181 that take place upon binding to the microtubule-associated activator protein TPX2 (PDB code 1OL5 or 4C3P, Supplementary Figure 6).[68, 69]

To test this hypothesis, we measured the binding of Aurora A to labeled $TPX2^{1-43}$ using microscale thermophoresis (K_D ~800 nM). As reported in Figure 6a, we found that this binding was indeed abolished in the presence of excess **9**. The incompatibility between **9** and TPX2 was further evidenced by the fact that TPX2 binding, which induced a 3-fold increase in the activity of Aurora A similar to other reports (Figure 6b),[70] reduced inhibition by **9** from IC_{50} = 2.0 nM to IC_{50} = 1.4 μM (Figure 6c). In control human cells, TPX2 helps in the localization of Aurora A to the spindle microtubules, but not to the centrosomes.[70, 71] Our findings raised the possibility that addition of **9** should prevent localization from taking place strictly on the spindle microtubules.[71] Indeed, we found that Aurora A remained localized at centrosomes in the presence of **9** but was notably displaced from the spindle microtubules, as is the case for **1** (Figure 6d).[72]

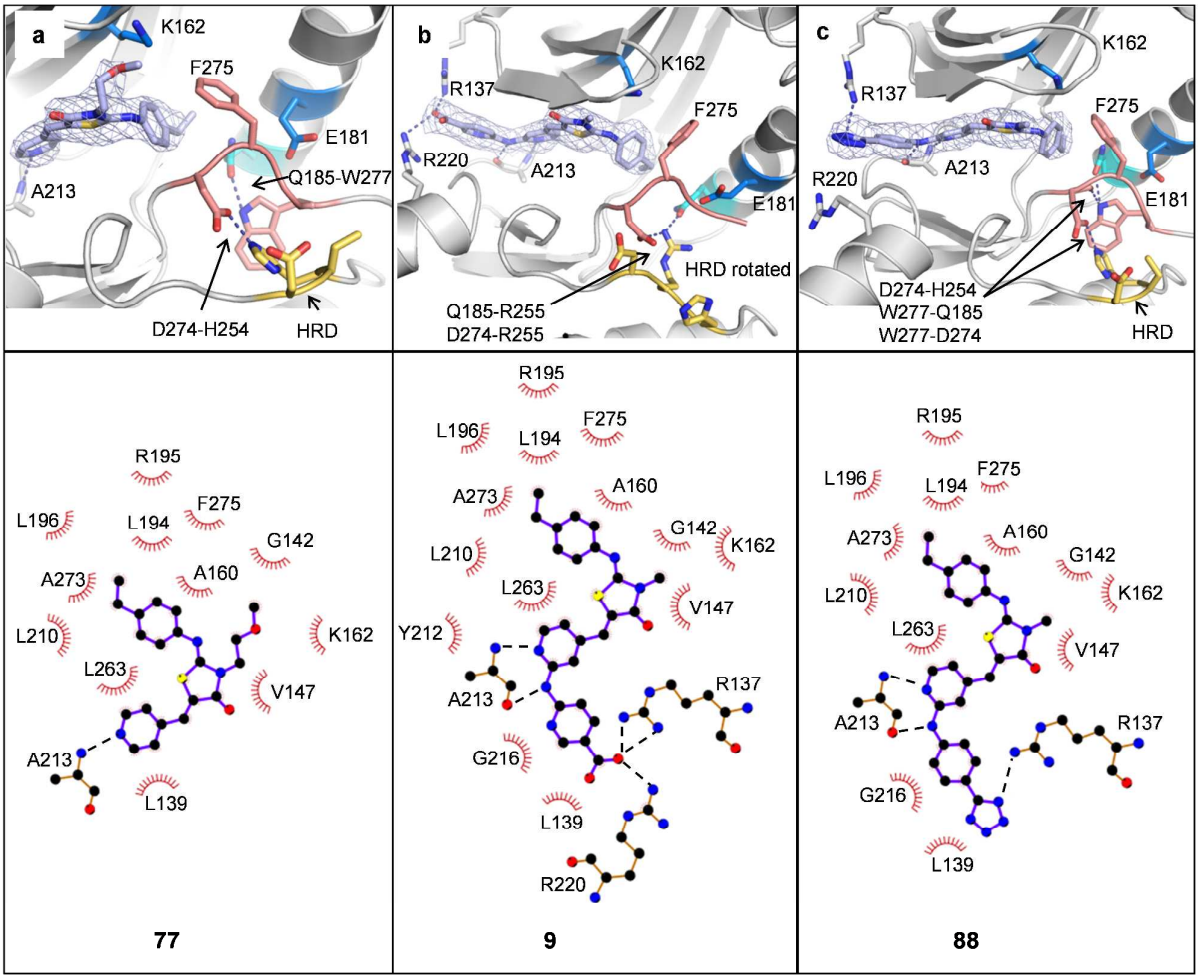

Figure 5. Crystal structures of the 4-thiazolidinone derivatives bound to Aurora A. The $2F_o$-F_c electron density map contoured at 1 sigma around the compounds is shown to highlight their unambiguous position in the pocket. Lys162 and Glu181 (blue), DFG motif (pink) and HRD motif (yellow). The catalytic pocket of Aurora A acquires an inactive conformation upon binding to **77** (**a**), **9** (**b**) and **88** (**c**). The lower panels show schematic representations of the interactions between the compounds and the protein. Dashed lines indicate hydrogen bonds, in particular interactions between the aminopyridine portion of the inhibitors and the hinge region (A213) and between the anionic carboxyl or tetrazole group and the guanidinium groups of R137 and R220. Residues involved in hydrophobic interactions are highlighted with a red arc.

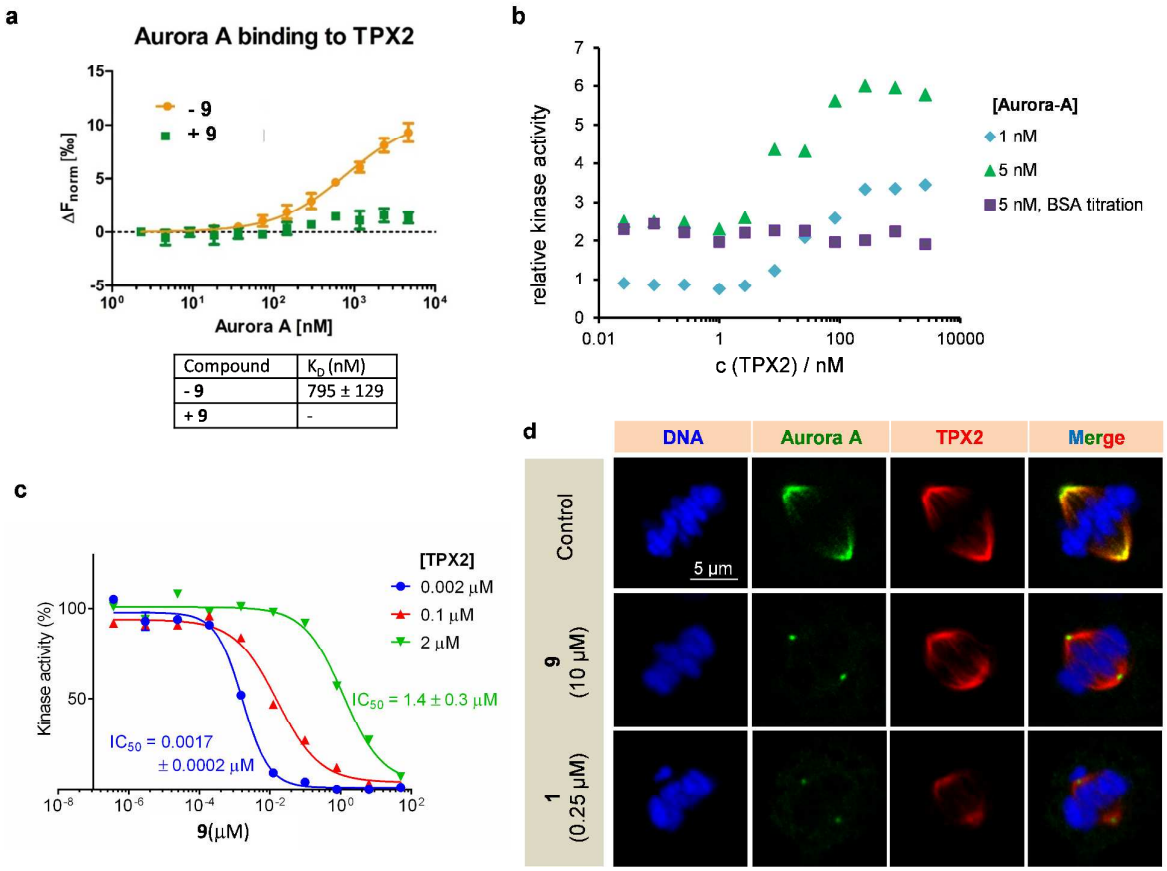

Figure 6. Binding of Aurora A to **9** excludes TPX2. **(a)** Microscale thermophoresis (MST) analysis of TPX2 binding to Aurora A kinase in presence and absence of compound **9**. Three independent measurements were performed; error bars represent the standard deviation (SD). **(b)** Aurora A kinase activity in the presence of TPX2 or control protein BSA. **(c)** IC_{50} curves for **9** in the presence of different TPX2 concentrations. **(d) 9** impairs localization of Aurora A at the mitotic spindle. Representative images of HeLa Kyoto cells treated with compound **9** overnight and stained for DNA (blue), Aurora A (green) and TPX2 (red). TPX2 co-localizes with Aurora A in control cells (top row). **9** impairs Aurora A localization at the spindle microtubules but does not affect centrosomal Aurora A. Aurora A is also present at centrosomes but not on spindle microtubules in cells treated with **1** (MLN8237).

Compound 9 selectively inhibits Aurora A in cells

We next set out to test the impact of **9** on mitotic progression of human tissue culture cells. Treatment of HeLa cells with **9** resulted in a dose-dependent increase in the mitotic index, as observed also with the reference inhibitor **1** and as expected from the role of Aurora A for timely progression through mitosis (Figure 7a).[24] Inhibitor **9** also decreased phosphorylation of Aurora A Thr288, an autophosphorylation site that marks Aurora A kinase activity (IC_{50} = 760 nM, Figure 7b).[73] Furthermore, **9** induced defective chromosome alignment during metaphase, with a phenotypic EC_{50} value of 6 μM, in line with the requirement of Aurora A activity for proper spindle dynamics (Figure 7c/d).[18, 24, 74]

Many Aurora A kinase inhibitors also target Aurora B in the cellular context. To address whether this may be the case also for **9**, we examined the distribution of phospho-Histone H3 Ser10, a histone modification that is imparted during early mitosis by Aurora B.[75] We found that this feature remained unchanged in cells treated with **9**, whereas it was absent in cells treated with the Aurora B inhibitor ZM447439 (**94**) (Figure 7f/g).[76] Furthermore the massive accumulation of cells with 8N and 16N DNA contents observed by flow cytometry upon treatment with **94**, which is a hallmark of defective cytokinesis following Aurora B inactivation, also did not occur with **9** even when provided at 10 μM (Figure 7h).[76] We conclude that in contrast to other Aurora A inhibitors, including the reference inhibitor **1**,[23, 77] our inhibitor **9** had no effect on Aurora B activity in cells.

To unequivocally test whether the effect of **9** on human cells was specific to Aurora A inhibition we performed phenotypic rescue experiments using cells expressing GFP-Aurora A-Arg137Ala or GFP-Aurora A-Trp277Ala mutants, which were predicted by examination of the crystal structure to be insensitive to **9**. As shown in Figure 7e, we found that these proteins were insensitive to the addition of **9**, demonstrating that the phenotype normally induced by this compound was indeed caused by Aurora A inhibition.[65, 67]

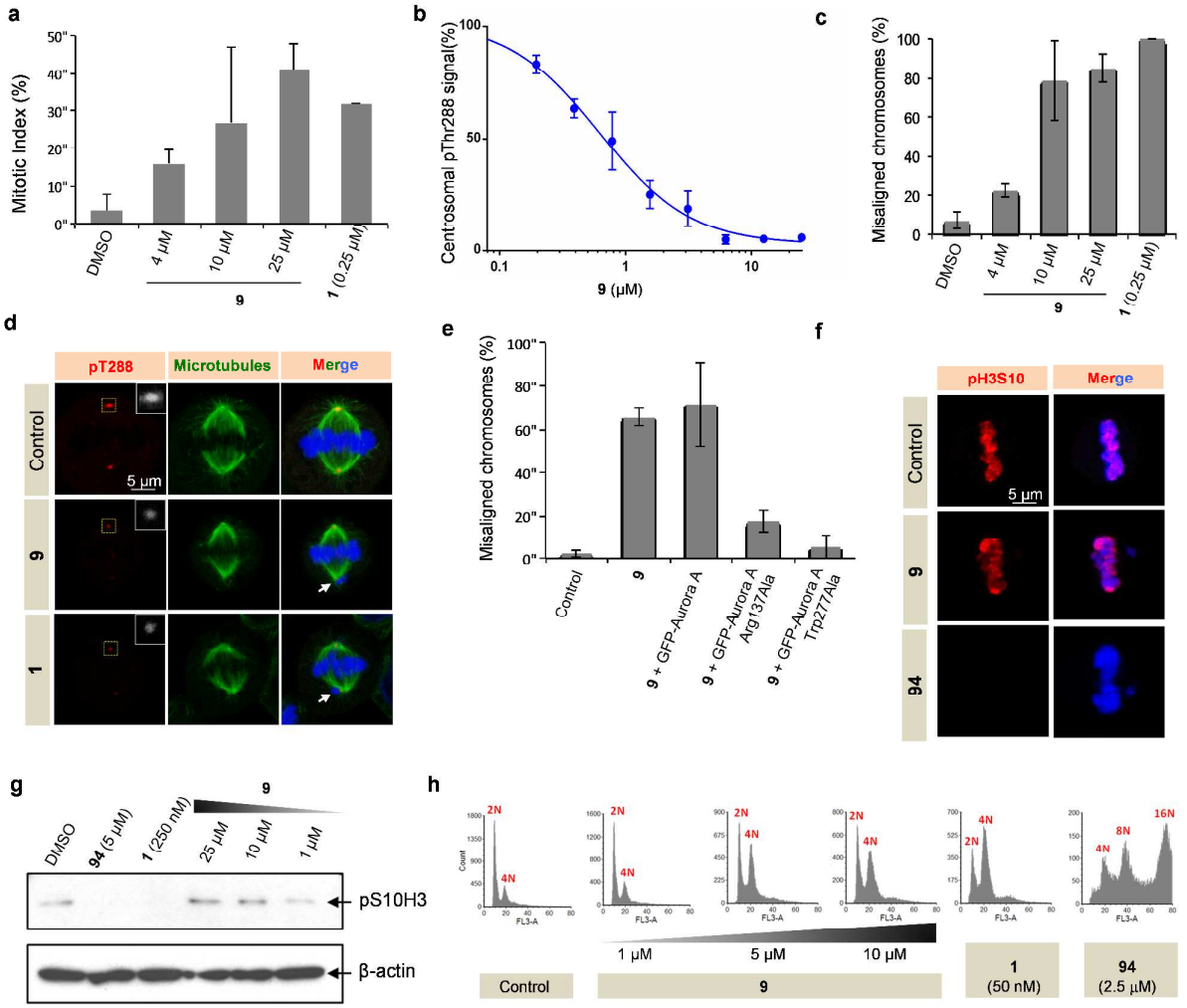

Figure 7. Inhibitor **9** yields an Aurora A specific inhibition phenotype in cells without impairing Aurora B function. **(a)** Mitotic index of HeLa Kyoto cells after overnight incubation with indicated compounds. The experiment was repeated twice and error bars represent SD. **(b)** Centrosomal pThr288 Aurora A levels in HeLa Kyoto cells after overnight incubation with indicated concentrations of **9**. More than 10 cells were analyzed in every condition. The experiment was repeated twice and the error bars represent SD. **(c)** Chromosome misalignment phenotype of HeLa Kyoto cells incubated with indicated compounds. The experiment was repeated twice and error bars represent SD. **(d)** Representative images of HeLa Kyoto cells after overnight incubation with indicated compounds. The cells were stained for pThr288 Aurora A (red), α-tubulin (green), and DNA (blue). Impaired alignment of chromosomes on the metaphase plate is indicated by white arrows. **(e)** Chromosome misalignment phenotype of HeLa Kyoto cells. The cells were transfected

with the indicated GFP-Aurora A constructs before incubation with **9** overnight. The bars represent mean phenotype ± SD of two independent experiments. At least 100 cells were analyzed in every condition. Note that cells expressing the highest amount of GFP-Aurora A, GFP-Aurora A Arg137Ala and GFP-Aurora A Trp277Ala were considered for the analysis; cells expressing lower levels of the mutant transgenes exhibited less or no rescue (data not shown). **(f)** Representative images of HeLa Kyoto cells after overnight incubation with indicated compounds and staining for pHis-H3 (red) and DNA (blue). **(g)** Western blot of lysates from cells synchronized in prometaphase with 100 nM nocodazole and treated with the indicated inhibitors. β-actin was used as loading control. **(h)** DNA content analysis of cells treated for 48 h with the indicated compounds. The cells were stained with propidium iodide and analyzed using flow cytometry.

Compound 9 shows moderate reactivity with glutathione

Despite of its high selectivity towards Aurora A the cellular activity of **9** (EC_{50} > 1 μM) was much weaker than its biochemical activity (IC_{50} = 2 nM). To understand whether this lower activity might be caused by covalent reaction of the electrophilic double bond of **9** we measured its reactivity towards the intracellular nucleophile glutathione (GSH) under physiological conditions. Conversion to a GSH adduct was indeed detected, however only to a limited extent (50 % conversion after 24 h with 5 mM GSH, pH 7.4, 37°C, Figure 8), suggesting that a significant portion of the inhibitor remained unreacted within the cell and was available for inhibition of Aurora A. Nevertheless analogs of **9** lacking the electrophilic double bond were prepared as described above (Scheme 4) and investigated as alternatives. Diastereomeric cyclopropanes *rac*-**89**/*rac*-**90** were more than 400-fold less active than their precursor **79**. On the other hand its reduced double bond analog *rac*-**91** was only 7-fold less active, and the reduced double bond analog of **9**, *rac*-**92**, was also still quite potent (IC_{50} = 24 nM). However this derivative did not show any activity in cells despite the fact that it cannot form GSH adducts.

Taken together, these data suggest that GSH reactivity is insufficient to explain the discrepancy between the IC_{50} values of cellular versus biochemical activity of **9** on Aurora A and B presented above (Aurora A: biochemical IC_{50} = 2.0 nM, cellular IC_{50} (pT288) = 760 nM, Aurora B/INCENP: biochemical IC_{50} = 149 nM, cellular IC_{50} (pH3) > 25 μM). This activity difference is probably a consequence of the higher ATP concentration in cells (1 mM) compared to *in vitro* assays (20 μM) and the presence of competing ligands such as TPX2 (Figure 6d), as well as the presence of a carboxylate group which might reduce cellular uptake. The same effects probably explain the weaker cellular versus biochemical activities reported for inhibitor **1** (Aurora A: biochemical IC_{50} = 0.04 nM, cellular IC_{50} (pT288) = 6.7 nM, Aurora B/INCENP: biochemical IC_{50} = 1.1 nM, cellular IC_{50} (pH3) = 1.5 μM), as well as for MK-5108, a further selective Aurora A inhibitor (Aurora A: biochemical IC_{50} = 0.064 nM, cellular IC_{50} (pT288) = 300 nM, Aurora B/INCENP: biochemical IC_{50} = 1.49 nM, cellular IC_{50} (pH3) > 10 μM).[22, 23, 78]

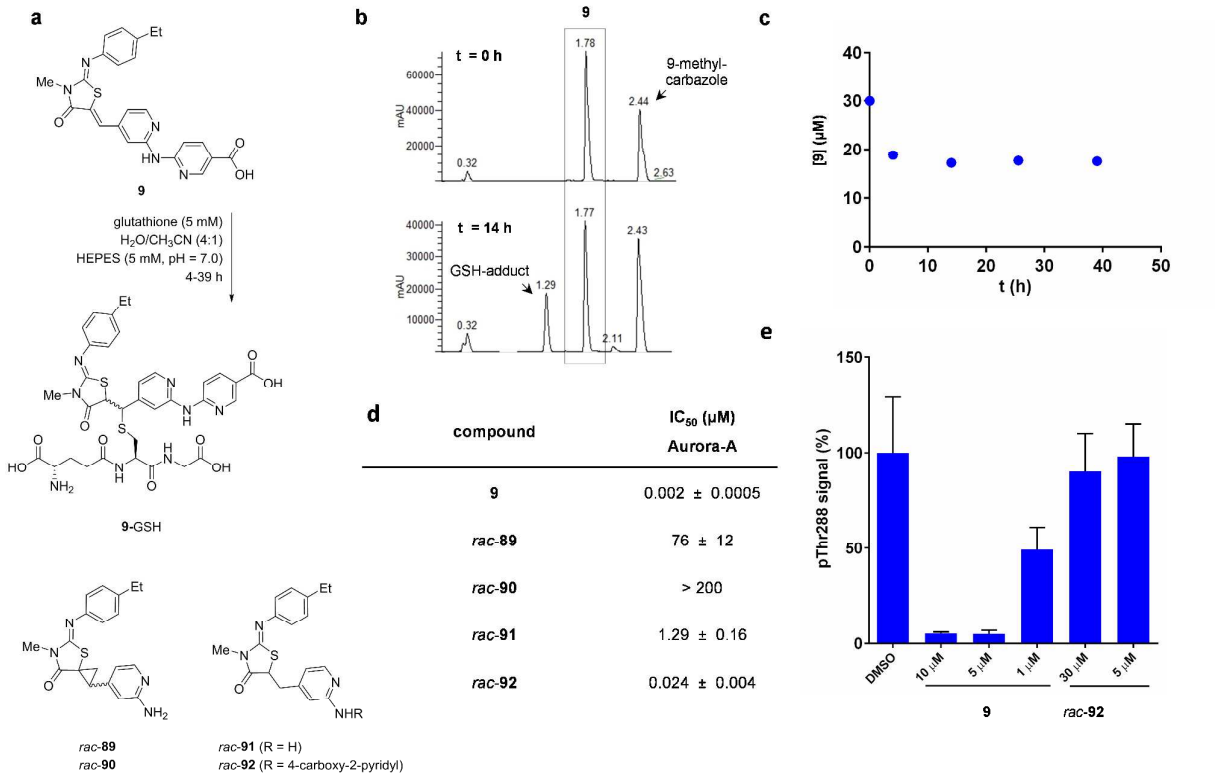

Figure 8. In vitro reactivity of **9** towards glutathione (GSH). Inhibitor **9** (30 μM) was incubated with GSH (5 mM) in H_2O/CH_3CN (4:1) at pH = 7.0, and the reaction was followed by LC-MS. **a.** Reaction scheme and structures of modified analogs. **b.** LC chromatogram of the reaction mixture after t = 0 h and t = 14 h. The product formed with a retention time t_{ret} = 1.29 min is identified by MS as the GSH-adduct of **9**. 9-methylcarbazole (t_{ret} = 2.44 min) was used as internal control. **c.** Concentration of compound **9** during the course of the reaction as determined by integration of the absorption peaks (at 310 nm) of compound **9** at t_{ret} = 1.78 min.The average of two independent experiments is shown, SD is < 5 % for all data points. **d.** Aurora A inhibition in the HTRF biochemical assay. **e.** Cellular pThr288 Aurora A levels of cells incubated with **9** or *rac*-**92** overnight at the indicated concentrations. The experiment was repeated twice and the error bars represent SD. Derivative *rac*-**92** does not reduce pThr288 levels in cells, although having an IC_{50} of 24 nM in the biochemical assay. Numbers represent average IC_{50} ± SD of two independent experiments.

Conclusion

To identify new inhibitors of Aurora A kinase we performed scaffold hopping LBVS using our recently reported method xLOS, a 3D shape and pharmacophore similarity algorithm, and assembled a kinase discovery set with very low compound and scaffold overlap with known kinase inhibitors and screening compounds. We then performed biochemical activity screening against Aurora A and optimization for two screening hits, benzimidazole **5** and thiazolidinone **7**. While benzimidazole **5** did not yield potent inhibitors, we successfully optimized thiazolidinone **7** by elaboration of the hinge-binding motif using structure-based drug design and discovered the potent inhibitor **9** with IC_{50} = 2 nM. This type II inhibitor locks the kinase in an inactive conformation and competes with the activator protein TPX2. Inhibitor **9** shows strong binding selectivity for Aurora kinases against the entire kinome, displays a highly specific Aurora A inhibition phenotype without Aurora B specific effects.

Experimental Section

Virtual screening. Virtual screening was performed using xLOS, an in-house developed 3D-ligand based virtual screening method. Two rounds of virtual screening were performed. In the first round, the ZINC database containing ~12M commercial compounds[39] was screened using each of the 16 known inhibitors of Aurora A and other kinases as seed molecule. For each seed (one stereoisomer) and database (all possible stereoisomers), a single lowest energy 3D-model was generated using CORINA program available from Molecular Networks Pvt. Ltd. These 3D-models were used by xLOS to calculate the xLOS similarity score between seed and database molecule as described previously.[33] For database molecules only best scoring stereoisomer was retained in the list. The search was limited to catalogs from Princeton Molecular Research Inc. (~800,000 cpds) and Otava Chemicals (~300,000 cpds). For each of the 16 reference molecules the top 1000 scoring

compounds were selected. The resulting 16,000 compounds were further analyzed by clustering and visual analysis to select structurally diverse compounds. In the second round 15 hits identified in first round of virtual screening were used in the same manner.

Scaffold analysis. The Kinase ChEMBL was downloaded from the ChEMBL database website (https://www.ebi.ac.uk/chembl/). The screening commercial set was created by combining commercially available screening compounds for kinases from three different vendors namely ChemBridge (http://www.chembridge.com/), Life Chemicals (http://www.lifechemicals.com/) and Otava (http://www.otavachemicals.com/). The Kinase 50 nM and Aurora 50 nM sets were created by selecting the compounds from ChEMBL database with reported IC_{50} of ≤50 nM against any kinases and Aurora kinase targets respectively. Molecules were processed using in-house written java program utilizing Java Chemistry library (JChem) from ChemAxon, Pvt. Ltd as starting point. Molecules were checked for valence error, counter ions were removed and ionization states were adjusted to pH 7.4. Molecules were stored in non-stereo smiles format and duplicate molecules were removed from each database. Within each database, each molecule was converted to Bemis-Murcko Scaffold (BMS) using the StructuralFrameworksPlugin available in the JChem library from ChemAxon Pvt. Ltd. For each database, the list of unique BMS was generated, followed by calculation of the number of compounds represented by each BMS. For the shared scaffold analysis the unique SMILES of scaffolds were used for comparing molecules.

Chemistry. All reagents were purchased from commercial sources and were used without further purification. Flash chromatography purifications were performed with silica Gel 60 (Fluka, 0.040–0.063 nm, 230–400 mesh ASTM). Low resolution mass spectra were obtained by electron spray ionization (ESI-MS) in the positive mode on a Thermo Scientific LCQ Fleet. High resolution mass spectra were obtained by electron spray ionization (HR-ESI-MS) in the positive mode recorded on a Thermo Scientific LTQ Orbitrap XL. ^{1}H and ^{13}C-NMR spectra were measured on a Bruker Avance 300 spectrometer (at 300 MHz and 75 MHz, respectively) or on a Bruker AVANCE II 400 spectrometer (at 400 MHz and 101 MHz, respectively). ^{1}H and ^{13}C chemical shifts are quoted

relative to solvent signals, and resonance multiplicities are reported as s (singlet), d (doublet), t (triplet), q (quartet), p (pentet), and m (multiplet); br = broad peak. Compound purities were assessed by analytical reversed phase HPLC (RP-HPLC) at a detection wavelength of 254 nm or 310 nm. The purity of tested compounds was > 95 %, unless otherwise stated (Supplementary Table 2). Analytical RP-HPLC was performed on a Dionex Ultimate 3000 RSLC System (DAD-3000 RS Photodiode Array Detector) using a Dionex Acclaim RSLC 120 column (C18, 3.0 x 50 mm, particle size 2.2 µm, 120 Å pore size) and a flow rate of 1.2 mL min^{-1}. Data were recorded and processed with Dionex Chromeleon Management System (version 6.8) and Xcalibur (version 2.2, Thermo Scientific). Eluents for analytical RP-HPLC were as follows: (A) milliQ-deionized water containing 0.05 % TFA, and (D) HPLC-grade acetonitrile/milliQ-deionized water (9:1) containing 0.05 % TFA. Conditions for analytical RP-HPLC were as follows: From A/D (7:3) to 100 % D (2.2 min) followed by 100 % D (1 min). Preparative RP-HPLC was performed with a Waters Prep LC4000 Chromatography System using a Reprospher 100 column (Dr. Maisch GmbH, C18-DE, 100 x 30 mm, particle size 5 µM, pore size 100 Å) and a Waters 489 Tunable Absorbance Detector operating at 214 nm. Eluents for preparative RP-HPLC were as follow: (A) milliQ-deionized water containing 0.1 % TFA, and (D) HPLC-grade acetonitrile/milliQ-deionized water (9:1) containing 0.1 % TFA.

1'*H*-[1,2'-bibenzo[*d*]imidazol]-2(3*H*)-one (5). A solution of compound **25** (150 mg, 0.463 mmol, 1 eq.) and K_2CO_3 (194 mg, 1.39 mmol, 3 eq.) in DMF (4 mL) was stirred at 110 °C for 14 h. DMF was evaporated *in vacuo*, and EtOAc (20 mL) and brine (20 mL) were added. The organic phase was separated and washed with H_2O (3 x 20 mL). EtOAc was removed *in vacuo*. The crude was purified by FC (SiO_2; hexane/EtOAc 1:2) to afford **5** as gray powder (46 mg, 0.19 mmol, 40 %). m.p. > 300°C (dec.). ^{1}H NMR (300 MHz, DMSO-d_6) δ 11.69 (s, 1H), 8.59 – 8.18 (m, 1H), 7.87 – 7.44 (m, 2H), 7.50 – 7.08 (m, 5H); ^{13}C NMR (75 MHz, DMSO-d_6) δ 152.42, 143.91, 128.56, 127.02, 123.41, 121.68, 121.61, 113.41, 109.45; HR-ESI-MS (*m/z*): calculated for $[M + H]^+$ $C_{14}H_{11}ON_4$ 251.0927, found 251.0923.

1-(1*H*-Benzo[*d*]imidazol-2-yl)-5-hydroxy-1*H*-benzo[*d*]imidazol-2(3*H*)-one (6). Purification of compound **40** by HPLC (Reprospher C_{18}; 10-60 % D/A) gave as a second fraction **6** (19 mg, 0.071 mmol, 70 %) as a white solid. m.p. 297.4-299.8 °C (dec.); ^{1}H-NMR (DMSO-d_6, 300 MHz): δ 11.47 (s, 1H), 9.41 (s, 1H), 8.17 (d, J = 8.6 Hz, 1H), 7.59 (dd, J = 5.9, 3.2 Hz, 2H), 7.17 (dd, J = 6.0, 3.2 Hz, 2H), 6.61 (dd, J = 8.6, 2.3 Hz, 1H), 6.57 (d, J = 2.2 Hz, 1H); ^{13}C-NMR (DMSO-d_6, 75 MHz): δ 154.17, 152.65, 144.10, 129.51, 121.60, 119.57, 114.26, 108.40, 97.02; HR-ESI-MS (*m/z*): calculated for $[M + H]^+$ $C_{14}H_{11}O_2N_4$ 267.0877, found 267.0872.

(2*Z*,5*Z*)-2-((3,4-dimethylphenyl)imino)-3-methyl-5-(pyridin-4-ylmethylene)thiazolidin-4-one (7). This compound was purchased from Princeton Biomolecular (no. OSSK_393940). ^{1}H NMR (300 MHz, $CDCl_3$) δ 8.57 (d, J = 4.0 Hz, 2H), 7.55 (d, J = 1.5 Hz, 1H), 7.23 (d, J = 4.4 Hz, 2H), 7.07 (d, J = 7.8 Hz, 1H), 6.72 – 6.66 (m, 2H), 3.39 (s, 3H), 2.21 (s, 6H); ^{13}C NMR (75 MHz, $CDCl_3$) δ 166.18, 150.13, 149.07, 145.49, 141.33, 137.91, 133.64, 130.54, 127.68, 126.85, 123.42, 122.32, 118.04, 29.99, 19.99, 19.37; HR-ESI-MS (*m/z*): 324.1175, calcd for $[M + H]^+$ $C_{18}H_{18}ON_3S$: 324.1165.

(2*Z*,5*Z*)-2-((4-ethylphenyl)imino)-3-methyl-5-(pyridin-4-ylmethylene)thiazolidin-4-one (8). This compound was initially purchased, and later resynthesized as follows: a solution of **54** (702 mg, 3.00 mmol, 1.0 eq.) and piperidine (0.65 mL, 6.6 mmol, 2.2 eq.) in EtOH (5 mL) was treated with 4-pyridinecarboxaldehyde (0.56 mL, 6.0 mmol, 2.0 eq.) and heated to 78 °C. After 12 h, the reaction mixture was cooled to 0 °C, filtered, and the filter residue washed with ice-cold EtOH (3 x 5 mL). The yellow solid was further purified by FC (SiO_2; hexane/EtOAc 2:1) to afford the **8** as yellow solid (203 mg, 0.627 mmol, 20.9 %). m.p. 167.3-168.0°C. ^{1}H NMR (300 MHz, $CDCl_3$) δ 8.58 – 8.56 (m, 2H), 7.55 (d, J = 1.5 Hz, 1H), 7.24 – 7.14 (m, 4H), 6.86 (d, J = 8.2 Hz, 2H), 3.39 (s, 3H), 2.61 (q, J = 7.6 Hz, 2H), 1.20 (t, J = 7.6 Hz, 3H); ^{13}C NMR (75 MHz, $CDCl_3$) δ 166.15, 150.30, 150.25, 149.15, 145.27, 141.29, 128.88, 127.00, 123.35, 120.94, 29.99, 28.39, 15.52; ESI-MS (*m/z*): 324.12.

6-((4-((*Z*)-((*Z*)-2-((4-ethylphenyl)imino)-3-methyl-4-oxothiazolidin-5-ylidene)methyl)pyridin-2-yl)amino)nicotinic acid (9). Degassed dioxane (1.2 mL) was added to a flask containing amine **79** (100 mg, 0.296 mmol, 1.0 eq.), $Pd_2(dba)_3$ (5.1 mg, 0.0088 mmol, 0.03 eq.), Xantphos (10 mg, 0.018 mmol, 0.06 eq.), Cs_2CO_3 (116 mg, 0.355 mmol, 1.2 eq.), and 6-bromonicotinic acid (65.9 mg, 0.326 mmol, 1.1 eq.) under argon. The suspension was degassed and refilled with argon (5 x) and then heated to 100 °C. The reaction mixture was stirred overnight at 100 °C, then cooled to room temperature, filtered, and concentrated *in vacuo*. The crude was purified by RP-HPLC (A/D 70:30 to A/D 45:55, 40 min gradient) to afford **9** as yellow solid after lyophylization (38 mg, 0.083 mmol, 28 %). ^{1}H NMR (400 MHz, DMSO-d_6) δ 10.71 (s, 1H), 8.70 (d, J = 2.3 Hz, 1H), 8.37 – 8.36 (m, 1H), 8.16 – 8.15 (m, 2H), 7.67 (s, 1H), 7.47 (d, J = 8.8 Hz, 1H), 7.32 (d, J = 8.3 Hz, 2H), 7.19 (dd, J = 5.4, 1.7 Hz, 1H), 7.00 (d, J = 8.2 Hz, 2H), 3.36 (s, 3H), 2.61 (q, J = 7.6 Hz, 2H), 1.17 (t, J = 7.6 Hz, 3H); ^{13}C NMR (101 MHz, DMSO-d_6) δ 166.07, 165.47, 156.34, 153.46, 149.42, 148.97, 147.38, 145.14, 142.61, 140.51, 138.74, 128.78, 127.07, 126.83, 120.82, 118.02, 111.55, 110.76, 29.73, 27.53, 15.48; HR-ESI-MS (*m/z*): 460.1435, calcd for $[M + H]^+$ $C_{24}H_{22}O_3N_5S$: 460.1438.

1,3-dihydro-2*H*-benzo[*d*]imidazol-2-one (13). A solution of 1,2-diaminobenzene (10.0 g, 92.5 mmol) in DMF (93 mL) was treated with *N*,*N*'-carbonyldiimidazole (30.2 g, 186 mmol) and stirred at room temperature for 18 h. After removal of the DMF *in vacuo*, the resulting white solid was washed with H_2O (4 x 50 mL) and dried on high vacuum to give **13** (12.4 g, 99 %) as a white solid. m.p. > 300 °C (dec.); ^{1}H NMR (DMSO-d_6, 300 MHz): δ 10.57 (s, 1H), 6.91 (s, 2H); ^{13}C NMR (DMSO-d_6, 75 MHz): δ 155.29, 129.68, 120.41, 108.49; HR-ESI-MS (*m/z*): calculated for $[M + H]^+$ $C_7H_7ON_2$ 135.0553, found 135.0550.

4-Methyl-1*H*-benzo[*d*]imidazol-2(3*H*)-one (14). A solution of 2,3-diaminotoluene (3.50 g, 28.7 mmol) in DMF (28.7 mL) was treated with *N*,*N*'-carbonyldiimidazole (4.65 g, 28.7 mmol) and the solution was stirred at room temperature for 15 h. After addition of H_2O (100 mL), the reaction mixture was extracted with EtOAc (3 x 200 mL) and the combined organic phases were dried over $MgSO_4$ and concentrated to give **14** (4.24 g, 28.6 mmol, quant.) as a brown solid. m.p. 218.6-220.4

°C; ^{1}H NMR (DMSO-d_6, 300 MHz): δ 10.73 (s, 1H), 10.60 (s, 1H), 6.85 – 6.78 (m, 1H), 6.77 – 6.70 (m, 2H), 2.25 (s, 3H); ^{13}C-NMR (DMSO-d_6, 75 MHz): δ 155.68, 129.35, 128.67, 121.70, 120.48, 118.29, 106.21, 16.25; HR-ESI-MS (*m/z*): calculated for $[M + H]^+$ $C_8H_8ON_2Na$ 171.0529, found 171.0527.

5-Methyl-1*H*-benzo[*d*]imidazol-2(3*H*)-one (15). Following the procedure for **14**, conversion of 3,4-diaminotoluene (1.70 g, 13.9 mmol) gave **15** as light gray solid (2.04 g, 13.8 mmol, 99 %) after filtration and washing with H_2O (4 x 30 mL). m.p. 277.2-279.2 °C; ^{1}H NMR (DMSO-d_6, 300 MHz): δ 10.46 (d, J = 10.9 Hz, 2H), 6.77 (s, 1H), 6.73 (s, 2H), 2.27 (s, 3H); ^{13}C NMR (DMSO-d_6, 75 MHz): δ 155.41, 129.84, 129.33, 127.43, 120.86, 108.99, 108.14, 21.01; HR-ESI-MS (*m/z*): calculated for $[M + H]^+$ $C_8H_9N_2O$ 149.0709, found 149.0704.

5-Bromo-1*H*-benzo[*d*]imidazol-2(3*H*)-one (16). Following the procedure for **14,** conversion of 3,4-diaminobromobenzene (2.50 g, 13.4 mmol) gave **16** as brown solid (2.83 g, 13.3 mmol, quant.) after filtration and washing with H_2O (5 x 70 mL). m.p. > 300 °C (dec.); ^{1}H NMR (DMSO-d_6, 300 MHz): δ 10.76 (s, 2H), 7.08 – 7.03 (m, J = 10.2 Hz, 2H), 6.86 (d, J = 8.0 Hz, 1H); ^{13}C NMR (DMSO-d_6, 75 MHz): δ 155.07, 131.23, 129.01, 122.92, 112.02, 111.05, 110.09; HR-ESI-MS (*m/z*): calculated for $[M + H]^+$ $C_7H_6ON_2Br$ 212.9658, found 212.9662.

5-(Trifluoromethyl)-1*H*-benzo[*d*]imidazol-2(3*H*)-one (17). Following the procedure for **14**, conversion of 3,4-diaminotrifluoromethylbenzene (2.50 g, 14.2 mmol) gave **17** as brown solid (2.06 g, 10.2 mmol, 73 %) after filtration and washing with H_2O (5 x 20 mL). m.p. 280.1-282.0 °C; ^{1}H NMR (DMSO-d_6, 300 MHz): δ 11.06 (s, 1H), 10.96 (s, 1H), 7.29 (m, 1H), 7.16 (s, 1H), 7.09 (d, J = 8.2 Hz, 1H); ^{13}C NMR (DMSO-d_6, 75 MHz): δ 155.35, 132.87, 129.86, 121.27, 120.85, 117.87, 108.56, 104.93; HR-ESI-MS (*m/z*): calculated for $[M + H]^+$ $C_8H_6ON_2F_3$ 203.0427, found 203.0423.

5,6-Dichloro-1*H*-benzo[*d*[imidazol-2(3*H*)-one (18). Following the procedure for **14**, conversion of 4,5-diamino-1,2-dichlorobenzene (2.50 g, 14.2 mmol) gave **18** as brown solid (2.67 g, 13.2 mmol, 95 %) after filtration and washing with H_2O (5 x 20 mL). m.p. > 300 °C (dec.); ^{1}H NMR (DMSO-

d_6, 300 MHz): δ 10.91 (s, 2H), 7.10 (s, 2H); ^{13}C NMR (DMSO-d_6, 75 MHz): δ 155.18, 129.85, 122.36, 109.75; HR-ESI-MS (*m/z*): calculated for $[M + H]^+$ $C_7H_5ON_2Cl_2$ 202.9773, found 202.9770.

2-chloro-1*H*-benzo[*d*]imidazole (19). A solution of **13** (4.31 g, 32.1 mmol) in $POCl_3$ (30 mL) was refluxed at 100 °C for 15 h. The reaction mixture was slowly poured into icecold H_2O (150 mL) and the pH was adjusted to pH = 7 using NaOH (6 M). The yellowish solid was filtered and washed with H_2O (3 x 50 mL) to give **19** (4.42 g, 91 %) as a yellowish solid. m.p. 192.1-193.5 °C; ^{1}H NMR (DMSO-d_6, 300 MHz): δ 13.22 (s, 1H), 7.51 (m, 2H), 7.21 (m, 2H); ^{13}C NMR (DMSO-d_6, 75 MHz): δ 150.90, 129.08, 126.59, 124.40, 121.68, 112.15, 109.69; HR-ESI-MS (*m/z*): calculated for $[M + H]^+$ $C_7H_6N_2Cl$ 153.0214, found 153.0214.

2-Chloro-4-methyl-1*H*-benzo[*d*]imidazole (20). A solution of **14** (3.50 g, 23.6 mmol) in $POCl_3$ (22.0 mL) was refluxed at 100 °C; for 16 h. H_2O was slowly added to the reaction mixture and then poured into icecold H_2O (100 mL) and the pH was adjusted to pH = 7 using NaOH (5M) to precipitate a white solid. The white suspension was extracted with EtOAc (3 x 100 mL), dried over $MgSO_4$ and concentrated to give a white crude product. Purification by flash chromatography (SiO_2; 10-40 % EtOAc/hexane) gave **20** (1.00 g, 6.02 mmol, 26 %) as a white solid. m.p. 138.2-140.9 °C; ^{1}H NMR (DMSO-d_6, 300 MHz): δ 13.18 (s, 1H), 7.31 (dd, J = 38.8, 7.1 Hz, 1H), 7.10 (t, J = 6.8 Hz, 1H), 7.00 (d, J = 7.3 Hz, 1H), 2.47 (s, 3H); ^{13}C NMR (DMSO-d_6, 75 MHz): mixture of two isomers δ 142.08, 141.71, 138.33, 137.68, 134.39, 134.20, 127.89, 123.33, 122.78, 122.17, 121.97, 120.98, 115.68, 108.42, 16.65, 16.33; HR-ESI-MS (*m/z*): calculated for $[M + H]^+$ $C_8H_8N_2Cl$ 167.0371, found 167.0367.

2-Chloro-5-methyl-1*H*-benzo[*d*]imidazole (21). Following the procedure for **20**, conversion of **15** (1.00 g, 6.75 mmol) gave **21** as brown solid (530 mg, 3.19 mmol, 48 %) after extraction with EtOAc (3 x 50 mL). m.p. 161.7-162.8 °C; ^{1}H NMR (DMSO-d_6, 300 MHz): δ 13.04 (s, 1H), 7.53 – 7.13 (m, 2H), 7.03 (m, 1H), 2.39 (s, 3H); ^{13}C NMR (DMSO-d_6, 75 MHz): δ 155.44, 137.98, 135.53,

130.07, 123.66, 120.85, 117.29, 21.15; HR-ESI-MS (*m/z*): calculated for $[M + H]^+$ $C_8H_8N_2Cl$ 167.0371, found 167.0367.

5-Bromo-2-chloro-1*H*benzo[*d*]imidazole (22). Following the procedure for **20**, conversion of **16** (2.50 g, 11.8 mmol) gave **22** as brown solid (2.40 g, 10.4 mmol, 89 %) after extraction with EtOAc (3 x 100 mL). m.p. 198.0-199.2 °C; ^{1}H NMR (DMSO-d_6, 300 MHz): δ 13.46 (s, 1H), 7.75 (d, J = 1.5 Hz, 1H), 7.50 (d, J = 8.5 Hz, 1H), 7.39 (dd, J = 8.6, 1.9 Hz, 1H); ^{13}C NMR (DMSO-d_6, 75 MHz): δ 152.14, 139.90, 135.70, 130.29, 125.35, 117.33, 114.69; HR-ESI-MS (*m/z*): calculated for $[M + H]^+$ $C_7H_5N_2BrCl$ 230.9319, found 230.9315.

2-Chloro-5-(trifluoromethyl)-1*H*-benzo[*d*]imidazole (23). Following the procedure for **20**, conversion of **17** (1.50 g, 7.42 mmol) gave **23** as light brown solid (1.11 g, 5.05 mmol, 72 %) after filtration and washing with H_2O (5 x 50 mL). m.p. 184.7-185.9 °C; ^{1}H NMR (DMSO-d_6, 300 MHz): δ 13.76 (s, 1H), 7.89 (s, 1H), 7.71 (d, J = 8.4 Hz, 1H), 7.55 (dd, J = 8.5, 1.3 Hz, 1H); ^{13}C NMR (DMSO-d_6, 75 MHz): δ 141.51, 130.16, 126.56, 123.34, 122.96, 119.35, 119.29, 119.25; HR-ESI-MS (*m/z*): calculated for $[M + H]^+$ $C_8H_5N_2ClF_3$ 221.0088, found 221.0083.

2,5,6-Trichloro-1*H*-benzo[*d*]imidazole (24). Following the procedure for **20**, conversion of **18** (2.50 g, 12.4 mmol) gave **24** as brown solid (1.99 g, 9.00 mmol, 73 %) after extraction with EtOAc (3 x 100 mL). m.p. 218.1-219.9 °C; ^{1}H NMR (DMSO-d_6, 300 MHz): δ 13.65 (s, 1H), 7.82 (s, 2H); ^{13}C NMR (DMSO-d_6, 75 MHz): δ 141.92, 138.36, 124.76, 116.11; HR-ESI-MS (*m/z*): calculated for $[M + H]^+$ $C_7H_4N_2Cl_3$ 220.9435, found 220.9437.

***Tert*-butyl (2-((1*H*-benzo[*d*]imidazol-2-yl)amino)phenyl)carbamate (25).** A solution of **19** (350 mg, 2.29 mmol, 1.0 eq.), *tert*-butyl (2-aminophenyl)carbamate (477 mg, 2.29 mmol, 1.0 eq.), and KH_2PO_4 (312 mg, 2.29 mmol, 1.0 eq.) in *n*-BuOH (5 mL) was heated to 90 °C and stirred for 12 h. The reaction mixture was cooled to RT, EtOAc (20 mL) and H_2O (20 mL) were added, and the organic layer was extracted with H_2O (3 x 20 mL). Evaporation of EtOAc *in vacuo* afforded **25** as pale brown solid (145 mg, 0.458 mmol, 20 %). ^{1}H NMR (300 MHz, DMSO-d_6) δ 12.81 (s, 2H),

10.82 (s, 1H), 9.13 (s, 1H), 7.82 (dd, J = 8.0, 1.5 Hz, 1H), 7.53 (dd, J = 7.9, 1.7 Hz, 1H), 7.42 (dt, J = 6.6, 3.1 Hz, 3H), 7.33 – 7.18 (m, 3H), 1.45 (s, 9H). ^{13}C NMR (75 MHz, DMSO-d_6) δ 153.02, 149.32, 134.79, 129.87, 128.07, 127.33, 126.82, 124.63, 123.33, 123.12, 111.59, 79.44, 28.03; HR-ESI-MS (*m/z*): calculated for $[M + H]^+$ $C_{18}H_{21}O_2N_4$ 325.1659, found 325.1654.

***Tert*-butyl 2-(4-methyl-1*H*-benzo[*d*]imidazol-2-ylamino)phenylcarbamate (26).** A solution of **20** (0.810 g, 4.88 mmol) and *tert*-butyl (2-aminophenyl)carbamate (1.02 g, 4.88 mmol) in *n*-BuOH (9.8 mL) was treated with KH_2PO_4 (0.664 g, 4.88 mmol) and stirred at 115 °C for 17 h. After addition of H_2O (40 mL), the reaction mixture was extracted with EtOAc (3 x 15 mL) and the combined organic phases were dried over $MgSO_4$ and concentrated to give a brown crude product. Purification by flash chromatography (SiO_2; 10-100 % EtOAc/hexane) gave **26** (425 mg, 1.26 mmol, 26 %) as a brownish solid. m.p. 106.3-109.0 °C; ^{1}H NMR (DMSO-d_6, 300 MHz): δ 11.16 (s, 1H), 8.93 (s, 1H), 8.09 (s, 1H), 7.39 (s, 1H), 7.15 (dd, J = 16.1, 7.7 Hz, 2H), 6.99 (t, J = 7.4 Hz, 1H), 6.93 – 6.75 (m, 3H), 2.41 (s, 3H), 1.45 (s, 9H); ^{13}C-NMR (DMSO-d_6, 75 MHz): δ 172.02, 153.75, 150.79, 129.66, 125.18, 121.93, 120.98, 120.37, 120.06, 108.45, 79.11, 28.10, 16.59; HR-ESI-MS (*m/z*): calculated for $[M + H]^+$ $C_{19}H_{23}O_2N_4$ 339.1816, found 339.1814.

***Tert*-butyl 2-(5-methyl-1*H*-benzo[*d*]imidazol-2-ylamino)phenylcarbamate (27).** Following the procedure for **26**, conversion of **21** (300 mg, 1.81 mmol) gave **27** as brown solid (170 mg, 0.51 mmol, 27 %) after purification by flash chromatography (SiO_2; 1-15 % MeOH/DCM). m.p. 166.4-166.8 °C; ^{1}H NMR (DMSO-d_6, 300 MHz): δ 10.44 (d, J = 10.9 Hz, 1H), 8.74 (s, 1H),8.07 (d, J = 7.8 Hz, 1H), 7.40 (d, J = 7.6 Hz, 1H), 7.22 – 7.11 (m, 2H), 7.10 – 6.97 (m, 2H), 6.78 (m, 2H), 2.35 (s, 3H), 1.45 (s, 9H); ^{13}C NMR (DMSO-d_6, 75 MHz): δ 155.36, 153.65, 129.81, 129.28, 129.04, 128.20, 127.40, 125.08, 122.11, 121.24, 120.81, 120.53, 108.94, 108.09, 79.15, 28.07, 21.21; HR-ESI-MS (*m/z*): calculated for $[M + H]^+$ $C_{19}H_{23}O_2N_4$ 339.1816, found 339.1809.

***Tert*-butyl 2-(5-bromo-1*H*-benzo[*d*]imidazol-2-ylamino)phenylcarbamate (28).** Following the procedure for **26**, conversion of **22** (700 mg, 3.04 mmol) gave **28** as brown solid (480 mg, 1.19

mmol, 40 %) after purification by flash chromatography (SiO_2; 0-10 % MeOH/DCM). m.p. 176.2-178.2 °C; ^{1}H NMR (DMSO-d_6, 300 MHz): δ 11.26 (s, 1H), 8.62 (d, J = 27.6 Hz, 2H), 8.08 (s, 1H), 7.42 (dd, J = 18.1, 5.0 Hz, 2H), 7.28 – 7.07 (m, 3H), 7.02 (t, J = 7.1 Hz, 1H), 1.45 (s, 9H); ^{13}C-NMR (DMSO-d_6, 75 MHz): δ 153.66, 152.14, 133.26, 128.46, 125.14, 122.55, 120.90, 79.22, 28.06; HR-ESI-MS (*m/z*): calculated for $[M + H]^+$ $C_{18}H_{20}O_2N_4Br$ 403.0764, found 403.0757.

***Tert*-butyl 2-(5-(trifluoromethyl)-1*H*-benzo[*d*]imidazol-2-ylamino)phenylcarbamate (29).** Following the procedure for **26**, conversion of **23** (500 mg, 2.27 mmol) was gave **29** as brown solid (750 mg, 1.91 mmol, 84 %) after purification by flash chromatography (SiO_2; 1:1 hexane/EtOAc). m.p. 176.5-177.6 °C; ^{1}H NMR (DMSO-d_6, 300 MHz): δ 11.40 (s, 1H), 8.68 (s, 1H), 8.09 (d, J = 7.9 Hz, 1H), 7.60 (s, 1H), 7.43 (t, J = 8.0 Hz, 2H), 7.31 (m, 1H), 7.19 (td, J = 8.1, 1.5 Hz, 1H), 7.05 (td, J = 7.7, 1.4 Hz, 1H), 1.45 (s, 9H); ^{13}C NMR (DMSO-d_6, 75 MHz): δ 153.64, 133.04, 128.69, 127.15, 125.13, 123.56, 122.80, 121.17, 79.24, 28.05; HR-ESI-MS (*m/z*): calculated for $[M + H]^+$ $C_{19}H_{20}O_2N_4F_3$ 393.1533, found 393.1532.

***Tert*-butyl 2-(5,6-dichloro-1*H*-benzo[*d*]imidazol-2-ylamino)phenylcarbamate (30).** Following the procedure for **26**, conversion of **24** (700 mg, 3.18 mmol) gave **30** as brown solid (700 mg, 1.78 mmol, 56 %) after washing the obtained solid after extraction with hexane/EtOAc (4:1, 20 mL). ^{1}H NMR (DMSO-d_6, 300 MHz): δ 11.30 (s, 1H), 8.67 (d, J = 17.8 Hz, 2H), 8.08 (d, J = 7.9 Hz, 1H), 7.50 (s, 2H), 7.39 (d, J = 9.4 Hz, 1H), 7.18 (td, J = 7.9, 1.5 Hz, 1H), 7.04 (td, J = 7.7, 1.4 Hz, 1H), 1.45 (s, 9H); ^{13}C NMR (DMSO-d_6, 75 MHz): δ 153.70, 153.32, 133.02, 128.72, 125.78, 125.15, 124.19, 123.64, 122.83, 121.20, 110.92, 79.27, 28.09; HR-ESI-MS (*m/z*): calculated for $[M + H]^+$ $C_{18}H_{19}O_2N_4Cl_2$ 393.0880, found 393.0882.

2-(1*H*-benzo[*d*]imidazol-2-ylamino)-4-chloroaniline (31). A solution of *tert*-butyl 2-amino-4-chlorophenylcarbamate (300 mg, 1.24 mmol) and **19** (190 mg, 1.24 mmol) in *n*-BuOH (2.5 mL) was treated with KH_2PO_4 (170 mg, 1.24 mmol) and stirred at 90 °C; for 17 h. After addition of H_2O (50 mL), the reaction mixture was extracted with EtOAc (3 x 15 mL) and the combined organic

phases were dried over $MgSO_4$ and concentrated to give a dark violet solid. Purification by flash chromatography (SiO_2; 10-100 % EtOAc/hexane) gave **31** (300 mg, 1.16 mmol, 92 %) as a violet solid. m.p. 122.8-124.3 °C; ^{1}H NMR (DMSO-d_6, 300 MHz): δ 10.67 (s, 1H), 9.12 (s, 2H), 7.43 – 7.36 (m, 3H), 7.26 – 7.17 (m, 4H), 6.89 – 6.84 (m, 1H); ^{13}C NMR (DMSO-d_6, 75 MHz): δ 149.15, 144.17, 129.89, 128.71, 127.43, 123.14, 120.37, 118.81, 117.14, 111.54; HR-ESI-MS (*m/z*): calculated for $[M + H]^+$ $C_{13}H_{12}N_4Cl$ 259.0745, found 259.0752.

***Tert*-butyl 2-(1*H*-benzo[*d*]imidazol-2-ylamino)-5-chlorophenylcarbamate (32).** A solution of *tert*-butyl 2-amino-5-chlorophenylcarbamate (260 mg, 1.07 mmol) and **19** (0.16 g, 1.07 mmol) in *n*-BuOH (2.1 mL) was treated with KH_2PO_4 (150 mg, 1.07 mmol) and stirred at 90 °C for 24 h. After addition of H_2O (40 mL), the reaction mixture was extracted with EtOAc (3 x 20 mL) and the combined organic phases were dried over $MgSO_4$ and concentrated to give a brownish solid. Purification by flash chromatography (SiO_2; 10-100 % EtOAc/hexane) gave **32** (160 mg, 41 %) as a violet solid. m.p. 154.5-155.8 °C; ^{1}H NMR (DMSO-d_6, 300 MHz): δ 12.39 (s, 1H), 9.24 (s, 1H), 7.92 (d, J = 2.2 Hz, 1H), 7.64 (d, J = 8.5 Hz, 1H), 7.37 (m, 2H), 7.25 (m, 3H), 1.45 (s, 9H); ^{13}C NMR (DMSO-d_6, 75 MHz): δ 152.85, 149.85, 136.09, 131.75, 130.68, 128.87, 125.70, 124.05, 122.96, 122.03, 111.63, 80.10, 27.98; HR-ESI-MS (*m/z*): calculated for $[M + H]^+$ $C_{18}H_{20}O_2N_4Cl$ 359.1269, found 359.1275.

1-(4-Methyl-1*H*-benzo[*d*]imidazol-2-yl)-1*H*-benzo[*d*]imidazol-2(3*H*)-one (33). A solution of **26** (170 mg, 0.503 mmol) in DMF (2.5 mL) was treated with K_2CO_3 (207 mg, 1.51 mmol) and stirred at 110 °C for 22 h. After addition of H_2O (20 mL), the reaction mixture was extracted with EtOAc (3 x 15 mL) and the combined organic phases were dried over $MgSO_4$ and concentrated to give a brown crude product. Purification by HPLC (Reprospher C_{18}; 10-70 % D/A) gave **33** (86.0 mg, 0.33 mmol, 65 %) as a white solid. m.p. 278.3-280.7 °C. ^{1}H NMR (DMSO-d_6, 300 MHz): δ 11.66 (s, 1H), 8.37 (dd, J = 5.4, 3.4 Hz, 1H), 7.44 (d, J = 7.8 Hz, 1H), 7.25 – 7.12 (m, 3H), 7.09 (t, J = 7.6 Hz, 1H), 7.01 (d, J = 7.3 Hz, 1H), 2.58 (s, 3H); ^{13}C-NMR (DMSO-d_6, 75 MHz): δ 152.43, 143.13,

128.58, 127.23, 125.85, 123.32, 122.12, 121.74, 121.56, 113.19, 110.63, 109.41, 16.46; HR-ESI-MS (*m/z*): calculated for $[M + H]^+$ $C_{15}H_{13}ON_4$ 265.1084, found 265.1078.

1-(5-Methyl-1*H*-benzo[*d*]imidazol-2-yl)-1*H*-benzo[*d*]imidazol-2(3*H*)-one (34). A solution of **27** (150 mg, 0.442 mmol) in DMF (2.2 mL) was treated with K_2CO_3 (180 mg, 1.32 mmol) and stirred at 110 °C for 47 h. After addition of H_2O (30 mL), the reaction mixture was extracted with EtOAc (3 x 20 mL) and the combined organic phases were dried over $MgSO_4$ and concentrated to give a brown solid. Purification by flash chromatography (SiO_2; 1-10 % MeOH/DCM) gave **34** (20 mg, 0.076 mmol, 14 %) as a gray solid. m.p. > 300 °C (dec.). ^{1}H NMR (DMSO-d_6, 300 MHz): δ 12.29 (s, 1H), 11.64 (s, 1H), 8.44 – 8.32 (m, 1H), 7.49 (m, 1H), 7.41 (d, J = 5.1 Hz, 1H), 7.24 – 7.11 (m, 3H), 7.01 (dd, J = 8.2, 1.2 Hz, 1H), 2.42 (s, 3H); ^{13}C NMR (DMSO-d_6, 75 MHz): mixture of two isomers δ 152.39, 143.83, 143.48, 140.81, 138.53, 132.57, 130.87, 130.42, 130.32, 128.53, 127.06, 123.29, 122.91, 122.92, 121.54, 117.65, 117.33, 113.35, 111.67, 111.38, 109.36, 21.37, 21.25; HR-ESI-MS (*m/z*): calculated for $[M + H]^+$ $C_{15}H_{13}ON_4$ 265.1084, found 265.1083.

1-(5-Bromo-1*H*-benzo[*d*]imidazol-2-yl)-1*H*-benzo[*d*]imidazol-2(3*H*)-one (35). A solution of **28** (480 mg, 1.20 mmol) in DMF (6 mL) was treated with K_2CO_3 (500 mg, 3.60 mmol) and stirred at 110 °C for 15 h. After addition of H_2O (50 mL), the reaction mixture was extracted with EtOAc (3 x 30 mL) and the combined organic phases were dried over $MgSO_4$ and concentrated to give a light brown solid. Purification by flash chromatography (SiO_2; 1-10 % MeOH/DCM) gave **35** (10 mg, 0.030 mmol, 2 %) as a light brown solid. m.p. > 300 °C (dec.). ^{1}H NMR (DMSO-d_6, 300 MHz): δ 12.57 (d, J = 15.7 Hz, 1H), 11.72 (s, 1H), 8.46 – 8.34 (m, 1H), 7.86 – 7.74 (m, 1H), 7.58 (dd, J = 8.5, 3.6 Hz, 1H), 7.33 (m, 1H), 7.26 – 7.12 (m, 3H); ^{13}C NMR (DMSO-d_6, 75 MHz): two sets of signals: first set with high intensity δ 152.35, 128.61, 126.81, 124.43, 123.56, 121.64, 113.64, 113.55, 109.49: second set with low intensity δ 155.20, 155.00, 145.01, 144.74, 142.07, 139.68, 133.67, 131.58, 131.19, 129.63, 128.97, 122.85, 120.32, 120.10, 119.42, 114.51, 110.98, 110.02, 108.40; HR-ESI-MS (*m/z*): calculated for $[M + H]^+$ $C_{14}H_{10}ON_4Br$ 329.0033, found 329.0035.

1-(5-(Trifluoromethyl)-1*H*-benzo[*d*]imidazol-2-yl)-1*H*-benzo[*d*]imidazol-2(3*H*)-one (36). A solution of **29** (400 mg, 1.02 mmol) in DMF (6.4 mL) was treated with K_2CO_3 (420 mg, 3.06 mmol) and stirred at 110 °C for 46 h. After addition of H_2O (50 mL), the reaction mixture was extracted with EtOAc (3 x 20 mL) and the combined organic phases were dried over $MgSO_4$ and concentrated to give a white solid. Purification by flash chromatography (SiO_2; 0-3 % MeOH/DCM) gave **36** (40.0 mg, 0.13 mmol, 12 %) as a white solid. m.p. 269.7-270.5 °C. ^{1}H NMR (DMSO-d_6, 300 MHz): δ 12.79 (d, J = 9.8 Hz, 1H), 11.75 (d, J = 6.9 Hz, 1H), 8.44 (td, J = 6.7, 2.8 Hz, 1H), 7.97 (s, 1H), 7.80 (d, J = 8.3 Hz, 1H), 7.57 – 7.47 (m, 1H), 7.20 (dd, J = 21.7, 9.1 Hz, 3H); ^{13}C NMR (DMSO-d_6, 75 MHz): δ 152.35, 146.40, 145.92, 143.22, 140.16, 135.04, 132.03, 128.69, 126.80, 123.69, 121.69, 118.23, 113.61, 112.67, 109.56; ^{19}F NMR (DMSO-d_6, 376 MHz): δ -58.81 (t, J = 27.2 Hz); HR-ESI-MS (*m/z*): calculated for $[M + H]^+$ $C_{15}H_{10}ON_4F_3$ 319.0812, found 319.0822.

1-(5,6-Dichloro-1*H*-benzo[*d*]imidazol-2-yl)-1*H*-benzo[*d*]imidazol-2(3*H*)-one (37). A solution of **30** (500 mg, 1.28 mmol) in DMF (6.4 mL) was treated with K_2CO_3 (530 mg, 3.84 mmol) and stirred at 110 °C for 19 h. After addition of H_2O (50 mL), the reaction mixture was extracted with EtOAc (3 x 20 mL) and the combined organic phases were dried over $MgSO_4$ and concentrated to give a brown solid. Purification by flash chromatography (SiO_2; 0-10 % MeOH/DCM) gave **37** (21 mg, 0.066 mmol, 5 %) as a white solid. m.p. > 300 °C (dec.); ^{1}H NMR (DMSO-d_6, 300 MHz): δ 12.65 (s, 1H), 11.75 (s, 1H), 8.43 – 8.33 (m, 1H), 7.84 (d, J = 24.9 Hz, 2H), 7.19 (m, 3H); ^{13}C NMR (DMSO-d_6, 75 MHz): δ 152.31, 146.01, 128.65, 126.66, 123.87, 123.72, 121.69, 118.82, 113.63, 113.14, 109.56; HR-ESI-MS (*m/z*): calculated for $[M + H]^+$ $C_{14}H_9ON_4Cl_2$ 319.0148, found 319.0150.

1-(1*H*-Benzo[*d*]imidazol-2-yl)-7-hydroxy-1*H*-benzo[*d*]imidazol-2(3*H*)-one (38). A solution of 3-*tert*-butyldimethylsiloxy-1,2-diaminobenzene (500 mg, 2.10 mmol) and **19** (319 mg, 2.10 mmol) in *n*-BuOH (4.2 mL) was treated with KH_2PO_4 (286 mg, 2.10 mmol) and stirred at 120 °C for 16 h. After addition of H_2O (40 mL), the reaction mixture was extracted with EtOAc (3 x 40 mL) and the

combined organic phases were dried over $MgSO_4$ and concentrated to give a white solid. A solution of this intermediate (65 mg, 0.27 mmol) in DMF (0.3 mL) was then treated with *N*,*N*'-carbonyldiimidazole(44 mg, 0.27 mmol) and stirred at room temperature for 17 h. After addition of H_2O (10 mL), the reaction mixture was extracted with EtOAc (3 x 10 mL) and the combined organic phases were dried over $MgSO_4$ and concentrated to give a white solid. Purification by HPLC (Reprospher C_{18}; 30-40 % D/A) afforded a good separation from **42** to give **38** (11 mg, 0.041 mmol, 15 %) as a white solid. m.p. 220.6-222.2 °C; ^{1}H NMR (DMSO-d_6, 300 MHz): δ 11.65 (s, 1H), 9.67 (s, 1H), 8.44 (dd, J = 6.1, 3.0 Hz, 1H), 7.21 (dd, J = 5.4, 3.7 Hz, 2H), 7.17 – 7.12 (m, 1H), 7.11 – 7.05 (m, 1H), 6.99 (t, J = 7.9 Hz, 1H), 6.59 (dd, J = 7.7, 0.9 Hz, 1H); ^{13}C NMR (DMSO-d_6, 75 MHz): δ 157.98, 152.52, 142.61, 128.53, 127.09, 123.38, 122.58, 121.58, 113.53, 109.42, 107.35; HR-ESI-MS (*m/z*): calculated for $[M + H]^+$ $C_{14}H_{11}O_2N_4$ 267.0877, found 267.0871.

1-(1*H*-Benzo[*d*]imidazol-2-yl)-6-chloro-1*H*-benzo[*d*]imidazol-2(3*H*)-one (39). A solution of **31** (150 mg, 0.582 mmol) in DMF (0.6 mL) was treated with *N*,*N*'-carbonyldiimidazole (94.1 mg, 0.582 mmol) and stirred at room temperature for 40 h. After addition of H_2O (30 mL), the reaction mixture was extracted with EtOAc (3 x 15 mL) and the combined organic phases were dried over $MgSO_4$ and concentrated to give a violet solid. Purification by HPLC (Reprospher C_{18}; 30-100 % D/A) gave **39** (5.0 mg, 0.018 mmol, 3 %) as a white solid. m.p. > 300 °C (dec.); ^{1}H NMR (DMSO-d_6, 300 MHz): δ 11.84 (s, 1H), 8.46 (d, J = 2.1 Hz, 1H), 7.67 – 7.62 (m, 2H), 7.29 – 7.25 (m, 1H), 7.22 – 7.14 (m, 3H); ^{13}C NMR (DMSO-d_6, 75 MHz): δ 152.33, 143.57, 127.86, 127.63, 125.56, 123.11, 121.80, 113.26, 110.65; HR-ESI-MS (*m/z*): calculated for $[M + H]^+$ $C_{14}H_{10}ON_4Cl$ 285.0538, found 285.0543.

1-(1*H*-Benzo[*d*]imidazol-2-yl)-6-hydroxy-1*H*-benzo[*d*]imidazol-2(3*H*)-one (40). A solution of 4-*tert*-butyldimethylsiloxy-1,2-diaminobenzene (0.60 g, 2.52 mmol) and **52** (0.38 g, 2.5 mmol) in *n*-BuOH (5.0 mL) was treated with KH_2PO_4 (0.34 g, 2.5 mmol) and stirred at 120 °C for 18 h. After addition of H_2O (40 mL), the reaction mixture was extracted with EtOAc (3 x 100 mL) and the

combined organic phases were dried over $MgSO_4$ and concentrated to give a white product, which was used for the next step without further purification.

A solution of this intermediate (150 mg, 0.424 mmol) in DMF (0.4 mL) was treated with *N*,*N*'-carbonyldiimidazole (68.0 mg, 0.424 mmol) and stirred at room temperature for 17 h. After addition of H_2O (20 mL), the reaction mixture was extracted with EtOAc (3 x 20 mL) and the combined organic phases were dried over $MgSO_4$ and concentrated to give a white solid. Purification by HPLC (Reprospher C_{18}; 65-85 % D/A) gave 1-(1*H*-benzo[*d*]imidazol-2-yl)-5/6-*tert*-butyldimethylsilylether-1*H*-benzo[*d*]imidazol-2(3*H*)-one (52 mg, 0.14 mmol, 33 %) as a white solid. m.p. 201.2-204.0 °C; ^{1}H NMR (DMSO-d_6, 300 MHz): mixture of two isomers with the same chemical shift δ 11.53 (s, 1H), 8.25 (d, J = 8.6 Hz, 1H), 7.60 (dd, J = 5.9, 3.2 Hz, 2H), 7.18 (dd, J = 6.0, 3.1 Hz, 2H), 6.71 (dd, J = 8.6, 2.3 Hz, 1H), 6.60 (d, J = 2.2 Hz, 1H), 0.97 (s, 9H), 0.21 (s, 6H); ^{13}C-NMR (DMSO-d_6, 75 MHz): mixture of two isomers with the same chemical shift δ 158.43, 152.63, 151.53, 144.01, 129.47, 121.61, 121.51, 114.76, 114.25, 113.02, 101.51, 25.59, 17.95, -4.56; HR-ESI-MS (*m/z*): calculated for $[M + H]^+$ $C_{20}H_{25}O_2N_4Si$ 381.1741, found 381.1737.

This intermediate (37 mg, 0.10 mmol) in THF (0.6 mL) was treated with a solution of TBAF·$3H_2O$ (32 mg, 0.10 mmol) in THF (0.2 mL) and stirred at 0 °C for 5 min, and at room temperature for 1 h. The reaction mixture was extracted with HCl (1M) / ice water (1:1) and EtOAc (3 x 10 mL) and the combined organic phases were dried over $MgSO_4$ and concentrated to give a brown crude product. Purification by HPLC (Reprospher C_{18}; 10-60 % D/A) gave **40** (2.0 mg, 0.008 mmol, 7 %) as the first fraction (separated from **6**) as a white solid. m.p. 151.4-154.4 °C; ^{1}H NMR (DMSO-d_6, 300 MHz): δ 11.63 (s, 1H), 9.11 (s, 1H), 8.32 (dd, J = 6.0, 3.1 Hz, 1H), 7.39 (d, J = 8.6 Hz, 1H), 7.22 – 7.16 (m, 2H), 7.16 – 7.11 (m, 1H), 6.99 (d, J = 2.2 Hz, 1H), 6.66 (dd, J = 8.6, 2.3 Hz, 1H); ^{13}C-NMR (DMSO-d_6, 101 MHz): δ 153.12, 152.35, 142.90, 128.49, 127.07, 123.22, 121.51, 113.24, 111.05, 109.35; HR-ESI-MS (*m/z*): calculated for $[M + H]^+$ $C_{14}H_{11}O_2N_4$ 267.0877, found 267.0872.

1-(1*H*-Benzo[*d*]imidazol-2-yl)-5-chloro-1*H*-benzo[*d*]imidazol-2(3*H*)-one (41). A solution of **32** (120 mg, 0.34 mmol) in DMF (1.7 mL) was treated with K_2CO_3 (140 mg, 1.02 mmol) and stirred at 110 °C for 38 h. After addition of H_2O (20 mL), the reaction mixture was extracted with EtOAc (3 x 15 mL) and the combined organic phases were dried over $MgSO_4$ and concentrated to give a gray solid. Purification by flash chromatography (SiO_2; 0-5 % MeOH/DCM) gave **41** (14 mg, 0.049 mmol, 14 %) as a white solid. m.p. > 300 °C (dec.); ^{1}H NMR (DMSO-d_6, 300 MHz): δ 12.44 (s, 1H), 11.84 (s, 1H), 8.40 (d, J = 8.6 Hz, 1H), 7.65 – 7.58 (m, 2H), 7.27 (dd, J = 8.6, 2.1 Hz, 1H), 7.22 – 7.16 (m, 3H); ^{13}C NMR (DMSO-d_6, 75 MHz): δ 152.32, 143.61, 129.87, 127.45, 125.97, 121.38, 114.64, 109.38; HR-ESI-MS (*m/z*): calculated for $[M + H]^+$ $C_{14}H_{10}ON_4Cl$ 285.0538, found 285.0544.

1-(1*H*-Benzo[*d*]imidazol-2-yl)-4-hydroxy-1*H*-benzo[*d*]imidazol-2(3*H*)-one (42). Purification of the reaction to form **38** by HPLC (Reprospher C_{18}; 30-40 % C/A) afforded also a second fraction in form of **42** (14 mg, 0.053 mmol, 19 %) as a white solid. m.p. 153.2-155.7 °C; ^{1}H NMR (DMSO-d_6, 400 MHz) δ 11.51 (s, 1H), 9.95 (s, 1H), 7.88 (d, J = 8.0 Hz, 1H), 7.61 (dd, J = 6.0, 3.2 Hz, 2H), 7.18 (dd, J = 6.0, 3.2 Hz, 2H), 7.00 (t, J = 8.1 Hz, 1H), 6.71 (d, J = 7.4 Hz, 1H); ^{13}C-NMR (DMSO-d_6, 75 MHz): δ 152.37, 144.07, 141.61, 128.27, 122.00, 121.60, 116.73, 110.31, 105.00; HR-ESI-MS (*m/z*): calculated for $[M + H]^+$ $C_{14}H_{11}O_2N_4$ 267.0877, found 267.0874.

***Tert*-butyl 2-amino-4-methylphenylcarbamate and *tert*-butyl 2-amino-5-methylphenylcarbamate (43).** An ice-cold solution of 3,4-diaminotoluene (5.00 g, 40.9 mmol) and guanidine hydrochloride (0.587 g, 6.14 mmol) in EtOH (41 mL) was treated with Boc_2O (8.93 g, 40.9 mmol) and the solution was stirred at room temperature for 2 h. EtOH was removed *in vacuo*. Flash chromatography (SiO_2; 1:6 EtOAc/hexane) gave **43** (6.22 g, 28.1 mmol, 68 %) as a white solid. m.p. 101.9-104.1 °C; ^{1}H NMR (DMSO-d_6, 300 MHz): mixture of two isomers δ 8.20 (d, J = 16.8 Hz, 1H), 7.02 (d, J = 7.9 Hz, 1H), 6.50 (tdd, J = 51.4, 8.0, 1.6 Hz, 2H), 4.66 (d, J = 33.8 Hz, 2H), 2.13 (s, 3H), 1.45 (d, J = 3.2 Hz, 9H); ^{13}C NMR (DMSO-d_6, 75 MHz): mixture of two isomers δ 153.72, 153.53, 141.19, 133.88, 125.30, 124.84, 124.68, 123.82, 121.24, 117.01, 116.12, 115.85,

78.56, 78.44, 28.18, 20.69, 20.19; HR-ESI-MS (*m/z*): calculated for $[M + H]^+$ $C_{12}H_{19}O_2N_2$ 223.1441, found 223.1442.

1-(1*H*-benzo[*d*]imidazol-2-yl)-5-methyl-1*H*-benzo[*d*]imidazol-2(3*H*)-one and 1-(1*H*-benzo[*d*]imidazol-2-yl)-6-methyl-1*H*-benzo[*d*]imidazol-2(3*H*)-one (44). A solution of **43** (1.00 g, 4.50 mmol) and **19** (0.684 g, 4.50 mmol) in *n*-BuOH (9.0 mL) was treated with KH_2PO_4 (612 mg, 1.81 mmol, 4.50 mmol) and stirred at 95 °C for 15 h. After addition of H_2O (50 mL), the reaction mixture was extracted with EtOAc (3 x 30 mL) and the combined organic phases were dried over $MgSO_4$ and concentrated to give a white solid, which was used for the next step without further purification. This product (800 mg, 2.37 mmol) was dissolved in DMF (12 mL) and treated with K_2CO_3 (983 mg, 7.11 mmol) and stirred at 110 °C for 18 h. After addition of H_2O (50 mL), the reaction mixture was extracted with EtOAc (3 x 40 mL) and the combined organic phases were dried over $MgSO_4$ and concentrated to give a brownish solid. Purification by HPLC (Reprospher C_{18}; 40-55 % D/A) gave **44** (123 mg, 20 %) as a white solid. m.p. 271.9-273.5 °C; ^{1}H NMR (DMSO-d_6, 300 MHz): mixture of two isomers (ratio 5:1) with the same chemical shift δ 11.55 (s, 1H), 8.23 (s, 1H), 7.63 (dd, J = 6.0, 3.2 Hz, 2H), 7.19 (dd, J = 5.9, 3.2 Hz, 2H), 7.03 (d, J = 0.8 Hz, 2H), 2.42 (s, 3H); ^{13}C-NMR (DMSO-d_6, 75 MHz): mixture of two isomers δ 152.58, 152.54, 144.02, 143.97, 130.78, 127.14, 126.34, 123.90, 122.14, 121.68, 113.79, 109.14, 21.30, 21.04; HR-ESI-MS (*m/z*): calculated for $[M + H]^+$ $C_{15}H_{13}ON_4$ 265.1084, found 265.1082.

3-(1*H*-Benzo[*d*]imidazol-2-yl)-2,3-dihydro-2-oxo-1*H*-benzo[*d*]imidazole-6-carboxylic acid (45). H_5IO_6 (249 mg, 1.09 mmol) was dissolved in MeCN (2.9 mL) under vigorous stirring and CrO_3 (6.0 mg, 0.2 eq.) was added to the transparent solution and stirred at room temperature for 5 min. The orange solution was slowly treated with **44** (82.0 mg, 0.310 mmol) and stirred for 1 h. H_2O (5.0 mL) was added and the reaction mixture was extracted with EtOAc (4 x 20 mL). The combined organic phases were dried over $MgSO_4$ and concentrated to give a white solid. Separation from **46** by HPLC (Reprospher C_{18}; 30-65 % D/A) gave **45** (42.0 mg, 0.14 mmol, 46 %) as a white solid. m.p. > 300 °C (dec.); ^{1}H NMR (DMSO-d_6, 300 MHz): δ 12.91 (s, 1H), 12.05 (s, 1H), 8.98 (s, 1H),

7.87 (dd, *J* = 8.2, 1.5 Hz, 1H), 7.66 (dd, *J* = 5.8, 3.1 Hz, 2H), 7.27 – 7.16 (m, 3H); ^{13}C-NMR (DMSO-d_6, 75 MHz): δ 167.31, 152.63, 143.60, 132.50, 126.92, 125.57, 124.10, 121.77, 114.51, 109.06; HR-ESI-MS (*m/z*): calculated for $[M + H]^+$ $C_{15}H_{11}O_3N_4$ 295.0826, found 295.0824.

1-(1*H*-Benzo[*d*]imidazol-2-yl)-2,3-dihydro-2-oxo-1*H*-benzo[*d*]imidazole-5-carboxylic acid (46). Purification of **45** by HPLC (Reprospher C_{18}; 30-65 % D/A) gave as a second fraction product **46** (16 mg, 0.054 mmol, 18 %) as a white solid. m.p. > 300 °C (dec.); ^{1}H NMR (DMSO-d_6, 300 MHz): δ 11.91 (s, 1H), 8.47 (d, *J* = 8.4 Hz, 1H), 7.87 (dd, *J* = 8.5, 1.6 Hz, 1H), 7.68 – 7.61 (m, 3H), 7.21 (dd, *J* = 6.0, 3.2 Hz, 2H); ^{13}C-NMR (DMSO-d_6, 101 MHz): δ 167.04, 152.52, 143.47, 128.61, 125.73, 123.66, 121.83, 112.97, 110.01; HR-ESI-MS (*m/z*): calculated for $[M + H]^+$ $C_{15}H_{11}O_3N_4$ 295.0826, found 295.0827.

3-(1*H*-Benzo[*d*]imidazol-2-yl)-2,3-dihydro-*N*-methyl-2-oxo-1*H*-benzo[*d*]imidazole-6-carboxamide (47). A solution of **45** (4.0 mg, 0.014 mmol) in DMF (0.5 mL) was treated with BOP (6.6 mg, 0.015 mmol), triethylamine (0.011 mL, 0.070 mmol) and methylamine hydrochloride (4.7 mg, 0.070 mmol) and stirred at room temperature for 4 h. The reaction crude was directly purified by HPLC (Reprospher C_{18}; 15-60 % C/A) to give **47** (2.5 mg, 0.0081 mmol, 58 %) as a white solid. m.p. > 300 °C (dec.); ^{1}H NMR (DMSO-d_6, 300 MHz): δ 11.92 (s, 1H), 8.81 (d, *J* = 1.3 Hz, 1H), 8.45 (d, *J* = 4.5 Hz, 1H), 7.70 (dd, *J* = 8.2, 1.7 Hz, 1H), 7.66 (dd, *J* = 6.0, 3.2 Hz, 2H), 7.24 – 7.16 (m, 3H), 2.81 (d, *J* = 4.5 Hz, 3H); ^{13}C-NMR (DMSO-d_6, 101 MHz): δ 166.73, 152.66, 143.55, 130.86, 128.57, 126.99, 122.57, 121.75, 112.72, 108.69, 26.35; HR-ESI-MS (*m/z*): calculated for $[M + H]^+$ $C_{16}H_{14}O_2N_5$ 308.1142, found 308.1141.

1-(1*H*-Benzo[*d*]imidazol-2-yl)-2,3-dihydro-*N*-methyl-2-oxo-1*H*-benzo[*d*]imidazole-5-carboxamide (48). A solution of **46** (2.5 mg, 0.0085 mmol) in DMF (0.5 mL) was treated with BOP (4.5 mg, 0.010 mmol), triethylamine (0.011 mL, 0.050 mmol) and methylamine hydrochloride (3.4 mg, 0.050 mmol) and stirred at room temperature for 4 h. The reaction crude was directly purified by HPLC (Reprospher C_{18}; 15-60 % D/A) to give **48** (1.5 mg, 0.0049 mmol, 54 %) as a

white solid. m.p. 172.5-175.0 °C; ^{1}H NMR (DMSO-d_6, 300 MHz): δ 11.91 (s, 1H), 8.50 (d, J = 4.6 Hz, 1H), 8.41 (d, J = 8.4 Hz, 1H), 7.74 (dd, J = 8.4, 1.7 Hz, 1H), 7.66 – 7.60 (m, 3H), 7.20 (dd, J = 6.0, 3.2 Hz, 2H), 2.80 (d, J = 4.5 Hz, 3H); ^{13}C-NMR (DMSO-d_6, 101 MHz): δ 166.17, 152.62, 144.64, 143.62, 131.02, 129.81, 129.03, 121.76, 120.98, 112.70, 108.27, 26.29; HR-ESI-MS (*m/z*): calculated for $[M + H]^+$ $C_{16}H_{14}O_2N_5$ 308.1142, found 308.1141.

2-Chloro-1-methyl-1*H*-benzo[*d*]imidazole (49). A solution of **19** (1.00 g, 6.58 mmol) in DMF (10 mL) at 0 °C was treated with NaH (0.284 g, 11. 8 mmol) and stirred for 15 min. MeI (0.431 mL, 6.91 mmol) was added and the mixture was stirred for 15 min. The reaction mixture was then poured into H_2O (75 mL) and the white precipitate was filtered and washed with H_2O (3 x 30 mL). The white solid was dried *in vacuo* to give **49** (604 mg, 3.64 mmol, 55 %) as a white solid. m.p. 115.2-117.8 °C; ^{1}H NMR (DMSO-d_6, 300 MHz): δ 7.59 (m, 2H), 7.28 (m, 2H), 3.79 (s, 3H); ^{13}C NMR (DMSO-d_6, 75 MHz): δ 141.02, 140.24, 135.61, 122.80, 122.29, 118.46, 110.46, 30.49; HR-ESI-MS (*m/z*): calculated for $[M + H]^+$ $C_8H_8ClN_2$ 167.0371, found 167.0370.

2-Chloro-1-methyl-1*H*-benzo[*d*]imidazole (50). A solution of **49** (500 mg, 3.01 mmol) and *tert*-butyl (2-aminophenyl)carbamate (627 mg, 3.01 mmol) in *n*-BuOH (6.0 mL) was treated with KH_2PO_4 (410 mg, 3.01 mmol) and stirred at 90 °C; for 22 h. Reaction control indicated incomplete reaction. The temperature was elevated to 120 °C and the reaction mixture was stirred for additional 22 h. After addition of H_2O (60 mL), the reaction mixture was extracted with EtOAc (3 x 30 mL) and the combined organic phases were dried over $MgSO_4$ and concentrated to give a reddish solid. Purification by flash chromatography (SiO_2; 5-100 % EtOAc/hexane) gave **50** (302 mg, 0.89 mmol, 30 %) as an off-white solid. m.p. 212.7-214.9 °C; ^{1}H NMR (DMSO-d_6, 300 MHz): δ 8.99 (s, 1H), 7.78 (d, J = 7.7 Hz, 1H), 7.48 (d, J = 7.7 Hz, 1H), 7.31 – 7.25 (m, 2H), 7.16 – 6.99 (m, 5H), 3.67 (s, 3H), 1.45 (d, J = 0.8 Hz, 9H); ^{13}C NMR (DMSO-d_6, 75 MHz): mixture of isomers δ 155.23, 153.62, 152.67, 151.39, 141.99, 141.43, 141.63, 134.92, 134.54, 132.39, 130.07, 129.65, 129.48, 128.98, 124.70, 124.34, 124.06, 123.37, 123.29, 122.90, 122.84, 122.66, 122.32, 121.32, 120.79, 120.43, 120.34, 119.58, 119.16, 116.23, 115.90, 110.69, 110.37, 110.02, 109.58, 108.42, 107.97, 107.49,

79.40, 48.57, 28.03; HR-ESI-MS (*m/z*): calculated for $[M + H]^+$ $C_{19}H_{23}O_2N_4$ 339.1816, found 339.1815.

1-(1-Methyl-1*H*-benzo[*d*]imidazol-2-yl)-1*H*-benzo[*d*]imidazol-2(3*H*)-one (51). A solution of **50** (222 mg, 0.656 mmol) in DMF (3.3 mL) was treated with K_2CO_3 (274 mg, 1.98 mmol) and stirred at 110 °C for 16 h. After addition of H_2O (40 mL), the reaction mixture was extracted with EtOAc (3 x 20 mL) and the combined organic phases were dried over $MgSO_4$ and concentrated to give a solid. Purification by flash chromatography (SiO_2; 5-100 % EtOAc/hexane) gave **51** (84.0 mg, 0.32 mmol, 48 %) as a white solid, m.p. 239.4-241.6 °C. ^{1}H NMR (DMSO-d_6, 300 MHz): δ 11.45 (s, 1H), 7.74 – 7.65 (m, 2H), 7.41 – 7.29 (m, 2H), 7.17 – 7.03 (m, 4H), 3.75 (s, 3H); ^{13}C NMR (DMSO-d_6, 75 MHz): δ 152.65, 141.97, 140.62, 134.91, 129.46, 128.96, 122.89, 122.83, 122.31, 121.31, 119.14, 110.69, 110.01, 109.56, 30.42; HR-ESI-MS (*m/z*): calculated for $[M + H]^+$ $C_{15}H_{13}ON_4$ 265.1084, found 265.1082.

***Tert*-butyl 2-aminophenylmethylcarbamate (52).** A solution of *tert*-butyl methyl 2-nitrophenylcarbamate (6.30 g, 25.0 mmol) in dioxane/H_2O (5:1, 166 mL) was treated with $Na_2S_2O_4$ (17.4 g, 100 mmol) and $NaHCO_3$ (21.0 g, 250 mmol) and refluxed at 100 °C for 45 min. After addition of H_2O (90 mL), the reaction mixture was extracted with EtOAc (3 x 70 mL) and the combined organic phases were dried over $MgSO_4$ and concentrated to give an orange solid. Purification by flash chromatography (Si_2O; 5-100 % EtOAc/hexane) gave **52** (1.19 g, 5.36 mmol, 22 %) as a light brown solid. m.p. 87.4-89.6 °C; ^{1}H NMR (DMSO-d_6, 300 MHz): δ 7.00 – 6.83 (m, 2H), 6.69 (d, J = 7.7 Hz, 1H), 6.50 (t, J = 7.4 Hz, 1H), 4.85 (s, 2H), 2.98 (s, 3H), 1.30 (s, 9H); ^{13}C NMR (DMSO-d_6, 75 MHz): δ 154.39, 144.09, 128.28, 127.83, 127.39, 116.02, 115.38, 78.53, 35.63, 27.99; HR-ESI-MS (*m/z*): calculated for $[M + H]^+$ $C_{12}H_{19}O_2N_2$ 223.1441, found 223.1443.

1-(1*H*-Benzo[*d*]imidazol-2-yl)-3-methyl-1*H*-benzo[*d*]imidazol-2(3*H*)-one (53). A solution of **52** (1.10 g, 4.95 mmol) and **19** (0.684 g, 4.95 mmol) in *n*-BuOH (10 mL) was treated with KH_2PO_4 (0.612 g, 4.95 mmol) and stirred at 120 °C for 24 h. After addition of H_2O (40 mL), the reaction

mixture was extracted with EtOAc (3 x 30 mL) and the combined organic phases were dried over $MgSO_4$ and concentrated to give a white crude solid. Purification by HPLC (Reprospher C_{18}; 20-80 % D/A) gave **53** (8.00 mg, 0.03 mmol, 1 %) as a white solid. m.p. 258.3-260.5 °C. ^{1}H NMR (DMSO-d_6, 300 MHz): δ 12.47 (s, 1H), 8.51 – 8.39 (m, 1H), 7.67 – 7.59 (m, 2H), 7.37 – 7.17 (m, 5H), 3.48 (s, 3H); ^{13}C NMR (DMSO-d_6, 75 MHz): δ 151.68, 143.78, 130.10, 125.78, 123.37, 122.01, 121.70, 113.29, 108.53, 27.14; HR-ESI-MS (*m/z*): calculated for $[M + H]^+$ $C_{15}H_{13}ON_4$ 265.1084, found 265.1087.

(*Z*)-2-((4-ethylphenyl)imino)-3-methylthiazolidin-4-one (54). A solution of 4-ethylaniline (2.15 mL, 17.3 mmol, 1.15 eq.) in EtOH (50 mL) was treated with methyl isothiocyanate (1.01 g, 15.0 mmol, 1.0 eq.) and stirred at 78 °C for 12 h. The solution was then treated with NaOAc (6.23 g, 75.0 mmol, 5.0 eq.) and ethyl chloroacetate (3.22 mL, 30.0 mmol, 2.0 eq.) and stirred at 78 °C for another 5 h. EtOH was evaporated *in vacuo* to afford crude **54** as yellow oil (2.25 g, 9.60 mmol, 64.0 %), which was used for the next step without further purification. ^{1}H NMR (300 MHz, DMSO-d_6) δ 7.19 (d, J = 8.4 Hz, 2H), 7.88 – 6.83 (m, 2H), 4.00 (s, 2H), 3.15 (s, 3H), 2.59 (q, J = 7.6 Hz, 2H), 1.18 (t, J = 7.6 Hz, 3H); ^{13}C NMR (75 MHz, DMSO-d_6) δ 171.91, 155.36, 145.75, 139.53, 128.50, 120.76, 32.54, 29.15, 27.57, ESI-MS (*m/z*): 235.09.

(*Z*)-2-((3-ethylphenyl)imino)-3-methylthiazolidin-4-one (55). Using the same procedure as for **54**, this compound was obtained from 3-ethylaniline (2.10 g, 17.3 mmol, 1.15 eq.) as brown oil (3.08 g, 13.2 mmol, 88 %). ^{1}H NMR (300 MHz, $CDCl_3$) δ 7.18 (t, J = 7.6 Hz, 1H), 6.93 – 6.89 (m, 1H), 6.75 – 6.71 (m, 2H), 3.73 (s, 2H), 3.24 (s, 3H), 2.57 (q, J = 7.6 Hz, 2H), 1.16 (t, J = 7.6 Hz, 3H); ^{13}C NMR (75 MHz, $CDCl_3$) δ 171.80, 155.10, 147.75, 145.60, 129.17, 124.44, 120.63, 118.21, 32.84, 29.75, 28.84, 15.47; HR-ESI-MS (*m/z*): 235.0897, calcd for $[M + H]^+$ $C_{12}H_{15}ON_2S$: 235.0900.

(*Z*)-2-((2-ethylphenyl)imino)-3-methylthiazolidin-4-one (56). Using the same procedure as for **54**, this compound was obtained from 2-ethylaniline (2.09 g, 17.3 mmol, 1.15 eq.) as brown oil

(3.23 g, 13.8 mmol, 92 %). ^{1}H NMR (300 MHz, $CDCl_3$) δ 7.18 – 7.00 (m, 3H), 6.80 – 6.77 (m, 1H), 3.73 (s, 2H), 3.27 (s, 3H), 2.47 (q, *J* = 7.5 Hz, 2H), 1.09 (t, *J* = 7.5 Hz, 3H); ^{13}C NMR (75 MHz, $CDCl_3$) δ 171.81, 154.40, 145.87, 136.08, 129.04, 126.54, 125.03, 119.88, 32.93, 29.72, 29.67, 24.66, 14.49; HR-ESI-MS (*m/z*): 235.0898, calcd for $[M + H]^+$ $C_{12}H_{15}ON_2S$: 235.0900.

(*Z*)-3-methyl-2-((4-propylphenyl)imino)thiazolidin-4-one (57). Using the same procedure as for **54**, this compound was obtained from 4-propylaniline (2.34 g, 17.3 mmol, 1.15 eq.) as brown oil (3.40 g, 13.7 mmol, 91 %). ^{1}H NMR (300 MHz, $CDCl_3$) δ 7.08 (d, *J* = 8.3 Hz, 2H), 6.82 (d, *J* = 8.3 Hz, 2H), 3.73 (s, 2H), 3.25 (s, 3H), 2.53 – 2.48 (m, 2H), 1.63 – 1.51 (m, 2H), 0.87 (t, *J* = 7.3 Hz, 3H); ^{13}C NMR (75 MHz, $CDCl_3$) δ 171.13, 144.61, 138.59, 128.64, 120.26, 36.91, 32.17, 29.13, 23.91, 13.19; HR-ESI-MS (*m/z*): 249.1049, calcd for $[M + H]^+$ $C_{13}H_{17}ON_2S$: 249.1056.

(*Z*)-2-((4-isopropylphenyl)imino)-3-methylthiazolidin-4-one (58). Using the same procedure as for **54**, this compound was obtained from 4-isopropylaniline (2.34 g, 17.3 mmol, 1.15 eq.) as brown oil (3.62 g, 14.6 mmol, 97 %). ^{1}H NMR (300 MHz, $CDCl_3$) δ 7.11 (d, *J* = 8.4 Hz, 2H), 6.81 (d, *J* = 8.3 Hz, 2H), 3.70 (s, 2H), 3.21 (s, 3H), 2.88 – 2.74 (m, 1H), 1.16 (d, *J* = 7.0 Hz, 6H); ^{13}C NMR (75 MHz, $CDCl_3$) δ 171.83, 154.52, 145.53, 145.21, 127.21, 120.88, 33.60, 32.80, 29.67, 24.10; HR-ESI-MS (*m/z*): 249.1054, calcd for $[M + H]^+$ $C_{13}H_{17}ON_2S$: 249.1056.

(*Z*)-2-((4-butylphenyl)imino)-3-methylthiazolidin-4-one (59). Using the same procedure as for **54**, this compound was obtained from 4-butylaniline (2.58 g, 17.3 mmol, 1.15 eq.) as brown oil (3.07 g, 11.7 mmol, 78 %). ^{1}H NMR (300 MHz, $CDCl_3$) δ 7.08 (d, *J* = 8.3 Hz, 2H), 6.81 (d, *J* = 8.3 Hz, 2H), 3.73 (s, 2H), 3.24 (s, 3H), 2.75 – 2.39 (m, 2H), 1.66 – 1.42 (m, 2H), 1.42 – 1.16 (m, 2H), 1.09 – 0.66 (m, 3H); ^{13}C NMR (75 MHz, $CDCl_3$) δ 171.79, 154.87, 145.27, 139.43, 129.22, 120.90, 35.17, 33.66, 32.82, 29.76, 22.39, 14.02; HR-ESI-MS (*m/z*): 263.1204, calcd for $[M + H]^+$ $C_{14}H_{19}ON_2S$: 263.1213.

(*Z*)-2-((4-(*tert*-butyl)phenyl)imino)-3-methylthiazolidin-4-one (60). Using the same procedure as for **54**, this compound was obtained from 4-*tert*-butylaniline (2.58 g, 17.3 mmol, 1.15 eq.) as brown

oil (3.20 g, 12.2 mmol, 81 %). ^{1}H NMR (300 MHz, $CDCl_3$) δ 7.28 (d, J = 8.6 Hz, 2H), 6.84 (d, J = 8.6 Hz, 2H), 3.73 (s, 2H), 3.24 (s, 3H), 1.25 (s, 9H); ^{13}C NMR (75 MHz, $CDCl_3$) δ 171.79, 154.65, 147.63, 144.98, 126.14, 120.63, 34.45, 32.82, 31.48, 29.76; HR-ESI-MS (*m/z*): 263.1206, calcd for $[M + H]^+$ $C_{14}H_{19}ON_2S$: 263.1213.

(*Z*)-3-methyl-2-((4-(trifluoromethyl)phenyl)imino)thiazolidin-4-one (61). Using the same procedure as for **54**, this compound was obtained from 4-(trifluoromethyl)aniline (2.79 g, 17.3 mmol, 1.15 eq.) as brown oil (3.95 g, 14.4 mmol, 96 %). ^{1}H NMR (300 MHz, $CDCl_3$) δ 7.52 (d, J = 8.4 Hz, 2H), 6.97 (d, J = 8.1 Hz, 2H), 3.76 (s, 2H), 3.22 (s, 3H); ^{13}C NMR (75 MHz, $CDCl_3$) δ 171.59, 155.99, 151.18, 151.15, 127.24 – 121.37 (m), 32.87, 29.65, 29.61; HR-ESI-MS (*m/z*): 275.0458, calcd for $[M + H]^+$ $C_{11}H_{10}ON_2F_3S$: 275.0460.

(*Z*)-2-((4-bromophenyl)imino)-3-methylthiazolidin-4-one (62). Using the same procedure as for **54**, this compound was obtained from 4-bromoaniline (2.98 g, 17.3 mmol, 1.15 eq.) as brown oil (3.82 g, 13.4 mmol, 89 %). ^{1}H NMR (300 MHz, $CDCl_3$) δ 7.38 (d, J = 8.5 Hz, 2H), 6.78 (d, J = 8.6 Hz, 2H), 3.75 (s, 2H), 3.23 (s, 3H); ^{13}C NMR (75 MHz, $CDCl_3$) δ 171.61, 155.77, 146.89, 132.37, 122.95, 117.80, 32.90, 29.77, 29.72; HR-ESI-MS (*m/z*): 284.9687, calcd for $[M + H]^+$ $C_{10}H_{10}ON_2BrS$: 284.9692.

(2*Z*,5*Z*)-2-((3-ethylphenyl)imino)-3-methyl-5-(pyridin-4-ylmethylene)thiazolidin-4-one (63). Using the same procedure as for **8**, this compound was obtained from **55** (702 mg, 3.00 mmol, 1.0 eq.) as yellow solid (795 mg, 2.46 mmol, 82 %). m.p. 116.2-116.8°C.^{1}H NMR (300 MHz, DMSO-d_6) δ 8.68 – 8.66 (m, 2H), 7.72 (s, 1H), 7.47 (d, J = 6.2 Hz, 2H), 7.34 (t, J = 7.6 Hz, 1H), 7.07 (dt, J = 7.6, 1.3 Hz, 1H), 6.88 – 6.84 (m, 2H), 3.36 (s, 3H), 2.64 (q, J = 7.6 Hz, 2H), 1.21 (t, J = 7.6 Hz, 3H); ^{13}C NMR (75 MHz, DMSO-d_6) δ 165.42, 150.41, 149.29, 147.55, 145.27, 140.41, 129.38, 126.86, 126.67, 124.52, 123.17, 120.42, 117.93, 29.70, 28.01, 15.34; HR-ESI-MS (*m/z*): 324.1164, calcd for $[M + H]^+$ $C_{18}H_{18}ON_3S$: 324.1165.

(2*Z*,5*Z*)-2-((2-ethylphenyl)imino)-3-methyl-5-(pyridin-4-ylmethylene)thiazolidin-4-one (64). Using the same procedure as for **8**, this compound was obtained from **56** (702 mg, 3.00 mmol, 1.0 eq.) as yellow solid (882 mg, 2.73 mmol, 91 %). m.p. 107.7-110.8°C. ^{1}H NMR (300 MHz, DMSO-d_6) δ 8.76 – 8.65 (m, 2H), 7.72 (s, 1H), 7.46 (d, J = 6.2 Hz, 2H), 7.33 – 7.14 (m, 3H), 6.93 (dd, J = 7.6, 1.4 Hz, 1H), 2.57 – 2.50 (m, 2H), 1.11 (t, J = 7.5 Hz, 3H); ^{13}C NMR (75 MHz, DMSO-d_6) δ 165.44, 150.43, 148.98, 145.69, 140.38, 135.66, 129.02, 126.86, 126.78, 126.74, 125.26, 123.15, 119.78, 29.67, 24.07, 14.50; HR-ESI-MS (*m/z*): 324.1164, calcd for $[M + H]^+$ $C_{18}H_{18}ON_3S$: 324.1165.

(2*Z*,5*Z*)-3-methyl-2-((4-propylphenyl)imino)-5-(pyridin-4-ylmethylene)thiazolidin-4-one (65). Using the same procedure as for **8**, this compound was obtained from **57** (744 mg, 3.00 mmol, 1.0 eq.) as yellow solid (485 mg, 1.44 mmol, 48 %). m.p. 131.6-133.3°C. ^{1}H NMR (300 MHz, $CDCl_3$) δ 8.59 – 8.57 (m, 2H), 7.56 (s, 1H), 7.24 (dd, J = 4.5, 1.7 Hz, 2H), 7.13 (d, J = 8.2 Hz, 2H), 6.85 (d, J = 8.3 Hz, 2H), 3.40 (s, 3H), 2.56 – 2.51 (m, 2H), 1.64 – 1.56 (m, 2H), 0.90 (t, J = 7.3 Hz, 3H); ^{13}C NMR (75 MHz, $CDCl_3$) δ 166.13, 150.12, 149.06, 145.24, 141.34, 139.82, 129.48, 127.63, 126.91, 123.40, 120.86, 37.59, 30.01, 24.56, 13.89; HR-ESI-MS (*m/z*): 338.1320, calcd for $[M + H]^+$ $C_{19}H_{20}ON_3S$: 338.1322.

(2*Z*,5*Z*)-2-((4-isopropylphenyl)imino)-3-methyl-5-(pyridin-4-ylmethylene)thiazolidin-4-one (66). Using the same procedure as for **8**, this compound was obtained from **58** (744 mg, 3.00 mmol, 1.0 eq.) as yellow solid (880 mg, 2.61 mmol, 87 %). m.p. 159.2-159.3°C. ^{1}H NMR (300 MHz, $CDCl_3$) δ 8.58 (d, J = 6.2 Hz, 2H), 7.55 (s, 1H), 7.23 (d, J = 6.2 Hz, 2H), 7.18 (d, J = 8.4 Hz, 2H), 6.86 (d, J = 8.3 Hz, 2H), 3.39 (s, 3H), 2.86 (dt, J = 14.0, 7.1 Hz, 1H), 1.21 (d, J = 6.9 Hz, 6H); ^{13}C NMR (75 MHz, $CDCl_3$) δ 166.08, 150.18, 148.87, 145.90, 145.21, 141.23, 127.55, 127.43, 126.89, 123.33, 120.89, 33.63, 29.96, 24.03; HR-ESI-MS (*m/z*): 338.1321, calcd for $[M + H]^+$ $C_{19}H_{20}ON_3S$: 338.1322.

(2*Z*,5*Z*)-2-((4-butylphenyl)imino)-3-methyl-5-(pyridin-4-ylmethylene)thiazolidin-4-one (67). Using the same procedure as for **8**, this compound was obtained from **59** (786 mg, 3.00 mmol, 1.0 eq.) as yellow solid (748 mg, 2.13 mmol, 71 %). m.p. 104.6-105.2°C. ^{1}H NMR (300 MHz, $CDCl_3$) δ 8.57 (d, *J* = 6.2 Hz, 2H), 7.55 (s, 1H), 7.22 (d, *J* = 6.2 Hz, 2H), 7.13 (d, *J* = 8.3 Hz, 2H), 6.84 (d, *J* = 8.3 Hz, 2H), 3.39 (s, 3H), 2.88 – 2.31 (m, 2H), 1.77 – 1.42 (m, 2H), 1.31 (q, *J* = 7.4 Hz, 3H), 0.87 (t, *J* = 7.3 Hz, 3H); ^{13}C NMR (75 MHz, $CDCl_3$) δ 166.13, 150.26, 149.07, 145.21, 141.18, 140.02, 129.42, 127.50, 126.98, 123.36, 120.88, 35.20, 33.64, 29.99, 22.45, 14.03; HR-ESI-MS (*m/z*): 352.1471, calcd for $[M + H]^+$ $C_{20}H_{22}ON_3S$: 352.1478.

(2*Z*,5*Z*)-2-((4-(*tert*-butyl)phenyl)imino)-3-methyl-5-(pyridin-4-ylmethylene)thiazolidin-4-one (68). Using the same procedure as for **8**, this compound was obtained from **60** (786 mg, 3.00 mmol, 1.0 eq.) as yellow solid (453 mg, 1.29 mmol, 43 %). m.p. 154.9-158.4°C.^{1}H NMR (300 MHz, $CDCl_3$) δ 8.58 – 8.56 (m, 2H), 7.55 (s, 1H), 7.33 (d, *J* = 8.6 Hz, 2H), 7.21 (d, *J* = 6.2 Hz, 2H), 6.87 (d, *J* = 8.5 Hz, 2H), 3.38 (s, 3H), 1.27 (s, 9H); ^{13}C NMR (75 MHz, $CDCl_3$) δ 166.16, 150.56, 148.92, 148.20, 144.87, 140.90, 127.28, 127.09, 126.37, 123.28, 120.63, 34.53, 31.47, 29.99; HR-ESI-MS (*m/z*): 352.1470, calcd for $[M + H]^+$ $C_{20}H_{22}ON_3S$: 352.1478.

(2*Z*,5*Z*)-3-methyl-5-(pyridin-4-ylmethylene)-2-((4-(trifluoromethyl)phenyl)imino)thiazolidin-4-one (69). Using the same procedure as for **8**, this compound was obtained from **61** (822 mg, 3.00 mmol, 1.0 eq.) as yellow solid (643 mg, 1.77 mmol, 59 %).m.p. 167.7-168.6°C. ^{1}H NMR (300 MHz, DMSO-d_6) δ 8.69 – 8.67 (m, 12), 7.82 – 7.77 (m, 3H), 7.50 (dd, *J* = 4.6, 1.7 Hz, 2H), 7.26 (d, *J* = 8.6 Hz, 2H), 3.38 (s, 3H); ^{13}C NMR (75 MHz, DMSO-d_6) δ 165.37, 151.10, 150.87, 150.54, 140.14, 127.62, 126.79, 126.74, 126.10, 126.07, 125.48, 125.05, 124.63, 123.19, 122.50, 121.79, 29.72; HR-ESI-MS (*m/z*): 364.0724, calcd for $[M + H]^+$ $C_{17}H_{13}ON_3F_3S$: 364.0726.

(2*Z*,5*Z*)-2-((4-bromophenyl)imino)-3-methyl-5-(pyridin-4-ylmethylene)thiazolidin-4-one (70). Using the same procedure as for **8**, this compound was obtained from **62** (855 mg, 3.00 mmol, 1.0 eq.) as yellow solid (426 mg, 1.77 mmol, 59 %). m.p. 191.9-192.3°C.^{1}H NMR (300 MHz, $CDCl_3$) δ

8.59 (d, *J* = 6.2 Hz, 2H), 7.58 (s, 1H), 7.43 (d, *J* = 8.6 Hz, 2H), 7.22 (d, *J* = 6.2 Hz, 2H), 6.81 (d, *J* = 8.6 Hz, 2H), 3.38 (s, 3H); ^{13}C NMR (75 MHz, $CDCl_3$) δ 165.93, 150.30, 150.23, 146.75, 140.94, 132.56, 127.63, 126.83, 123.27, 122.85, 118.44, 29.93; HR-ESI-MS (*m/z*): 373.9961, calcd for $[M + H]^+$ $C_{16}H_{13}ON_3BrS$: 373.9957.

(*Z*)-2-((4-ethylphenyl)imino)thiazolidin-4-one (71). 4-Ethylphenylisothiocyanate (2.00 g, 12.3 mmol, 1.0 eq.) was refluxed in a saturated NH_3 solution of MeOH (10 mL) for 18 h. The solution was cooled to room temperature and evaporated *in vacuo* to afford a pale yellow solid. The solid was added to a solution of ethyl chloroacetate (2.63 mL, 24.6 mmol, 2 eq.) and sodium acetate (2.98 g, 36.9 mmol, 3 eq.) in ethanol (33 mL), and the mixture was stirred at 78 °C for 6 h. After removal of EtOH *in vacuo*, the resulting solid was dissolved in EtOAc (200 mL) and washed with brine (5 x 40 mL) and water (5 x 40 mL). Evaporation of EtOAc *in vacuo* afforded the product as brown solid (2.41 g, 10.9 mmol, 89.0 %), which was used for the next steps without further purification.

(*Z*)-2-((4-ethylphenyl)imino)-3-ethylthiazolidin-4-one (72). Using the same procedure as for **54**, this compound was obtained from ethyl isothiocyanate (1.31 g, 15.0 mmol, 1.0 eq.) as yellow oil (2.61 g, 10.8 mmol, 72 %). ^{1}H NMR (300 MHz, DMSO-d_6) δ 7.21 (dd, *J* = 8.1, 1.5 Hz, 2H), 6.88 (dd, *J* = 8.2, 1.5 Hz, 2H), 4.02 (d, *J* = 1.4 Hz, 2H), 3.78 (qd, *J* = 7.0, 1.4 Hz, 2H), 2.61 (dt, *J* = 8.4, 7.0 Hz, 2H), 1.22 – 1.17 (m, 6H); ^{13}C NMR (75 MHz, DMSO-d_6) δ 171.65, 154.45, 145.75, 139.53, 128.49, 120.77, 37.35, 32.46, 27.57, 15.54, 12.27; ESI-MS (*m/z*): 249.11

(*Z*)-2-((4-ethylphenyl)imino)-3-(2-methoxyethyl)thiazolidin-4-one (73). A solution of 4-ethylaniline (2.15 mL, 17.3 mmol, 1.15 eq.) in EtOH (50 mL) was treated with 2-methoxyethyl isothiocyanate (1.76 g, 15.0 mmol, 1.0 eq.) and stirred at 78 °C for 12 h. The solution was then treated with NaOAc (6.23 g, 75.0 mmol, 5.0 eq.) and ethyl chloroacetate (3.22 mL, 30.0 mmol, 2.0 eq.) and stirred at 78 °C for another 5 h. EtOH was evaporated *in vacuo* to afford the crude title compound as brown solid (4.18 g, 15.0 mmol, quant.). m.p. 51.0-51.1°C.^{1}H NMR (300 MHz, $CDCl_3$) δ 7.09 (d, *J* = 8.2 Hz, 2H), 6.81 (d, *J* = 8.2 Hz, 2H), 3.99 (t, *J* = 5.6 Hz, 2H), 3.72 (s, 2H),

3.62 (t, *J* = 5.6 Hz, 2H), 3.29 (s, 3H), 2.55 (q, *J* = 7.6 Hz, 2H), 1.15 (t, *J* = 7.6 Hz, 3H); ^{13}C NMR (75 MHz, $CDCl_3$) δ 171.82, 154.23, 145.33, 140.66, 128.64, 120.95, 68.52, 58.65, 42.09, 32.74, 28.37, 15.60; HR-ESI-MS (*m/z*): 279.1159, calcd for $[M + H]^+$ $C_{14}H_{19}O_2N_2S$: 279.1162.

(*Z*)-3-(cyclohexylmethyl)-2-((4-ethylphenyl)imino)thiazolidin-4-one (74). Using the same procedure as for **54**, this compound was obtained from cyclohexylmethyl isothiocyanate (2.33 g, 15.0 mmol, 1.0 eq.) as brown oil (2.80 g, 8.85 mmol, 59 %). ^{1}H NMR (300 MHz, $CDCl_3$) δ 7.10 (d, *J* = 8.2 Hz, 2H), 6.81 (d, *J* = 8.2 Hz, 2H), 3.73 (s, 2H), 3.65 (d, *J* = 7.4 Hz, 2H), 2.57 (q, *J* = 7.6 Hz, 2H), 1.86 (ddd, *J* = 11.0, 7.7, 3.5 Hz, 1H), 1.65 – 1.61 (m, 5H), 1.23 – 0.92 (m, 8H); ^{13}C NMR (75 MHz, $CDCl_3$) δ 172.10, 154.70, 145.45, 140.67, 128.65, 120.93, 49.11, 35.88, 32.65, 30.69, 28.39, 26.32, 25.78, 15.64; HR-ESI-MS (*m/z*): 317.1674, calcd for $[M + H]^+$ $C_{18}H_{25}ON_2S$: 317.1682.

(2*Z*,5*Z*)-2-((4-ethylphenyl)imino)-5-(pyridin-4-ylmethylene)thiazolidin-4-one (75). Using the same procedure as for **8**, this compound was obtained from **71** (660 mg, 3.00 mmol, 1.0 eq.) as yellow solid (417 mg, 1.35 mmol, 45 %). m.p. > 300°C (dec.). ^{1}H NMR (300 MHz, DMSO-d_6) δ 12.15 (s, 1H), 8.74 (dd, *J* = 4.5, 1.7 Hz, 1H), 8.67 (dd, *J* = 4.5, 1.7 Hz, 1H), 7.71 – 7.69 (m, 2H), 7.60 – 7.56 (m, 1H), 7.47 (dd, *J* = 4.6, 1.7 Hz, 1H), 7.29 (dd, *J* = 8.6, 7.0 Hz, 2H), 7.02 (d, *J* = 8.1 Hz, 1H), 2.63 (qd, *J* = 7.6, 3.3 Hz, 2H), 1.25 – 1.18 (m, 3H); ^{13}C NMR (75 MHz, DMSO-d_6) δ 150.51, 150.47, 128.78, 128.38, 127.03, 126.34, 123.98, 123.10, 121.55, 120.82, 27.60, 15.52, 15.44; ESI-MS (*m/*z): 310.10.

(2*Z*,5*Z*)-3-ethyl-2-((4-ethylphenyl)imino)-5-(pyridin-4-ylmethylene)thiazolidin-4-one (76). This compound was prepared from **72** (744 mg, 3.00 mmol, 1.0 eq.) using the same procedure as for **8**. The yellow precipitate was further purified by FC (SiO_2; hexane/EtOAc 2:1) to afford the product as yellow solid (182 mg, 0.54 mmol, 18 %). m.p. 177.7-178.5°C. ^{1}H NMR (300 MHz, $CDCl_3$) δ 8.59 – 8.57 (m, 2H), 7.55 (s, 1H), 7.25 – 7.14 (m, 4H), 6.86 (d, *J* = 8.2 Hz, 2H), 4.00 (q, *J* = 7.1 Hz, 2H), 2.61 (q, *J* = 7.6 Hz, 2H), 1.30 (t, *J* = 7.1 Hz, 3H), 1.20 (t, *J* = 7.6 Hz, 3H); ^{13}C NMR (75 MHz,

$CDCl_3$) δ 165.86, 150.03, 148.31, 145.35, 141.50, 141.26, 128.87, 127.91, 126.67, 123.42, 120.95, 38.78, 28.40, 15.54, 12.81; ESI-MS (*m/*z): 338.13.

(2*Z*,5*Z*)-2-((4-ethylphenyl)imino)-3-(2-methoxyethyl)-5-(pyridin-4-ylmethylene)thiazolidin-4-one (77). A solution of **73** (834 mg, 3.00 mmol, 1.0 eq.) and piperidine (0.65 mL, 6.6 mmol, 2.2 eq.) in EtOH (5 mL) was treated with 4-pyridinecarboxaldehyde (0.56 mL, 6.0 mmol, 2.0 eq.) and heated to 78 °C. After 12 h, the reaction mixture was cooled to 0 °C, filtered, and the filter residue washed with ice-cold EtOH (3 x 5 mL).The yellow solid was further purified by FC (SiO_2; hexane/EtOAc 2:1) to afford **77** as yellow solid (361 mg, 0.984 mmol, 32.8 %). m.p. 112.9-114.0°C.^{1}H NMR (300 MHz, $CDCl_3$) δ 8.57 (d, *J* = 5.0 Hz, 2H), 7.55 (s, 1H), 7.23 (d, *J* = 6.2 Hz, 2H), 7.14 (d, *J* = 8.2 Hz, 1H), 6.84 (d, *J* = 8.2 Hz, 2H), 4.14 (t, *J* = 5.6 Hz, 2H), 3.69 (t, *J* = 5.6 Hz, 2H), 2.59 (q, *J* = 7.6 Hz, 3H), 1.19 (t, *J* = 7.6 Hz, 3H); ^{13}C NMR (75 MHz, $CDCl_3$) δ 166.10, 150.01, 148.54, 145.22, 141.44, 141.28, 128.86, 127.58, 127.01, 123.42, 120.93, 68.61, 58.72, 42.46, 28.39, 15.55; HR-ESI-MS (*m/z*): 368.1433, calcd for $[M + H]^+$ $C_{20}H_{22}O_2N_3S$: 368.1429.

(2*Z*,5*Z*)-3-(cyclohexylmethyl)-2-((4-ethylphenyl)imino)-5-(pyridin-4-ylmethylene)thiazolidin-4-one (78). Using the same procedure as for **8**, this compound was obtained from **74** (948 mg, 3.00 mmol, 1.0 eq.) as yellow solid (767 mg, 1.89 mmol, 63 %). m.p. 147.8-148.7°C.^{1}H NMR (300 MHz, $CDCl_3$) δ 8.57 (d, *J* = 5.3 Hz, 2H), 7.53 (s, 0H), 7.22 (d, *J* = 5.1 Hz, 1H), 7.15 (d, *J* = 7.9 Hz, 4H), 6.84 (d, *J* = 8.0 Hz, 2H), 3.79 (d, *J* = 7.4 Hz, 12), 2.60 (q, *J* = 7.6 Hz, 1H), 1.92 (dd, *J* = 13.3, 7.6 Hz, 5H), 1.67 – 1.62 (m, 2H), 1.22 – 0.99 (m, 8H); ^{13}C NMR (75 MHz, $CDCl_3$) δ 166.44, 150.30, 148.92, 145.45, 141.25, 141.19, 128.85, 127.51, 126.83, 123.35, 120.89, 49.44, 36.20, 30.73, 28.42, 26.30, 25.77, 15.60; HR-ESI-MS (*m/z*): 406.1941, calcd for $[M + H]^+$ $C_{24}H_{28}ON_3S$: 406.1948.

(2*Z*,5*Z*)-5-((2-aminopyridin-4-yl)methylene)-2-((4-ethylphenyl)imino)-3-methylthiazolidin-4-one (79). A solution of 4-thiazolidinone **54** (2.69 g, 11.5 mmol, 1.0 eq.) and piperidine (3.90 mL, 39.6 mmol, 3.44 eq.) in EtOH (6 mL) was treated with *tert*-Butyl(4-formylpyridin-2-yl)carbamate

(3.85 g, 17.3 mmol, 1.5 eq.) and stirred at 75 °C for 15 h. The solution was cooled to 0 °C and filtered. The yellow solid on the filter was washed with ice-cold EtOH (2 x 20 mL) and then added to TFA (6 mL). After 4 h, the solution was diluted with H_2O (100 mL) and CH_2Cl_2 (100 mL) and neutralized with NaOH (1 M) to pH = 7. The organic phase was washed with H_2O (3 x 20 mL), dried over $MgSO_4 \cdot 2H_2O$, and evaporated *in vacuo* to afford **79** as a yellow solid (2.45 g, 7.25 mmol, 63.1 %). m.p. 191.2-199.7°C. ^{1}H NMR (300 MHz, DMSO-d_6) δ 7.96 (d, J = 5.6 Hz, 1H), 7.52 (s, 1H), 7.25 (d, J = 8.3 Hz, 2H), 6.94 (d, J = 8.3 Hz, 2H), 6.65 (dd, J = 5.8, 1.6 Hz, 1H), 6.59 (d, J = 1.5 Hz, 1H), 3.33 (s, 3H), 2.62 (q, J = 7.6 Hz, 2H), 1.20 (t, J = 7.6 Hz, 3H); ^{13}C NMR (75 MHz, DMSO-d_6) δ 165.45, 158.85, 149.19, 145.86, 145.13, 142.69, 140.30, 128.78, 127.36, 126.35, 120.86, 111.78, 108.14, 29.72, 27.57, 15.41; HR-ESI-MS (*m/z*): 339.1271, calcd for $[M + H]^+$ $C_{18}H_{19}ON_4S$: 339.1274.

3-amino-N-(4-((*Z*)-((*Z*)-2-((4-ethylphenyl)imino)-3-methyl-4-oxothiazolidin-5-ylidene)methyl)pyridin-2-yl)propanamide (TFA salt) (80). A solution of **79** (100 mg, 0.296 mmol, 1.0 eq.), EDC·HCl (170 mg, 0.888 mmol, 3.0 eq.), and pyridine (71 µL, 0.888 mmol, 3.0 eq.) in DMF (2.0 mL) was treated with N-(*tert*-butoxycarbonyl)-3-aminopropionic acid (84 mg, 0.444 mmol, 1.5 eq.) and stirred overnight. Then, the solution was treated with EtOAc (10 mL), washed with H_2O (3 x 10 mL), and evaporated *in vacuo*. The crude was redissolved in TFA/THF (1:1) and stirred for 5 h. The mixture was then diluted with H_2O and neutralized with NaOH (1 M) to pH = 7. The organic phase was washed with H_2O (3 x 20 mL), dried over $MgSO_4 \cdot 2H_2O$, and evaporated *in vacuo*. The crude was purified by RP-HPLC (A(70%)/D(30%) to A(45%)/D(55%), 40 min gradient), and **80** was obtained as yellow solid after lyophilization (7.7 mg, 0.015 mmol, 5.1 %). ^{1}H NMR (300 MHz, DMSO-d_6) δ 10.86 (s, 1H), 8.41 (d, J = 5.3 Hz, 1H), 8.20 (s, 1H), 7.76 (s, 3H), 7.65 (s, 1H), 7.27 – 7.21 (m, 3H), 6.96 (d, J = 8.3 Hz, 2H), 3.35 (s, 3H), 3.07 (q, J = 6.2 Hz, 2H), 2.77 (t, J = 6.7 Hz, 2H), 2.63 (q, J = 7.6 Hz, 2H), 1.21 (t, J = 7.6 Hz, 3H); ^{13}C NMR (75 MHz, DMSO-d_6) δ 169.46, 165.39, 152.52, 149.06, 145.05, 142.31, 140.41, 128.74, 127.03, 126.80,

120.89, 119.12, 112.44, 34.61, 33.34, 29.77, 27.59, 15.50; HR-ESI-MS (*m/z*): 410.1638, calcd for $[M + H]^+$ $C_{21}H_{24}O_2N_2S$: 410.1645.

3-((4-((*Z*)-((*Z*)-2-((4-ethylphenyl)imino)-3-methyl-4-oxothiazolidin-5-ylidene)methyl)pyridin-2-yl)amino)-3-oxopropanoic acid (81). Using the same procedure as for **80**, this compound was obtained from mono-*tert*-butyl malonate (70 mg, 0.44 mmol, 1.5 eq.) as yellow solid (37 mg, 0.086 mmol, 29 %). m.p. 116.1-116.2°C. ^{1}H NMR (300 MHz, DMSO-d_6) δ 10.82 (s, 1H), 8.41 (d, J = 5.1 Hz, 1H), 8.21 (s, 1H), 7.66 (s, 1H), 7.26 (d, J = 8.3 Hz, 2H), 7.22 (dd, J = 5.3, 1.7 Hz, 1H), 6.96 (d, J = 8.2 Hz, 2H), 3.47 (s, 2H), 3.36 (s, 3H), 2.64 (q, J = 7.5 Hz, 2H), 1.22 (t, J = 7.6 Hz, 3H); ^{13}C NMR (75 MHz, DMSO-d_6) δ 169.11, 165.71, 165.36, 152.45, 149.01, 148.89, 145.01, 142.42, 140.35, 128.75, 127.04, 126.82, 120.85, 119.12, 112.35, 43.60, 29.75, 27.59, 15.44; HR-ESI-MS (*m/z*): 425.1274, calcd for $[M + H]^+$ $C_{21}H_{21}O_4N_4S$: 425.1278.

3-((4-((*Z*)-((*Z*)-2-((4-ethylphenyl)imino)-3-methyl-4-oxothiazolidin-5-ylidene)methyl)pyridin-2-yl)amino)-4-oxobutanoic acid (82). Succinic anhydride (443 mg, 4.43 mmol, 10 eq.) was added to a solution of amine **79** (150 mg, 0.443 mmol, 1 eq.) and pyridine (700 µL, 8.86 mmol, 20 eq.) in DMF (0.9 mL). The mixture was stirred for 12 h, and then EtOAc (40 mL) was added. The organic phase was washed with 1 M HCl (40 mL), brine (2 x 40 mL) and H_2O (20 mL). The solvent was evaporated *in vacuo*, and the crude was purified by RP-HPLC to afford the product as yellow solid after lyophylization (5.8 mg, 0.013 mmol, 3.1 %). ^{1}H NMR (300 MHz, DMSO-d_6) δ 10.69 (d, J = 1.8 Hz, 1H), 8.40 (dd, J = 5.3, 1.7 Hz, 1H), 8.24 (s, 1H), 7.66 (d, J = 1.7 Hz, 1H), 7.28 (dd, J = 8.4, 1.9 Hz, 2H), 7.20 (d, J = 5.3 Hz, 1H), 6.98 (dd, J = 8.4, 1.8 Hz, 2H), 3.37 (d, J = 1.8 Hz, 3H), 2.64 (dd, J = 4.8, 2.3 Hz, 4H), 1.23 (td, J = 7.6, 1.7 Hz, 3H); ^{13}C NMR (75 MHz, DMSO-d_6) δ 173.66, 171.30, 165.40, 152.79, 149.23, 148.88, 145.07, 142.24, 140.41, 128.73, 127.11, 126.71, 120.90, 118.66, 112.39, 30.89, 29.73, 28.42, 27.59, 15.46; HR-ESI-MS (*m/z*): 439.1431, calcd for $[M + H]^+$ $C_{22}H_{23}O_4N_4S$: 439.1435.

3-((4-((*Z*)-((*Z*)-2-((4-ethylphenyl)imino)-3-methyl-4-oxothiazolidin-5-ylidene)methyl)pyridin-2-yl)amino)-5-oxopentanoic acid (83). Glutaric anhydride (506 mg, 4.44 mmol, 15 eq.) was added to a solution of amine **79** (100 mg, 0.296 mmol, 1 eq.) and pyridine (239 µL, 2.96 mmol, 10 eq.) in DMF (2.0 mL). The solution was heated to 100 °C for 1 h. The yellow precipitate was filtered and washed with EtOAc (2 x 30 mL) and H_2O (30 mL). The product was dried on HV overnight to afford 90 mg (0.20 mmol, 67 %) of the product as yellow solid. m.p. 266.8-273.9°C. ^{1}H NMR (300 MHz, DMSO-d_6) δ 12.09 (s, 1H), 10.62 (s, 1H), 8.39 (d, J = 5.2 Hz, 1H), 8.27 (d, J = 1.8 Hz, 1H), 7.66 (s, 1H), 7.27 (d, J = 8.3 Hz, 2H), 7.20 (dd, J = 5.3, 1.6 Hz, 1H), 6.98 (d, J = 8.2 Hz, 2H), 3.37 (s, 3H), 2.64 (q, J = 7.6 Hz, 2H), 2.44 (t, J = 7.3 Hz, 2H), 2.27 (t, J = 7.4 Hz, 2H), 1.79 (p, J = 7.4 Hz, 2H), 1.22 (t, J = 7.6 Hz, 3H); ^{13}C NMR (75 MHz, DMSO-d_6) δ 174.02, 171.90, 165.41, 152.82, 149.27, 148.91, 145.09, 142.16, 140.41, 128.70, 127.13, 126.67, 120.90, 118.77, 112.43, 35.04, 32.91, 29.72, 27.58, 20.10, 15.46; HR-ESI-MS (*m/z*): 453.1594, calcd for $[M + H]^+$ $C_{23}H_{25}O_4N_4S$: 453.1591.

(2*Z*,5*Z*)-2-((4-ethylphenyl)imino)-3-methyl-5-((2-(phenylamino)pyridin-4-yl)methylene)thiazolidin-4-one (84): Degassed dioxane (1.2 mL) was added to a flask containing amine **79** (100 mg, 0.296 mmol, 1.0 eq.), $Pd_2(dba)_3$ (5.1 mg, 0.0088 mmol, 0.03 eq.), Xantphos (10 mg, 0.018 mmol, 0.06 eq.), Cs_2CO_3 (116 mg, 0.355 mmol, 1.2 eq.), and phenyl bromide (51 mg, 0.33 mmol, 1.1 eq.) under argon. The suspension was degassed and refilled with argon (5 x) and then heated to 100 °C. The reaction mixture was stirred overnight at 100 °C, then cooled to room temperature, filtered, and concentrated *in vacuo*. The crude was purified by FC (SiO_2; DCM, 0 to 2 % MeOH) to afford **84** as a yellow solid (43 mg, 0.104 mmol, 35 %). m.p. 181-182°C. ^{1}H NMR (300 MHz, $CDCl_3$) δ 8.09 (d, J = 5.4 Hz, 1H), 7.46 (s, 1H), 7.19 – 7.15 (m, 7H), 7.01 – 6.96 (m, 1H), 6.86 – 6.80 (m, 3H), 6.67 (dd, J = 5.4, 1.6 Hz, 1H), 3.38 (s, 3H), 2.65 (q, J = 7.5 Hz, 2H), 1.23 (t, J = 7.6 Hz, 3H); ^{13}C NMR (75 MHz, $CDCl_3$) δ 165.16, 155.39, 148.36, 146.90, 144.35, 142.25, 140.13, 138.25, 128.49, 128.45, 127.85, 127.80, 126.57, 126.14, 122.79, 120.15, 119.94, 113.60,

106.55, 28.86, 27.37, 14.50; HR-ESI-MS (*m/z*): 415.1581, calcd for $[M + H]^+$ $C_{24}H_{23}ON_4S$: 415.1587.

(2*Z*,5*Z*)-2-((4-ethylphenyl)imino)-3-methyl-5-((2-(pyridin-2-ylamino)pyridin-4-yl)methylene)thiazolidin-4-one (85). Using the same procedure as for **84** and after purification by RP-HPLC (A(70%)/D(30%) to A(45%)/D(55%), 40 min gradient), this compound was obtained from 2-bromopyridine (52 mg, 0.33 mmol, 1.1 eq.) as yellow solid after lyophilization (6.0 mg, 0.015 mmol, 4.9 %). ^{1}H NMR (300 MHz, DMSO-d_6) δ 8.39 (d, J = 5.4 Hz, 1H), 8.05 (s, 1H), 7.90 (s, 12), 7.72 (s, 1H), 7.36 – 7.30 (m, 3H), 7.24 (dd, J = 5.5, 1.7 Hz, 1H), 7.05 – 6.99 (m, 3H), 3.38 (s, 3H), 2.68 (q, J = 7.5 Hz, 2H), 1.25 (t, J = 7.5 Hz, 3H); ^{13}C NMR (75 MHz, DMSO-d_6) δ 165.52, 149.45, 145.34, 140.36, 128.77, 127.92, 126.61, 120.87, 117.68, 116.47, 113.33, 110.71, 69.76, 29.75, 27.58, 15.44.); HR-ESI-MS (*m/z*): 416.1531, calcd for $[M + H]^+$ $C_{23}H_{22}ON_5S$: 416.1540.

(2*Z*,5*Z*)-2-((4-ethylphenyl)imino)-5-((2-((4-(hydroxymethyl)phenyl)amino)pyridin-4-yl)methylene)-3-methylthiazolidin-4-one (86). Using the same procedure as for **84** and after purification by RP-HPLC (A(70%)/D(30%) to A(45%)/D(55%), 40 min gradient), this compound was obtained from 4-hydroxymethyl-1-bromobenzene (62 mg, 0.33 mmol, 1.1 eq.) as yellow solid afterr lyophilization (3.0 mg, 0.0070 mmol, 2.3 %). ^{1}H NMR (300 MHz, DMSO-d_6) δ 9.43 (s, 1H), 8.19 (d, J = 5.4 Hz, 1H), 7.62 (s, 1H), 7.55 (d, J = 8.5 Hz, 2H), 7.29 (d, J = 8.3 Hz, 2H), 7.22 (d, J = 8.5 Hz, 2H), 6.99 (d, J = 8.3 Hz, 2H), 6.90 – 6.87 (m, 2H), 4.44 (s, 2H), 3.37 (s, 3H), 2.66 (q, J = 7.6 Hz, 2H), 1.24 (t, J = 7.6 Hz, 3H); ^{13}C NMR (75 MHz, DMSO-d_6) δ 165.45, 155.98, 149.13, 147.32, 145.10, 142.06, 140.33, 139.21, 135.66, 128.79, 127.40, 127.14, 126.23, 120.86, 118.71, 113.86, 109.43, 62.73, 29.74, 27.56, 15.40; HR-ESI-MS (*m/z*): 445.1685, calcd for $[M + H]^+$ $C_{25}H_{25}O_2N_4S$: 445.1693.

4-((4-((*Z*)-((*Z*)-2-((4-ethylphenyl)imino)-3-methyl-4-oxothiazolidin-5-ylidene)methyl)pyridin-2-yl)amino)benzoic acid (87). Using the same procedure as for **84** and after purification by RP-HPLC (A(70%)/D(30%) to A(45%)/D(55%), 40 min gradient), this compound was obtained from

4-bromobenzoic acid (66 mg, 0.33 mmol, 1.1 eq.) as yellow solid after lyophilization (15 mg, 0.033 mmol, 11 %). ^{1}H NMR (300 MHz, DMSO-d_6) δ 9.74 (s, 1H), 8.31 (d, J = 6.0 Hz, 1H), 7.87 – 7.84 (m, 2H), 7.79 – 7.76 (m, 2H), 7.64 (s, 1H), 7.29 (d, J = 8.3 Hz, 2H), 7.00 – 6.97 (m, 4H), 3.37 (s, 3H), 2.65 (q, J = 7.6 Hz, 2H), 1.23 (t, J = 7.6 Hz, 3H); ^{13}C NMR (75 MHz, DMSO-d_6) δ 167.07, 165.46, 155.68, 149.08, 148.31, 145.43, 145.09, 141.79, 140.34, 130.43, 128.80, 127.35, 126.15, 122.23, 120.86, 116.86, 115.31, 110.23, 29.76, 27.55, 15.40; HR-ESI-MS (*m/z*): 459.1479, calcd for $[M + H]^+$ $C_{25}H_{23}O_3N_4S$: 459.1485.

(2*Z*,5*Z*)-5-((2-((4-(1*H*-tetrazol-5-yl)phenyl)amino)pyridin-4-yl)methylene)-2-((4-ethylphenyl)imino)-3-methylthiazolidin-4-one (88). Degassed dioxane (1.2 mL) was added to a flask containing amine **79** (100 mg, 0.296 mmol, 1.0 eq.), $Pd_2(dba)_3$ (5.1 mg, 0.0088 mmol, 0.03 eq.), Xantphos (10 mg, 0.018 mmol, 0.06 eq.), Cs_2CO_3 (116 mg, 0.355 mmol, 1.2 eq.), and 5-(4-bromophenyl)-1H-tetrazole (73.4 mg, 0.326 mmol, 1.1 eq.) under argon. The suspension was degassed and refilled with argon (5 x) and then heated to 100 °C. The reaction mixture was stirred overnight at 100 °C, then cooled to room temperature, filtered, and concentrated *in vacuo*. The crude was purified by RP-HPLC (A/D 70:30 to A/D 45:55, 40 min gradient) to afford the title compound as yellow solid after lyophilization (12 mg, 0.024 mmol, 8.2 %). ^{1}H NMR (400 MHz, DMSO-d_6) δ 9.72 (s, 1H), 8.30 – 8.29 (m, 1H), 7.95 – 7.92 (m, 2H), 7.89 – 7.87 (m, 2H), 7.62 (s, 1H), 7.27 (d, J = 8.3 Hz, 2H), 6.98 – 6.94 (m, 4H), 2.62 (q, J = 7.6 Hz, 2H), 1.21 (t, J = 7.6 Hz, 3H); ^{13}C NMR (101 MHz, DMSO-d_6) δ 165.45, 155.70, 149.07, 148.18, 145.08, 143.91, 141.81, 140.31, 128.79, 127.67, 127.34, 126.13, 120.85, 118.03, 115.11, 110.23, 29.74, 27.53, 15.38; HR-ESI-MS (*m/z*): 483.1712, calcd for $[M + H]^+$ $C_{25}H_{23}ON_8S$: 483.1710.

(*Z*)- and (*E*)-1-(2-aminopyridin-4-yl)-5-((4-ethylphenyl)imino)-6-methyl-4-thia-6-azaspiro[2.4]heptan-7-one *rac*-89 and *rac*-90. NaH (190 mg, 4.72 mmol, 4.0 eq.) was added to a solution of Me_3SOI (520 mg, 2.36 mmol, 2.0 eq.) in DMF (12 mL) at 0 °C. The reaction mixture was stirred for 15 min at 0 °C. Then, amine **79** (400 mg, 1.18 mmol, 1.0 eq.) dissolved in DMF (12 mL) was added to the reaction mixture at 0 °C. After 50 min, EtOAc (20 mL) and H_2O (20 mL)

were added, and the pH of the aqueous phase was adjusted to pH = 8 using 1 M HCl. The organic phase was separated, washed with H_2O (3 x 20 mL), and evaporated *in vacuo*. The crude was purified by FC (SiO_2; CH_2Cl_2, 0 to 3 % MeOH) to give a major isomer as off-white foam (156 mg, 0.437 mmol, 37.0 %) and a minor isomer as a colorless oil. The minor isomer was further purified by RP-HPLC to afford 5.0 mg (0.014 mmol, 1.3 %) of a white solid. The (*E*) or (*Z*) configuration of the two isomers could not be assigned.

Major isomer: ^{1}H NMR (400 MHz, $CDCl_3$) δ 7.90 (d, *J* = 6.1 Hz, 1H), 7.14 (d, *J* = 8.3 Hz, 2H), 6.83 (d, *J* = 8.3 Hz, 2H), 6.33 (dd, *J* = 5.6, 1.6 Hz, 1H), 6.28 (s, 1H), 5.01 (br s, 1H), 3.36 (s, 3H), 2.96 (dd, *J* = 9.5, 7.7 Hz, 1H), 2.61 (q, *J* = 7.6 Hz, 2H), 2.16 (dd, *J* = 9.5, 6.0 Hz, 1H), 1.66 (dd, *J* = 7.7, 6.0 Hz, 1H), 1.22 (t, *J* = 7.6 Hz, 3H); ^{13}C NMR (101 MHz, $CDCl_3$) δ 173.46, 157.78, 152.30, 147.70, 145.83, 145.55, 140.69, 128.72, 128.66, 120.77, 120.74, 112.90, 108.21, 38.09, 30.90, 29.95, 28.29, 20.48, 15.44; HR-ESI-MS (*m/z*): 353.1425, calcd for $[M + H]^+$ $C_{19}H_{21}ON_4S$: 353.1431.

Minor isomer: ^{1}H NMR (400 MHz, $CDCl_3$) δ 7.63 (s, 1H), 7.13 (d, *J* = 6.4 Hz, 2H), 6.86 (s, 3H), 6.68 (s, 1H), 3.22 (s, 3H), 2.58 (m, *J* = 7.6 Hz, 3H), 2.29 (s, 1H), 1.83 (s, 1H), 1.18 (t, *J* = 7.5 Hz, 3H); ^{13}C NMR (101 MHz, $CDCl_3$) δ 169.60, 153.07, 151.21, 150.88, 144.23, 140.24, 133.43, 127.79, 119.84, 113.16, 112.64, 35.00, 33.03, 29.21, 27.34, 19.35, 14.51; HR-ESI-MS (*m/z*): 353.1427, calcd for $[M + H]^+$ $C_{19}H_{21}ON_4S$: 353.1431

(±)-(*Z*)-5-((2-aminopyridin-4-yl)methyl)-2-((4-ethylphenyl)imino)-3-methylthiazolidin-4-one (*rac*-91). A flask containing amine **79** (150 mg, 0.444 mmol, 1.0 eq.), Pd/C (47 mg) and EtOAc (9 mL) was evacuated and refilled with argon (3 x). Then, H_2 was added via a septum inlet. The black suspension was stirred for 12 h and then filtered over celite. The celite was washed with EtOAc (3 x 20 mL). EtOAc was evaporated *in vacuo*, and the remaining crude was purified by FC (SiO_2; CH_2Cl_2, 0 to 5 % MeOH) to give the product as colorless oil (95 mg, 0.28 mmol, 63 %). ^{1}H NMR (300 MHz, DMSO-d_6) δ 7.80 (d, *J* = 5.2 Hz, 1H), 7.18 (d, *J* = 8.3 Hz, 2H), 6.82 (d, *J* = 8.2 Hz, 2H),

6.35 (dd, *J* = 5.3, 1.5 Hz, 1H), 6.25 (s, 1H), 5.90 (s, 2H), 4.75 – 4.70 (m, 1H), 3.29 (dd, *J* = 14.2, 4.1 Hz, 1H), 3.18 (s, 3H), 2.85 (dd, *J* = 14.2, 10.1 Hz, 1H), 2.58 (q, *J* = 7.6 Hz, 2H), 1.18 (t, *J* = 7.6 Hz, 3H); ^{13}C NMR (75 MHz, DMSO-d_6) δ 173.41, 159.88, 153.71, 147.86, 146.52, 145.67, 139.60, 128.50, 120.71, 112.29, 107.77, 47.97, 37.29, 29.26, 27.54, 15.49; HR-ESI-MS (*m/z*): 341.1424, calcd for $[M + H]^+$ $C_{18}H_{21}ON_4S$: 341.1431.

(±)-(*Z*)-6-((4-((2-((4-ethylphenyl)imino)-3-methyl-4-oxothiazolidin-5-yl)methyl)pyridin-2-yl)amino)nicotinic acid (*rac*-92). Degassed dioxane (0.6 mL) was added to a flask containing *rac*-**91** (50 mg, 0.248 mmol, 1.0 eq.), $Pd_2(dba)_3$ (2.6 mg, 0.0044 mmol, 0.03 eq.), Xantphos (5.0 mg, 0.009 mmol, 0.06 eq.), Cs_2CO_3 (58 mg, 0.178 mmol, 1.2 eq.), and 6-bromonicotinic acid (33 mg, 0.163 mmol, 1.1 eq.) under argon. The suspension was degassed and refilled with argon (5 x) and then heated to 100 °C. The reaction mixture was stirred overnight at 100 °C, then cooled to room temperature, filtered, and concentrated *in vacuo*. The crude was purified by RP-HPLC (A(70%)/D(30%) to A(45%)/D(55%), 40 min gradient) to give the product as off-white solid after lyophilization (18 mg, 0.040 mmol, 16 %). ^{1}H NMR (400 MHz, DMSO-d_6) δ 11.13 (s, 1H), 8.82 – 8.81 (m, 1H), 8.27 (d, *J* = 5.7 Hz, 1H), 8.23 (dd, *J* = 8.8, 2.3 Hz, 1H), 7.54 (d, *J* = 8.8 Hz, 1H), 7.48 (s, 1H), 7.14 (d, *J* = 8.3 Hz, 2H), 7.05 (d, *J* = 5.6 Hz, 1H), 6.79 (d, *J* = 8.3 Hz, 2H), 4.83 (dd, *J* = 9.1, 4.6 Hz, 1H), 3.49 (dd, *J* = 14.4, 4.6 Hz, 1H), 3.23 – 3.19 (m, 1H), 3.17 (s, 3H), 2.55 (q, *J* = 7.7 Hz, 2H), 1.15 (t, *J* = 7.6 Hz, 3H); ^{13}C NMR (101 MHz, DMSO-d_6) δ 173.13, 165.79, 155.83, 153.44, 151.65, 148.28, 145.57, 139.64, 139.37, 128.46, 120.65, 119.64, 118.17, 113.77, 111.97, 47.38, 37.38, 29.32, 27.49, 15.43; HR-ESI-MS (*m/z*): 462.1586, calcd for $[M + H]^+$ $C_{24}H_{24}O_3N_5S$: 462.1594.

(2*Z*,5*Z*)-3-methyl-2-(phenylimino)-5-(pyridin-4-ylmethylene)thiazolidin-4-one (93). This compound was purchased from Princeton Biomolecular (no. OSSL_047658). ^{1}H NMR (400 MHz, DMSO-d_6) δ 8.68 – 8.66 (m, 2H), 7.73 (s, 1H), 7.48 – 7.42 (m, 2H), 7.25 – 7.21 (m, 1H), 7.06 – 7.03 (m, 1H), 3.37 (s, 3H).

Aurora A purification. The clone of human Aurora A kinase domain (residues 122-403 in the pET24-d vector) was kindly provided by the Montoya laboratory (University of Copenhagen). The construct was transformed into *E. coli* BL21 (DE3) Rosetta cells and protein expression was induced with 0.5 mM IPTG at 20 °C for 12 hours. The cells were harvested at 6,000x*g* for 25 min at 4 °C and resuspended in lysis buffer (50 mM Tris-HCl, 500 mM NaCl, 1 mM PMSF, pH = 8.0). Disruption of the cells was performed by sonication cooled on ice, after which the debris were removed by centrifugation at 10,000x*g* for 30 min at 4 °C. Aurora A was purified by affinity chromatography using Ni-NTA resin from Qiagen following the manufacturer's instructions. After loading, the resin was washed with lysis buffer, followed by a second wash with 6 % elution buffer (50 mM Tris-HCl, 500 mM NaCl, 500 mM imidazole, pH = 8.0). Protein was eluted with 100 % elution buffer. The eluate was exchanged into final buffer (20 mM Tris-HCl, 200 mM NaCl, 0.5 mM EDTA, 2mM DTT, pH = 8.0) using a HiPrep 26/10 desalting column (GE Healthcare). The His-tag was cleaved with TEV protease at 4 °C overnight. The tag and minor impurities were removed by a second nickel affinity chromatography step. Aggregated and soluble Aurora A were separated from one another by size exclusion chromatography using a HiLoad 16/60 Superdex^{TM} 200 column (GE Healthcare) equilibrated in final buffer. Soluble Aurora A was concentrated using Vivaspin-15 concentrators (Sartorius Stedim Biotech). Protein concentration was determined by UV absorbance. Aurora A was flash frozen in liquid nitrogen and stored at -18 °C.

HTRF kinase assay. Aurora A and Aurora B kinases were assayed using the homogeneous time-resolved fluorescence (HTRF) KinEASE STK2 kit from Cisbio (France). For Aurora A, which was expressed and purified as described above, the enzymatic reaction (total volume 10 µL) was carried out with 3 nM Aurora A kinase domain, 1 µM biotinylated STK2 substrate, 20 µM ATP (~K_m) in kinase buffer (50 mM HEPES (pH 7.0), 0.02 % NaN_3, 0.1 mM Na_3VO_4, 0.01 % BSA, 5 mM $MgCl_2$, 0.01 % Triton X-100, 1 mM DTT), and either the test compound or the DMSO control (final DMSO concentration was 2 %). For Aurora B, the enzyme reaction (total volume 10 µL) was carried out with 8 nM Aurora B/INCENP complex (Millipore, no. 14-835), 1 µM biotinylated

STK2 substrate, 20 μM ATP (K_m = 26 μM) in kinase buffer (50 mM HEPES (pH 7.0), 0.02 % NaN_3, 0.1 mM Na_3VO_4, 0.01 % BSA, 5 mM $MgCl_2$, 0.01 % Triton X-100, 1 mM DTT), and either the test compound or the DMSO control (final DMSO concentration was 2 %). For both enzymes, the reactions were run for 30 min at room temperature and stopped by the addition of 10 μL of detection buffer containing EDTA, antiphospho-Ser/Thr antibody labeled with europium cryptate, and XL-665 conjugated streptavidin (62.5 nM final concentration). After incubation at room temperature for one hour, fluorescence was measured at 620 nm (europium cryptate) and 665 nm (XL-665) after excitation at 317 nm (lag time 60 μs, integration time 500 μs) using a Tecan Infinite M1000 PRO microplate reader (Greiner 384-well plates, white, non-binding, small volume). The ratio of fluorescence (665 nm/620 nm) was calculated for each well and the results were expressed as follows: specific signal = ratio (sample) – ratio (negative control), where ratio = 665 nm/620 nm x 10^4. Compounds were measured in 3-fold serial dilutions at 10 different concentrations, covering the concentration range from no to full inhibition. Each concentration was measured in duplicates, and two independent determinations were made for each IC_{50} value. IC_{50} curves were generated using a four-parameter logistic model (XLfit from IDBS).

Kinome profiling. The kinome profiling of compound **9** was conducted by DiscoveRx. In total, 456 kinases were assayed (scanMAX). For most assays, kinase-tagged T7 phage strains were grown in parallel in 24-well blocks in an *E. coli* host derived from the BL21 strain. *E. coli* were grown to log-phase and infected with T7 phage from a frozen stock (multiplicity of infection = 0.4) and incubated with shaking at 32°C until lysis (90-150 minutes). The lysates were centrifuged (6000 g) and filtered (0.2 μm) to remove cell debris. The remaining kinases were produced in HEK-293 cells and subsequently tagged with DNA for qPCR detection. Streptavidin-coated magnetic beads were treated with biotinylated small molecule ligands for 30 minutes at room temperature to generate affinity resins for kinase assays. The liganded beads were blocked with excess biotin and washed with blocking buffer (SeaBlock (Pierce), 1 % BSA, 0.05 % Tween 20, 1 mM DTT) to remove unbound ligand and to reduce non-specific phage binding. Binding reactions were assembled by

combining kinases, liganded affinity beads, and test compounds in 1x binding buffer (20 % SeaBlock, 0.17x PBS, 0.05 % Tween 20, 6 mM DTT). Test compounds were prepared as 40x stocks in 100% DMSO and directly diluted into the assay. All reactions were performed in polypropylene 384-well plates in a final volume of 0.04 ml. The assay plates were incubated at room temperature with shaking for 1 hour and the affinity beads were washed with wash buffer (1x PBS, 0.05 % Tween 20). The beads were then re-suspended in elution buffer (1x PBS, 0.05 % Tween 20, 0.5 μM non-biotinylated affinity ligand) and incubated at room temperature with shaking for 30 minutes. The kinase concentration in the eluates was measured by qPCR. Compound 114 was screened at 1 μM, and results for primary screen binding interactions were reported as % of control (PoC). PoC = (test compound signal – positive control signal)/(DMSO signal – positive control signal). PoC values at 1 μM **9** for all kinases were visualized using TREEspot (DiscoveRx). For the determination K_D values, an 11-point 3-fold serial dilution of **9** was prepared in 100 % DMSO at 100x final test concentration and subsequently diluted to 1x in the assay (final DMSO concentration = 1 %). K_D values were determined with a standard dose-response curve using the Hill equation.

Crystallization, structure solution and refinement. Aurora A kinase domain was concentrated to 150 μM and mixed with $MgSO_4$ and the corresponding compound (dissolved in DMSO) to a final concentration of 2 mM and 150 μM, respectively. Crystallization experiments were set up after incubation of the complex for 15 min on ice. The crystals were obtained by hanging drop vapor diffusion at 18° C, mixing 1 μl of sample solution with 1 μl of reservoir solution and equilibrating against 500 μl of reservoir solution. The crystals were flash frozen in liquid nitrogen under cryo-protection. The crystallization solutions found for each complex were: 4 % v/v Tacsimate pH 8.0, 12 % w/v PEG 3350, (10 % MPD added as cryo-protectant) for **6**/Aurora A; 0.3 M Ammonium citrate dibasic, 25% PEG 3350 (10 % MPD added as cryo-protectant) for **77**/Aurora A; 0.1 M Tris pH 8.0, 28 % PEG 4K (20 % glycerol added as cryo-protectant) for **9**/Aurora A; and 5 % MPD, 0.1 M Hepes pH 7.5, 10 % PEG 10K (20 % MPD added as cryo-protectant) for **88**/Aurora A.

Data were collected on beamline X06DA at the Swiss Light Source, Paul Scherrer Institut, Villigen, Switzerland, except the data set for the **77**/Aurora A complex that was collected on beamline X06SA, also at the Swiss Light Source. The wavelength was 1 Å and the temperature 100 K. The data were integrated and scaled with MOSFLM/SCALA[79, 80] or XDS[81] (crystallographic data statistics are shown in the Supporting Information). The structures were solved by molecular replacement using Phaser in CCP4[82] and PDB 1OL5 without ligand as template. All complexes crystallized in the $P6_122$ space group with one molecule per asymmetric unit. A first round of rigid body refinement was performed, followed by simulated annealing[83] and initial electron density maps showed the presence of the compounds. These were fitted using LigandFit in Phenix.[83] Several rounds of refinement (Phenix and Refmac5[82] (using TLS) and model building (Coot)[84] were subsequently carried out until convergence was reached. The final models have no Ramachandran outliers (except one residue in the **6**/Aurora A complex structure) and they lack 8 and 15 residues at the N- and C-terminus, respectively. In addition, in the complex structures of Aurora A with **77**, **9** and **88** , 13 residues in the activation loop were not visible (residues 279–291). In the **6**/Aurora A structure, 5 residues were not modeled (residues 287–291). The figures were compiled using Pymol[85] and Ligplot.[86]

TPX2 purification. The clone of human TPX2 N-terminal domain (residues 1-43), preceded by GST and a TEV cleavage site, was a generous gift from the Conti laboratory (MPI, Martinsried). The protein was expressed in *E.coli* Bl21 (DE3) cells using 0.1 mM IPTG at 20 °C for 12 hours. Cells were broken and the soluble fraction was isolated as explained above. TPX2 was purified using a GSTrap (GE Healthcare) equilibrated in 50 mM Tris, 150 mM NaCl, pH = 7.5. GST-TPX2 was eluted using final buffer plus 10 mM reduced glutathione. The GST-tag was cleaved with TEV protease at 4°C overnight. TPX2 (1-43) was isolated in a final step of size exclusion chromatography using a HiLoad 16/60 Superdex^{TM} 75 column (GE Healthcare) equilibrated in final buffer. Protein concentration was determined by UV absorbance. TPX2 was flash frozen in liquid nitrogen and stored at -18 °C.

Microscale thermophoresis. TPX2 was labeled using the Monolith NT.115 protein labeling kit RED (NanoTemper Technologies). The labeling was performed according to the manufacturer's instructions in the supplied labeling buffer applying a concentration of 44 μM peptide at room temperature for 30 min. Labeled TPX2 was adjusted to 400 nM with final buffer and 0.05 % Tween-20 (NanoTemper Technologies). Aurora A kinase with or without ligand was dissolved in final buffer supplemented with 0.05 % Tween-20, and a series of 12 dilutions (1:1) was prepared in the identical buffer, keeping the DMSO/ligand concentration constant (final concentrations 0.5 % and 125 μM, respectively). Final protein concentrations were between 4.4 nM and 150 μM. For the thermophoresis experiment, each protein dilution was mixed with one volume of labeled TPX2, which led to a final concentration of 200 nM for fluorescently labeled TPX2, 125 μM for the ligand and 2.2 nM to 75 μM for Aurora A. After 30 min incubation at 4 °C and centrifugation at 9,600x*g* for 2 min, the solution was filled into Monolith NT hydrophilic capillaries (NanoTemper Technologies). Thermophoresis was measured at room temperature with 5s/30s/5s laser off/on/off times. Instrument parameters were adjusted to 15 % LED intensity and 80 % MST power. Data of three independent measurements were analyzed (NT.Analysis software, version 1.5.41, NanoTemper Technologies) using the thermophoresis signal after 10 sec. Points measured above 4.7 μM Aurora A were rejected.

Cell culture experiments. HeLa Kyoto cells were cultured in high-glucose DMEM with GlutaMAX (Life Technologies) media supplemented with 10 % fetal calf serum (FCS) in a humidified 5 % CO_2 incubator at 37 °C. For plasmid transfections, cells were seeded at 80–90 % confluence. 4 μg of plasmid DNA in 100 μl OptiMEM and 4 μl of Lipofectamine 2000 (Life Technologies) in 100 μl OptiMEM were incubated in parallel for 5 minutes, mixed for 20 minutes and added to each well. All Aurora A clones were constructed using full-length Aurora A as a template with appropriate PCR primer pairs. The amplified products were subcloned into a pcDNA3-GFP vector.[87] GFP-Aurora A_{R137A} and GFP-Aurora A_{W277A} were engineered using a site directed mutagenesis kit (Agilent Technologies, no. 210515) with appropriate primers. For

determining the mitotic index and the chromosome misalignment phenotype, cells were incubated with various concentrations of compounds for 20 h before analysis. Cells were likewise treated with 0.25 μM MLN8237 (Selleckchem, no. S1133) or 5 μM ZM447439 (Selleckchem, no. S1103). For flow cytometry analysis, 50 nM MLN8037 and 2.5 μM ZM447439 were used. For rescue experiments, HeLa Kyoto cells were first transfected with GFP-Aurora A, GFP-Aurora A_{R137A} or GFP-Aurora A_{W277A} for 20 h, followed by incubation with **9** for another 20 h before cells were fixed with cold methanol and stained. To assess the impact of compound **9** on cell cycle progression, DNA content was analyzed after propidium iodide staining using FACS (BD Accuri C6 flow cytometer).

Indirect immunofluorescence. For immunofluorescence, cells were fixed in cold methanol, washed in PBT (PBS supplemented with 0.05 % Tween-20) and stained with the following primary antibodies: 1:200 rabbit anti-pT288 (Cell Signaling, C39D8), 1:200 rabbit anti-pH3S10 (Cell Signaling, D2C8), 1:500 mouse anti-α-tubulin (Transduction Laboratories, 612709), 1:300 mouse anti-GFP (MAB3580, Millipore), 1:200 anti-TPX2 (Santa Cruz Biotechnology, sc-32863), anti-Aurora A (Invitrogen, 458900). Secondary antibodies were anti-mouse conjugated to Alexa488 or Alexa568, as well as anti-rabbit conjugated to Alexa488 or Alexa568, all used at 1:500 (Invitrogen). Confocal images were acquired on a Zeiss LSM 710 confocal microscope equipped with a Axiocam MRm (B/W) CCD camera using a 63×NA 1.0 oil objective and processed in ImageJ and Adobe Photoshop, maintaining relative image intensities within a series.

Acknowledgements. This work was supported financially by the University of Bern and the Swiss National Science Foundation programs NCCR Chemical Biology and NCCR TransCure. MJM was funded by a Marie Heim-Vögtlin grant. We would like to thank Vincent Olieric at the SLS for his assistance and members of the Dal Peraro laboratory for helpful discussions and Clémence Delalande at the University of Bern for help with compound characterization.

Competing interests. The authors declare no competing financial interest.

Author contributions. FK designed and carried out the study. MJM designed, supervised and performed crystallographic and biophysical studies. SK designed and performed cell culture experiments. TS performed crystallographic and biophysical studies. SDB performed the synthesis of the indirubin-like series. MA performed and carried out virtual screening and scaffold analyses. PG and JLR designed and supervised the study. All authors interpreted data. FK, MJM, SK, PG and JLR wrote the paper.

Supporting Information Available. Structures of references inhibitors used for xLOS virtual screening (Supplementary Figure 1), 1st round hits (Supplementary Figure 2) and 2nd round hits (Supplementary Figure 3), ORTEP diagrams of **76** and **78** (Supplementary Figure 4), X-ray data collection table (Supplementary Table 1), Trp fluorescence data (Supplementary Figure 5), analysis of Aurora A conformations (Supplementary Figure 6), compound purities (Supplementary Table 2), and images of ^{1}H NMR and ^{13}C NMR spectra for final compounds and selected intermediates. SMILES files of kinase screening set and 2nd round LBVS annotated with PAINS flags. This material is available free of charge via the Internet at http://pubs.acs.org.

PDB ID Codes. 4ZS0 (Aurora A complex with **6**), 4ZTQ (Aurora A complex with **77**), 4ZTR (Aurora A complex with **9**), 4ZTS (Aurora A complex with **88**). Authors will release the atomic coordinates an experimental data upon article publication.

Corresponding Author Information. Pierre Gönczy: phone: +41216930711, e-mail: pierre.gonczy@epfl.ch, Jean-Louis Reymond: phone +41316314325, e-mail: jean-louis.reymond@dcb.unibe.ch

References

1. Klebe, G., Virtual Ligand Screening: Strategies, Perspectives and Limitations. *Drug Discovery Today* **2006,** *11*, 580-594.

2. Scior, T.; Bender, A.; Tresadern, G.; Medina-Franco, J. L.; Martinez-Mayorga, K.; Langer, T.; Cuanalo-Contreras, K.; Agrafiotis, D. K., Recognizing Pitfalls in Virtual Screening: A Critical Review. *J. Chem. Inf. Model.* **2012,** *52*, 867-881.

3. Heikamp, K.; Bajorath, J., The Future of Virtual Compound Screening. *Chem. Biol. Drug Des.* **2013,** *81*, 33-40.

4. Kolb, P.; Ferreira, R. S.; Irwin, J. J.; Shoichet, B. K., Docking and Chemoinformatic Screens for New Ligands and Targets. *Curr. Opin. Biotechnol.* **2009,** *20*, 429-436.

5. Forino, M.; Jung, D.; Easton, J. B.; Houghton, P. J.; Pellecchia, M., Virtual Docking Approaches to Protein Kinase B Inhibition. *J. Med. Chem.* **2005,** *48*, 2278-2281.

6. Geppert, H.; Vogt, M.; Bajorath, J., Current Trends in Ligand-Based Virtual Screening: Molecular Representations, Data Mining Methods, New Application Areas, and Performance Evaluation. *J. Chem. Inf. Model.* **2010,** *50*, 205-216.

7. Willett, P., Similarity-Based Virtual Screening Using 2d Fingerprints. *Drug Discovery Today* **2006,** *11*, 1046-1053.

8. Giganti, D.; Guillemain, H.; Spadoni, J. L.; Nilges, M.; Zagury, J. F.; Montes, M., Comparative Evaluation of 3d Virtual Ligand Screening Methods: Impact of the Molecular Alignment on Enrichment. *J. Chem. Inf. Model.* **2010,** *50*, 992-1004.

9. Lemmen, C.; Lengauer, T.; Klebe, G., Flexs: A Method for Fast Flexible Ligand Superposition. *J. Med. Chem.* **1998,** *41*, 4502-4520.

10. Andrews, K. M.; Cramer, R. D., Toward General Methods of Targeted Library Design: Topomer Shape Similarity Searching with Diverse Structures as Queries. *J. Med. Chem.* **2000,** *43*, 1723-1740.

11. Jain, A. N., Ligand-Based Structural Hypotheses for Virtual Screening. *J. Med. Chem.* **2004,** *47*, 947-961.

12. Korb, O.; Monecke, P.; Hessler, G.; Stutzle, T.; Exner, T. E., Pharmacophore: Multiple Flexible Ligand Alignment Based on Ant Colony Optimization. *J. Chem. Inf. Model.* **2010,** *50*, 1669-1681.

13. Nicholls, A.; McGaughey, G. B.; Sheridan, R. P.; Good, A. C.; Warren, G.; Mathieu, M.; Muchmore, S. W.; Brown, S. P.; Grant, J. A.; Haigh, J. A.; Nevins, N.; Jain, A. N.; Kelley, B., Molecular Shape and Medicinal Chemistry: A Perspective. *J. Med. Chem.* **2010,** *53*, 3862-3886.

14. Sheridan, R. P.; Miller, M. D.; Underwood, D. J.; Kearsley, S. K., Chemical Similarity Using Geometric Atom Pair Descriptors. *J. Chem. Inf. Comput. Sci.* **1996,** *36*, 128-136.

15. Schreyer, A. M.; Blundell, T., Usrcat: Real-Time Ultrafast Shape Recognition with Pharmacophoric Constraints. *J. Cheminf.* **2012,** *4*, 27-39.

16. Awale, M.; Jin, X.; Reymond, J. L., Stereoselective Virtual Screening of the Zinc Database Using Atom Pair 3d-Fingerprints. *J. Cheminf.* **2015,** *7*, 3.

17. Schneider, G.; Neidhart, W.; Giller, T.; Schmid, G., "Scaffold-Hopping" by Topological Pharmacophore Search: A Contribution to Virtual Screening. *Angew. Chem., Int. Ed. Engl.* **1999,** *38*, 2894-2896.

18. Marumoto, T.; Zhang, D.; Saya, H., Aurora-a - a Guardian of Poles. *Nat. Rev. Cancer* **2005,** *5*, 42-50.

19. Metz, J. T.; Johnson, E. F.; Soni, N. B.; Merta, P. J.; Kifle, L.; Hajduk, P. J., Navigating the Kinome. *Nat. Chem. Biol.* **2011,** *7*, 200-202.

20. Carmena, M.; Earnshaw, W. C., The Cellular Geography of Aurora Kinases. *Nat. Rev. Mol. Cell Biol.* **2003,** *4*, 842-854.

21. Shagisultanova, E.; Dunbrack, R. L., Jr.; Golemis, E. A., Issues in Interpreting the in Vivo Activity of Aurora-A. *Expert Opin. Ther. Targets* **2015,** *19*, 187-200.

22. de Groot, C. O.; Hsia, J. E.; Anzola, J. V.; Motamedi, A.; Yoon, M.; Wong, Y. L.; Jenkins, D.; Lee, H. J.; Martinez, M. B.; Davis, R. L.; Gahman, T. C.; Desai, A.; Shiau, A. K., A Cell Biologist's Field Guide to Aurora Kinase Inhibitors. *Front. Oncol.* **2015,** *5*, 285.

23. Manfredi, M. G.; Ecsedy, J. A.; Chakravarty, A.; Silverman, L.; Zhang, M.; Hoar, K. M.; Stroud, S. G.; Chen, W.; Shinde, V.; Huck, J. J.; Wysong, D. R.; Janowick, D. A.; Hyer, M. L.; Leroy, P. J.; Gershman, R. E.; Silva, M. D.; Germanos, M. S.; Bolen, J. B.; Claiborne, C. F.; Sells, T. B., Characterization of Alisertib (Mln8237), an Investigational Small-Molecule Inhibitor of Aurora a Kinase Using Novel in Vivo Pharmacodynamic Assays. *Clin. Cancer Res.* **2011,** *17*, 7614-7624.

24. Hoar, K.; Chakravarty, A.; Rabino, C.; Wysong, D.; Bowman, D.; Roy, N.; Ecsedy, J. A., Mln8054, a Small-Molecule Inhibitor of Aurora a, Causes Spindle Pole and Chromosome Congression Defects Leading to Aneuploidy. *Mol. Cell. Biol.* **2007,** *27*, 4513-4525.

25. Bemis, G. W.; Murcko, M. A., The Properties of Known Drugs. 1. Molecular Frameworks. *J. Med. Chem.* **1996,** *39*, 2887-2893.

26. Schuffenhauer, A.; Ertl, P.; Roggo, S.; Wetzel, S.; Koch, M. A.; Waldmann, H., The Scaffold Tree − Visualization of the Scaffold Universe by Hierarchical Scaffold Classification. *J. Chem. Inf. Model.* **2006,** *47*, 47-58.

27. Welsch, M. E.; Snyder, S. A.; Stockwell, B. R., Privileged Scaffolds for Library Design and Drug Discovery. *Curr. Opin. Chem. Biol.* **2010,** *14*, 347-361.

28. Aronov, A. M.; McClain, B.; Moody, C. S.; Murcko, M. A., Kinase-Likeness and Kinase-Privileged Fragments: Toward Virtual Polypharmacology. *J. Med. Chem.* **2008,** *51*, 1214-1222.

29. Yan, A.; Wang, L.; Xu, S.; Xu, J., Aurora-a Kinase Inhibitor Scaffolds and Binding Modes. *Drug Discovery Today* **2011,** *16*, 260-269.

30. Uitdehaag, J. C.; Verkaar, F.; Alwan, H.; de Man, J.; Buijsman, R. C.; Zaman, G. J., A Guide to Picking the Most Selective Kinase Inhibitor Tool Compounds for Pharmacological Validation of Drug Targets. *Br. J. Pharmacol.* **2012,** *166*, 858-876.

31. Hu, Y.; Bajorath, J., Exploring the Scaffold Universe of Kinase Inhibitors. *J. Med. Chem.* **2015,** *58*, 315-332.

32. Gaulton, A.; Bellis, L. J.; Bento, A. P.; Chambers, J.; Davies, M.; Hersey, A.; Light, Y.; McGlinchey, S.; Michalovich, D.; Al-Lazikani, B.; Overington, J. P., Chembl: A Large-Scale Bioactivity Database for Drug Discovery. *Nucleic Acids Res.* **2012,** *40*, D1100-D1107.

33. Simonin, C.; Awale, M.; Brand, M.; van Deursen, R.; Schwartz, J.; Fine, M.; Kovacs, G.; Häfliger, P.; Gyimesi, G.; Sithampari, A.; Charles, R. P.; Hediger, M.; Reymond, J. L., Optimization of Trpv6 Calcium Channel Inhibitors Using a New 3d Ligand Based Virtual Screening Method. *Angew. Chem., Int. Ed. Engl.* **2015,** *54*, 14748-14752.

34. Kearsley, S. K.; Smith, G., An Alternative Method for the Alignment of Molecular Structures: Maximizing Electrostatic and Steric Overlap. *Tet. Comput. Methodol.* **1990,** *3*, 615-633.

35. Kennewell, E. A.; Willett, P.; Ducrot, P.; Luttmann, C., Identification of Target-Specific Bioisosteric Fragments from Ligand-Protein Crystallographic Data. *J. Comput.-Aided Mol. Des.* **2006,** *20*, 385-394.

36. Awale, M.; Reymond, J. L., Atom Pair 2d-Fingerprints Perceive 3d-Molecular Shape and Pharmacophores for Very Fast Virtual Screening of Zinc and Gdb-17. *J. Chem. Inf. Model.* **2014,** *54*, 1892-1897.

37. Awale, M.; Jin, X.; Reymond, J. L., Stereoselective Virtual Screening of the Zinc Database Using Atom Pair 3d-Fingerprints. *J Cheminform* **2015,** *7*, 3.

38. Montalbetti, N.; Simonin, A.; Simonin, C.; Awale, M.; Reymond, J. L.; Hediger, M. A., Discovery and Characterization of a Novel Non-Competitive Inhibitor of the Divalent Metal Transporter Dmt1/Slc11a2. *Biochem. Pharmacol.* **2015,** *96*, 216-224.

39. Irwin, J. J.; Sterling, T.; Mysinger, M. M.; Bolstad, E. S.; Coleman, R. G., Zinc: A Free Tool to Discover Chemistry for Biology. *J. Chem. Inf. Model.* **2012,** *52*, 1757-1768.

40. Baell, J. B.; Holloway, G. A., New Substructure Filters for Removal of Pan Assay Interference Compounds (Pains) from Screening Libraries and for Their Exclusion in Bioassays. *J. Med. Chem.* **2010,** *53*, 2719-2740.

41. Sterling, T.; Irwin, J. J., Zinc 15--Ligand Discovery for Everyone. *J. Chem. Inf. Model.* **2015,** *55*, 2324-2337.

42. Degorce, F.; Card, A.; Soh, S.; Trinquet, E.; Knapik, G. P.; Xie, B., Htrf: A Technology Tailored for Drug Discovery - a Review of Theoretical Aspects and Recent Applications. *Curr. Chem. Genomics* **2009,** *3*, 22-32.

43. Ke, Y. Y.; Coumar, M. S.; Shiao, H. Y.; Wang, W. C.; Chen, C. W.; Song, J. S.; Chen, C. H.; Lin, W. H.; Wu, S. H.; Hsu, J. T.; Chang, C. M.; Hsieh, H. P., Ligand Efficiency Based Approach for Efficient Virtual Screening of Compound Libraries. *Eur. J. Med. Chem.* **2014,** *83*, 226-235.

44. Emanuel, S.; Rugg, C. A.; Gruninger, R. H.; Lin, R.; Fuentes-Pesquera, A.; Connolly, P. J.; Wetter, S. K.; Hollister, B.; Kruger, W. W.; Napier, C.; Jolliffe, L.; Middleton, S. A., The in Vitro and in Vivo Effects of Jnj-7706621: A Dual Inhibitor of Cyclin-Dependent Kinases and Aurora Kinases. *Cancer Res.* **2005,** *65*, 9038-9046.

45. Wyatt, P. G.; Woodhead, A. J.; Berdini, V.; Boulstridge, J. A.; Carr, M. G.; Cross, D. M.; Davis, D. J.; Devine, L. A.; Early, T. R.; Feltell, R. E.; Lewis, E. J.; McMenamin, R. L.; Navarro, E. F.; O'Brien, M. A.; O'Reilly, M.; Reule, M.; Saxty, G.; Seavers, L. C.; Smith, D. M.; Squires, M. S.; Trewartha, G.; Walker, M. T.; Woolford, A. J., Identification of N-(4-Piperidinyl)-4-(2,6-Dichlorobenzoylamino)-1h-Pyrazole-3-Carboxamide (At7519), a Novel Cyclin Dependent Kinase Inhibitor Using Fragment-Based X-Ray Crystallography and Structure Based Drug Design. *J. Med. Chem.* **2008,** *51*, 4986-4999.

46. Deng, X.; Roessler, A.; Brdar, I.; Faessler, R.; Wu, J.; Sales, Z. S.; Mani, N. S., Direct, Metal-Free Amination of Heterocyclic Amides/Ureas with Nh-Heterocycles and N-Substituted Anilines in $Pocl_3$. *J. Org. Chem.* **2011,** *76*, 8262-8269.

47. Davies, T. G.; Tunnah, P.; Meijer, L.; Marko, D.; Eisenbrand, G.; Endicott, J. A.; Noble, M. E., Inhibitor Binding to Active and Inactive Cdk2: The Crystal Structure of Cdk2-Cyclin a/Indirubin-5-Sulphonate. *Structure* **2001,** *9*, 389-397.

48. Hoessel, R.; Leclerc, S.; Endicott, J. A.; Nobel, M. E.; Lawrie, A.; Tunnah, P.; Leost, M.; Damiens, E.; Marie, D.; Marko, D.; Niederberger, E.; Tang, W.; Eisenbrand, G.; Meijer, L., Indirubin, the Active Constituent of a Chinese Antileukaemia Medicine, Inhibits Cyclin-Dependent Kinases. *Nat. Cell Biol.* **1999,** *1*, 60-67.

49. Ottana, R.; Carotti, S.; Maccari, R.; Landini, I.; Chiricosta, G.; Caciagli, B.; Vigorita, M. G.; Mini, E., In Vitro Antiproliferative Activity against Human Colon Cancer Cell Lines of Representative 4-Thiazolidinones. Part I. *Bioorg. Med. Chem. Lett.* **2005,** *15*, 3930-3393.

50. Vicini, P.; Geronikaki, A.; Anastasia, K.; Incerti, M.; Zani, F., Synthesis and Antimicrobial Activity of Novel 2-Thiazolylimino-5-Arylidene-4-Thiazolidinones. *Bioorg. Med. Chem.* **2006,** *14*, 3859-3864.

51. El-Barbary, A. A.; Khodair, A. I.; Pedersen, E. B.; Nielsen, C., Synthesis and Evaluation of Antiviral Activity of 2′-Deoxyuridines with 5-Methylene-2-Thiohydantoin Substituents in the 5-Position. *Monatsh. Chem.* **1994,** *125*, 593-598.

52. Bhandari, S. V.; Bothara, K. G.; Patil, A. A.; Chitre, T. S.; Sarkate, A. P.; Gore, S. T.; Dangre, S. C.; Khachane, C. V., Design, Synthesis and Pharmacological Screening of Novel Antihypertensive Agents Using Hybrid Approach. *Bioorg. Med. Chem.* **2009,** *17*, 390-400.

53. Richardson, C. M.; Nunns, C. L.; Williamson, D. S.; Parratt, M. J.; Dokurno, P.; Howes, R.; Borgognoni, J.; Drysdale, M. J.; Finch, H.; Hubbard, R. E.; Jackson, P. S.; Kierstan, P.; Lentzen, G.; Moore, J. D.; Murray, J. B.; Simmonite, H.; Surgenor, A. E.; Torrance, C. J., Discovery of a Potent Cdk2 Inhibitor with a Novel Binding Mode, Using Virtual Screening and Initial, Structure-Guided Lead Scoping. *Bioorg. Med. Chem. Lett.* **2007,** *17*, 3880-3885.

54. Dakin, L. A.; Block, M. H.; Chen, H.; Code, E.; Dowling, J. E.; Feng, X.; Ferguson, A. D.; Green, I.; Hird, A. W.; Howard, T.; Keeton, E. K.; Lamb, M. L.; Lyne, P. D.; Pollard, H.; Read, J.; Wu, A. J.; Zhang, T.; Zheng, X., Discovery of Novel Benzylidene-1,3-Thiazolidine-2,4-Diones as Potent and Selective Inhibitors of the Pim-1, Pim-2, and Pim-3 Protein Kinases. *Bioorg. Med. Chem. Lett.* **2012,** *22*, 4599-4604.

55. Zhou, H.; Wu, S.; Zhai, S.; Liu, A.; Sun, Y.; Li, R.; Zhang, Y.; Ekins, S.; Swaan, P. W.; Fang, B.; Zhang, B.; Yan, B., Design, Synthesis, Cytoselective Toxicity, Structure-Activity Relationships, and Pharmacophore of Thiazolidinone Derivatives Targeting Drug-Resistant Lung Cancer Cells. *J. Med. Chem.* **2008,** *51*, 1242-1251.

56. Kornev, A. P.; Haste, N. M.; Taylor, S. S.; Eyck, L. F., Surface Comparison of Active and Inactive Protein Kinases Identifies a Conserved Activation Mechanism. *Proc. Natl. Acad. Sci. U. S. A.* **2006,** *103*, 17783-17788.

57. Kornev, A. P.; Taylor, S. S.; Ten Eyck, L. F., A Helix Scaffold for the Assembly of Active Protein Kinases. *Proc. Natl. Acad. Sci. U. S. A.* **2008,** *105*, 14377-14382.

58. Jautelat, R.; Brumby, T.; Schafer, M.; Briem, H.; Eisenbrand, G.; Schwahn, S.; Kruger, M.; Lucking, U.; Prien, O.; Siemeister, G., From the Insoluble Dye Indirubin Towards Highly Active, Soluble Cdk2-Inhibitors. *Chembiochem* **2005,** *6*, 531-540.

59. Yin, J.; Zhao, M. M.; Huffmann, M.; McNamara, J. M., Pd-Catalyzed N-Arylation of Heteroarylamines. *Org. Lett.* **2002,** *4*.

60. Honda, R.; Korner, R.; Nigg, E. A., Exploring the Functional Interactions between Aurora B, Incenp, and Survivin in Mitosis. *Mol. Biol. Cell* **2003,** *14*, 3325-3341.

61. Fabian, M. A.; Biggs, W. H., 3rd; Treiber, D. K.; Atteridge, C. E.; Azimioara, M. D.; Benedetti, M. G.; Carter, T. A.; Ciceri, P.; Edeen, P. T.; Floyd, M.; Ford, J. M.; Galvin, M.; Gerlach, J. L.; Grotzfeld, R. M.; Herrgard, S.; Insko, D. E.; Insko, M. A.; Lai, A. G.; Lelias, J. M.; Mehta, S. A.; Milanov, Z. V.; Velasco, A. M.; Wodicka, L. M.; Patel, H. K.; Zarrinkar, P. P.; Lockhart, D. J., A Small Molecule-Kinase Interaction Map for Clinical Kinase Inhibitors. *Nat. Biotechnol.* **2005,** *23*, 329-336.

62. Karaman, M. W.; Herrgard, S.; Treiber, D. K.; Gallant, P.; Atteridge, C. E.; Campbell, B. T.; Chan, K. W.; Ciceri, P.; Davis, M. I.; Edeen, P. T.; Faraoni, R.; Floyd, M.; Hunt, J. P.; Lockhart, D. J.; Milanov, Z. V.; Morrison, M. J.; Pallares, G.; Patel, H. K.; Pritchard, S.; Wodicka, L. M.; Zarrinkar, P. P., A Quantitative Analysis of Kinase Inhibitor Selectivity. *Nat. Biotechnol.* **2008,** *26*, 127-132.

63. Knighton, D. R.; Zheng, J. H.; Ten Eyck, L. F.; Ashford, V. A.; Xuong, N. H.; Taylor, S. S.; Sowadski, J. M., Crystal Structure of the Catalytic Subunit of Cyclic Adenosine Monophosphate-Dependent Protein Kinase. *Science* **1991,** *253*, 407-414.

64. Schindler, T.; Bornmann, W.; Pellicena, P.; Miller, W. T.; Clarkson, B.; Kuriyan, J., Structural Mechanism for Sti-571 Inhibition of Abelson Tyrosine Kinase. *Science* **2000,** *289*, 1938-1942.

65. Girdler, F.; Gascoigne, K. E.; Eyers, P. A.; Hartmuth, S.; Crafter, C.; Foote, K. M.; Keen, N. J.; Taylor, S. S., Validating Aurora B as an Anti-Cancer Drug Target. *J. Cell Sci.* **2006,** *119*, 3664-3675.

66. Dodson, C. A.; Kosmopoulou, M.; Richards, M. W.; Atrash, B.; Bavetsias, V.; Blagg, J.; Bayliss, R., Crystal Structure of an Aurora-a Mutant That Mimics Aurora-B Bound to Mln8054: Insights into Selectivity and Drug Design. *Biochem. J.* **2010,** *427*, 19-28.

67. Sloane, D. A.; Trikic, M. Z.; Chu, M. L.; Lamers, M. B.; Mason, C. S.; Mueller, I.; Savory, W. J.; Williams, D. H.; Eyers, P. A., Drug-Resistant Aurora a Mutants for Cellular Target Validation of the Small Molecule Kinase Inhibitors Mln8054 and Mln8237. *ACS Chem. Biol.* **2010,** *5*, 563-576.

68. Eyers, P. A.; Erikson, E.; Chen, L. G.; Maller, J. L., A Novel Mechanism for Activation of the Protein Kinase Aurora A. *Curr. Biol.* **2003,** *13*, 691-697.

69. Neumayer, G.; Belzil, C.; Gruss, O. J.; Nguyen, M. D., Tpx2: Of Spindle Assembly, DNA Damage Response, and Cancer. *Cell. Mol. Life Sci.* **2014,** *71*, 3027-3047.

70. Zorba, A.; Buosi, V.; Kutter, S.; Kern, N.; Pontiggia, F.; Cho, Y. J.; Kern, D., Molecular Mechanism of Aurora a Kinase Autophosphorylation and Its Allosteric Activation by Tpx2. *Elife* **2014,** *3*, e02667.

71. Kufer, T. A.; Sillje, H. H.; Korner, R.; Gruss, O. J.; Meraldi, P.; Nigg, E. A., Human Tpx2 Is Required for Targeting Aurora-a Kinase to the Spindle. *J. Cell Biol.* **2002,** *158*, 617-623.

72. Kesisova, I. A.; Nakos, K. C.; Tsolou, A.; Angelis, D.; Lewis, J.; Chatzaki, A.; Agianian, B.; Giannis, A.; Koffa, M. D., Tripolin a, a Novel Small-Molecule Inhibitor of Aurora a Kinase, Reveals New Regulation of Hurp's Distribution on Microtubules. *PLoS One* **2013,** *8*, e58485.

73. Littlepage, L. E.; Wu, H.; Andresson, T.; Deanehan, J. K.; Amundadottir, L. T.; Ruderman, J. V., Identification of Phosphorylated Residues That Affect the Activity of the Mitotic Kinase Aurora-A. *Proc. Natl. Acad. Sci. U. S. A.* **2002,** *99*, 15440-15445.

74. Marumoto, T.; Honda, S.; Hara, T.; Nitta, M.; Hirota, T.; Kohmura, E.; Saya, H., Aurora-a Kinase Maintains the Fidelity of Early and Late Mitotic Events in Hela Cells. *J. Biol. Chem.* **2003,** *278*, 51786-51795.

75. Giet, R.; Glover, D. M., Drosophila Aurora B Kinase Is Required for Histone H3 Phosphorylation and Condensin Recruitment During Chromosome Condensation and to Organize the Central Spindle During Cytokinesis. *J. Cell. Biol.* **2001,** *152*, 669-682.

76. Ditchfield, C.; Johnson, V. L.; Tighe, A.; Ellston, R.; Haworth, C.; Johnson, T.; Mortlock, A.; Keen, N.; Taylor, S. S., Aurora B Couples Chromosome Alignment with Anaphase by Targeting Bubr1, Mad2, and Cenp-E to Kinetochores. *J. Cell. Biol.* **2003,** *161*, 267-280.

77. Harrington, E. A.; Bebbington, D.; Moore, J.; Rasmussen, R. K.; Ajose-Adeogun, A. O.; Nakayama, T.; Graham, J. A.; Demur, C.; Hercend, T.; Diu-Hercend, A.; Su, M.; Golec, J. M.; Miller, K. M., Vx-680, a Potent and Selective Small-Molecule Inhibitor of the Aurora Kinases, Suppresses Tumor Growth in Vivo. *Nat. Med.* **2004,** *10*, 262-267.

78. Shimomura, T.; Hasako, S.; Nakatsuru, Y.; Mita, T.; Ichikawa, K.; Kodera, T.; Sakai, T.; Nambu, T.; Miyamoto, M.; Takahashi, I.; Miki, S.; Kawanishi, N.; Ohkubo, M.; Kotani, H.;

Iwasawa, Y., Mk-5108, a Highly Selective Aurora-a Kinase Inhibitor, Shows Antitumor Activity Alone and in Combination with Docetaxel. *Mol. Cancer Ther.* **2010,** *9*, 157-166.

79. Evans, P., Scaling and Assessment of Data Quality. *Acta Cryst. D* **2006,** *62*, 72-82.

80. Leslie, A. G. W.; Powell, H. R.; Read, R. J.; Sussman, J. L., Processing Diffraction Data with Mosflm. *Nato Sci. Ser. II Math.* **2007,** *245*.

81. Kabsch, W., Xds. *Acta Cryst. D* **2010,** *66*, 125-132.

82. Winn, M. D.; Ballard, C. C.; Cowtan, K. D.; Dodson, E. J.; Emsley, P.; Evans, P. R.; Wilson, K. S., Overview of the Ccp4 Suite and Current Developments. *Acta Cryst. D* **2011,** *67*, 235-242.

83. Adams, P. D.; Afonine, P. V.; Bunkoczi, G.; Chen, V. B.; Davis, I. W.; Echols, N.; Headd, J. J.; Terwilliger, T. C.; Zwart, P. H., Phenix: A Comprehensive Python-Based System for Macromolecular Structure Solution. *Acta Cryst. D* **2010,** *66*, 213-221.

84. Emsley, P.; Lohkamp, B.; Scott, W. G.; Cowtan, K., Features and Development of Coot. *Acta Cryst. D* **2010,** *66*, 486-501.

85. DeLano, W. L., *The PyMOL Molecular Graphics System (2002) on World Wide Web* http://www.pymol.org.

86. Wallace, A. C.; Laskowski, R. A.; Thornton, J. M., Ligplot - a Program to Generate Schematic Diagrams of Protein Ligand Interactions. *Protein Eng.* **1995,** *8*, 127-134.

87. Merdes, A.; Heald, R.; Samejima, K.; Earnshaw, W. C.; Cleveland, D. W., Formation of Spindle Poles by Dynein/Dynactin-Dependent Transport of Numa. *J. Cell Biol.* **2000,** *149*, 851-862.

Graphics for the Table of Contents: